# Directed searches for gravitational waves from ultralight vector boson clouds around merger remnant and galactic black holes during the first part of the fourth LIGO–Virgo–KAGRA observing run

A. G. Abac,[1] I. Abouelfettouh,[2] F. Acernese,[3,4] K. Ackley,[5] C. Adamcewicz,[6] S. Adhicary,[7] D. Adhikari,[8,9]
N. Adhikari,[10] R. X. Adhikari,[11] V. K. Adkins,[12] S. Afroz,[13] A. Agapito,[14] D. Agarwal,[15]
M. Agathos,[16] N. Aggarwal,[17] S. Aggarwal,[18] O. D. Aguiar,[19] I.-L. Ahrend,[20] L. Aiello,[21,22] A. Ain,[23]
P. Ajith,[24] T. Akutsu,[25,26] S. Albanesi,[27,28] W. Ali,[29,30] S. Al-Kershi,[8,9] C. Alléné,[31] A. Allocca,[32,4]
S. Al-Shammari,[33] P. A. Altin,[34] S. Alvarez-Lopez,[35] W. Amar,[31] O. Amarasinghe,[33] A. Amato,[36,37]
F. Amicucci,[38,39] C. Amra,[40] A. Ananyeva,[11] S. B. Anderson,[11] W. G. Anderson,[11] M. Andia,[41]
M. Ando,[42] M. Andrés-Carcasona,[43] T. Andrić,[44,45,8,9] J. Anglin,[46] S. Ansoldi,[47,48] J. M. Antelis,[49]
S. Antier,[41] M. Aoumi,[50] E. Z. Appavuravther,[51,52] S. Appert,[11] S. K. Apple,[53] K. Arai,[11] A. Araya,[42]
M. C. Araya,[11] M. Arca Sedda,[44,45] J. S. Areeda,[54] N. Aritomi,[2] F. Armato,[29,30] S. Armstrong,[55]
N. Arnaud,[56] M. Arogeti,[57] S. M. Aronson,[12] K. G. Arun,[58] G. Ashton,[59] Y. Aso,[25,60] L. Asprea,[28]
M. Assiduo,[61,62] S. Assis de Souza Melo,[63] S. M. Aston,[64] P. Astone,[38] F. Attadio,[39,38] F. Aubin,[65]
K. AultONeal,[66] G. Avallone,[67] E. A. Avila,[49] S. Babak,[20] C. Badger,[68] S. Bae,[69] S. Bagnasco,[28]
L. Baiotti,[70] R. Bajpai,[71] T. Baka,[72,37] A. M. Baker,[6] K. A. Baker,[73] T. Baker,[74] G. Baldi,[75,76]
N. Baldicchi,[77,51] M. Ball,[78] G. Ballardin,[63] S. W. Ballmer,[79] S. Banagiri,[6] B. Banerjee,[44] D. Bankar,[80]
T. M. Baptiste,[12] P. Baral,[10] M. Baratti,[81,82] J. C. Barayoga,[11] B. C. Barish,[11] D. Barker,[2] N. Barman,[80]
P. Barneo,[83,84,85] F. Barone,[86,4] B. Barr,[87] L. Barsotti,[35] M. Barsuglia,[20] D. Barta,[88] A. M. Bartoletti,[89]
M. A. Barton,[87] I. Bartos,[46] A. Basalaev,[8,9] R. Bassiri,[90] A. Basti,[82,81] M. Bawaj,[77,51] P. Baxi,[91]
J. C. Bayley,[87] A. C. Baylor,[10] P. A. Baynard II,[57] M. Bazzan,[92,93] V. M. Bedakihale,[94] F. Beirnaert,[95]
M. Bejger,[96] D. Belardinelli,[22] A. S. Bell,[87] D. S. Bellie,[97] L. Bellizzi,[81,82] W. Benoit,[18] I. Bentara,[56]
J. D. Bentley,[98] M. Ben Yaala,[55] S. Bera,[99,100] F. Bergamin,[33] B. K. Berger,[90] S. Bernuzzi,[27]
M. Beroiz,[11] D. Bersanetti,[29] T. Bertheas,[101] A. Bertolini,[37,36] J. Betzwieser,[64] D. Beveridge,[73]
G. Bevilacqua,[102] N. Bevins,[103] R. Bhandare,[104] R. Bhatt,[11] D. Bhattacharjee,[105,106] S. Bhattacharyya,[107]
S. Bhaumik,[46] V. Biancalana,[102] A. Bianchi,[37,108] I. A. Bilenko,[109] G. Billingsley,[11] A. Binetti,[110]
S. Bini,[11,75,76] C. Binu,[111] S. Biot,[112] O. Birnholtz,[113] S. Biscoveanu,[97] A. Bisht,[9] M. Bitossi,[63,81]
M.-A. Bizouard,[114] S. Blaber,[115] J. K. Blackburn,[11] L. A. Blagg,[78] C. D. Blair,[73,64] D. G. Blair,[73]
N. Bode,[8,9] N. Boettner,[98] G. Boileau,[114] M. Boldrini,[38] G. N. Bolingbroke,[116] A. Bolliand,[117,40]
L. D. Bonavena,[46] R. Bondarescu,[83] F. Bondu,[118] E. Bonilla,[90] M. S. Bonilla,[54] A. Bonino,[119]
R. Bonnand,[31,117] A. Borchers,[8,9] V. Boschi,[81] S. Bose,[120] V. Bossilkov,[64] Y. Bothra,[37,108] A. Boudon,[56]
L. Bourg,[57] M. Boyle,[121] A. Bozzi,[63] C. Bradaschia,[81] P. R. Brady,[10] A. Branch,[64] M. Branchesi,[44,45]
I. Braun,[105] T. Briant,[122] A. Brillet,[114] M. Brinkmann,[8,9] P. Brockill,[10] E. Brockmueller,[8,9] A. F. Brooks,[11]
B. C. Brown,[46] D. D. Brown,[116] M. L. Brozzetti,[77,51] S. Brunett,[11] G. Bruno,[15] R. Bruntz,[123] J. Bryant,[119]
Y. Bu,[124] F. Bucci,[62] J. Buchanan,[123] O. Bulashenko,[83,84] T. Bulik,[125] H. J. Bulten,[37] A. Buonanno,[126,1]
K. Burtnyk,[2] R. Buscicchio,[127,128] D. Buskulic,[31] C. Buy,[101] R. L. Byer,[90] G. S. Cabourn Davies,[74]
R. Cabrita,[15] V. Cáceres-Barbosa,[7] L. Cadonati,[57] G. Cagnoli,[129] C. Cahillane,[79] A. Calafat,[99]
T. A. Callister,[130] E. Calloni,[32,4] S. R. Callos,[78] M. Canepa,[30,29] G. Caneva Santoro,[43] K. C. Cannon,[42]
H. Cao,[35] L. A. Capistran,[131] E. Capocasa,[20] E. Capote,[2,11] G. Capurri,[82,81] G. Carapella,[67,132]
F. Carbognani,[63] M. Carlassara,[8,9] J. B. Carlin,[124] T. K. Carlson,[133] M. F. Carney,[105] M. Carpinelli,[127,63]
G. Carrillo,[78] J. J. Carter,[8,9] G. Carullo,[119,134] A. Casallas-Lagos,[135] J. Casanueva Diaz,[63]
C. Casentini,[136,22] S. Y. Castro-Lucas,[137] S. Caudill,[133] M. Cavaglià,[106] R. Cavalieri,[63] A. Ceja,[54] G. Cella,[81]
P. Cerdá-Durán,[138,139] E. Cesarini,[22] N. Chabbra,[34] W. Chaibi,[114] A. Chakraborty,[13] P. Chakraborty,[8,9]
S. Chakraborty,[104] S. Chalathadka Subrahmanya,[98] J. C. L. Chan,[140] M. Chan,[115] K. Chang,[141] S. Chao,[142,141]
P. Charlton,[143] E. Chassande-Mottin,[20] C. Chatterjee,[144] Debarati Chatterjee,[80] Deep Chatterjee,[35]
M. Chaturvedi,[104] S. Chaty,[20] A. Chen,[145] A. H.-Y. Chen,[146] D. Chen,[147] H. Chen,[142] H. Y. Chen,[148]
S. Chen,[144] Yanbei Chen,[149] Yitian Chen,[121] H. P. Cheng,[150] P. Chessa,[77,51] H. T. Cheung,[91] S. Y. Cheung,[6]
F. Chiadini,[151,132] G. Chiarini,[8,9,93] A. Chiba,[152] A. Chincarini,[29] M. L. Chiofalo,[82,81] A. Chiummo,[4,63]
C. Chou,[146] S. Choudhary,[73] N. Christensen,[114,153] S. S. Y. Chua,[34] G. Ciani,[75,76] P. Ciecielag,[96]
M. Cieślar,[125] M. Cifaldi,[22] B. Cirok,[154] F. Clara,[2] J. A. Clark,[11,57] T. A. Clarke,[6] P. Clearwater,[155]
S. Clesse,[112] F. Cleva,[114,117] E. Coccia,[44,45,43] E. Codazzo,[156,157] P.-F. Cohadon,[122] S. Colace,[30]
E. Colangeli,[74] M. Colleoni,[99] C. G. Collette,[158] J. Collins,[64] S. Colloms,[87] A. Colombo,[159,128]

C. M. Compton,[2] G. Connolly,[78] L. Conti,[93] T. R. Corbitt,[12] I. Cordero-Carrión,[160] S. Corezzi,[77,51]
N. J. Cornish,[161] I. Coronado,[162] A. Corsi,[163] R. Cottingham,[64] M. W. Coughlin,[18] A. Couineaux,[38]
P. Couvares,[11,57] D. M. Coward,[73] R. Coyne,[164] A. Cozzumbo,[44] J. D. E. Creighton,[10] T. D. Creighton,[165]
P. Cremonese,[99] S. Crook,[64] R. Crouch,[2] J. Csizmazia,[2] J. R. Cudell,[166] T. J. Cullen,[11] A. Cumming,[87]
E. Cuoco,[167,168] M. Cusinato,[138] L. V. Da Conceição,[169] T. Dal Canton,[41] S. Dal Pra,[170]
G. Dálya,[101] B. D'Angelo,[29] S. Danilishin,[36,37] S. D'Antonio,[38] K. Danzmann,[9,8,9] K. E. Darroch,[123]
L. P. Dartez,[64] R. Das,[107] A. Dasgupta,[94] V. Dattilo,[63] A. Daumas,[20] N. Davari,[171,172] I. Dave,[104]
A. Davenport,[137] M. Davier,[41] T. F. Davies,[73] D. Davis,[11] L. Davis,[73] M. C. Davis,[18] P. Davis,[173,174]
E. J. Daw,[175] M. Dax,[1] J. De Bolle,[95] M. Deenadayalan,[80] J. Degallaix,[176] M. De Laurentis,[32,4]
F. De Lillo,[23] S. Della Torre,[128] W. Del Pozzo,[82,81] A. Demagny,[31] F. De Marco,[39,38] G. Demasi,[177,62]
F. De Matteis,[21,22] N. Demos,[35] T. Dent,[178] A. Depasse,[15] N. DePergola,[103] R. De Pietri,[179,180]
R. De Rosa,[32,4] C. De Rossi,[63] M. Desai,[35] R. DeSalvo,[181] A. DeSimone,[182] R. De Simone,[151,132]
A. Dhani,[1] R. Diab,[46] M. C. Díaz,[165] M. Di Cesare,[32,4] G. Dideron,[183] T. Dietrich,[1] L. Di Fiore,[4]
C. Di Fronzo,[73] M. Di Giovanni,[39,38] T. Di Girolamo,[32,4] D. Diksha,[37,36] J. Ding,[20,184] S. Di Pace,[39,38]
I. Di Palma,[39,38] D. Di Piero,[185,48] F. Di Renzo,[56] Divyajyoti,[33] A. Dmitriev,[119] J. P. Docherty,[87]
Z. Doctor,[97] N. Doerksen,[169] E. Dohmen,[2] A. Doke,[133] A. Domiciano De Souza,[186] L. D'Onofrio,[38]
F. Donovan,[35] K. L. Dooley,[33] T. Dooney,[72] S. Doravari,[80] O. Dorosh,[187] W. J. D. Doyle,[123] M. Drago,[39,38]
J. C. Driggers,[2] L. Dunn,[124] U. Dupletsa,[44] P.-A. Duverne,[20] D. D'Urso,[171,156] P. Dutta Roy,[46]
H. Duval,[188] S. E. Dwyer,[2] C. Eassa,[2] W. E. East,[183] M. Ebersold,[189,31] T. Eckhardt,[98] G. Eddolls,[79]
A. Effler,[64] J. Eichholz,[34] H. Einsle,[114] M. Eisenmann,[25] M. Emma,[59] K. Endo,[152] R. Enficiaud,[1]
L. Errico,[32,4] R. Espinosa,[165] M. Esposito,[4,32] R. C. Essick,[190] H. Estellés,[1] T. Etzel,[11] M. Evans,[35]
T. Evstafyeva,[183] B. E. Ewing,[7] J. M. Ezquiaga,[140] F. Fabrizi,[61,62] V. Fafone,[21,22] S. Fairhurst,[33]
A. M. Farah,[130] B. Farr,[78] W. M. Farr,[191,192] G. Favaro,[92] M. Favata,[193] M. Fays,[166] M. Fazio,[55]
J. Feicht,[11] M. M. Fejer,[90] R. Felicetti,[185,48] E. Fenyvesi,[88,194] J. Fernandes,[195] T. Fernandes,[196,138]
D. Fernando,[111] S. Ferraiuolo,[197,39,38] T. A. Ferreira,[12] F. Fidecaro,[82,81] P. Figura,[96] A. Fiori,[81,82]
I. Fiori,[63] M. Fishbach,[190] R. P. Fisher,[123] R. Fittipaldi,[198,132] V. Fiumara,[199,132] R. Flaminio,[31]
S. M. Fleischer,[200] L. S. Fleming,[201] E. Floden,[18] H. Fong,[115] J. A. Font,[138,139] F. Fontinele-Nunes,[18] C. Foo,[1]
B. Fornal,[202] K. Franceschetti,[179] F. Frappez,[31] S. Frasca,[39,38] F. Frasconi,[81] J. P. Freed,[66] Z. Frei,[203]
A. Freise,[37,108] O. Freitas,[196,138] R. Frey,[78] W. Frischhertz,[64] P. Fritschel,[35] V. V. Frolov,[64] G. G. Fronzé,[28]
M. Fuentes-Garcia,[11] S. Fujii,[204] T. Fujimori,[205] P. Fulda,[46] M. Fyffe,[64] B. Gadre,[72] J. R. Gair,[1]
S. Galaudage,[186] V. Galdi,[206] R. Gamba,[7] A. Gamboa,[1] S. Gamoji,[181] D. Ganapathy,[207] A. Ganguly,[80]
B. Garaventa,[29] J. García-Bellido,[208] C. García-Quirós,[189] J. W. Gardner,[34] K. A. Gardner,[115] S. Garg,[42]
J. Gargiulo,[63] X. Garrido,[41] A. Garron,[99] F. Garufi,[32,4] P. A. Garver,[90] C. Gasbarra,[21,22] B. Gateley,[2]
F. Gautier,[209] V. Gayathri,[10] T. Gayer,[79] G. Gemme,[29] A. Gennai,[81] V. Gennari,[101] J. George,[104]
R. George,[148] O. Gerberding,[98] L. Gergely,[154] Archisman Ghosh,[95] Sayantan Ghosh,[195] Shaon Ghosh,[193]
Shrobana Ghosh,[8,9] Suprovo Ghosh,[210] Tathagata Ghosh,[80] J. A. Giaime,[12,64] K. D. Giardina,[64]
D. R. Gibson,[201] C. Gier,[55] S. Gkaitatzis,[82,81] J. Glanzer,[11] F. Glotin,[41] J. Godfrey,[78] R. V. Godley,[8,9]
P. Godwin,[11] A. S. Goettel,[33] E. Goetz,[115] J. Golomb,[11] S. Gomez Lopez,[39,38] B. Goncharov,[44]
G. González,[12] P. Goodarzi,[211] S. Goode,[6] A. W. Goodwin-Jones,[15] M. Gosselin,[63] R. Gouaty,[31]
D. W. Gould,[34] K. Govorkova,[35] A. Grado,[77,51] V. Graham,[87] A. E. Granados,[18] M. Granata,[176]
V. Granata,[212,132] S. Gras,[35] P. Grassia,[11] J. Graves,[57] C. Gray,[2] R. Gray,[87] G. Greco,[51] A. C. Green,[37,108]
L. Green,[213] S. M. Green,[74] S. R. Green,[214] C. Greenberg,[133] A. M. Gretarsson,[66] H. K. Griffin,[18] D. Griffith,[11]
H. L. Griggs,[57] G. Grignani,[77,51] C. Grimaud,[31] H. Grote,[33] S. Grunewald,[1] D. Guerra,[138] D. Guetta,[215]
G. M. Guidi,[61,62] A. R. Guimaraes,[12] H. K. Gulati,[94] F. Gulminelli,[173,174] H. Guo,[145] W. Guo,[73]
Y. Guo,[37,36] Anuradha Gupta,[216] I. Gupta,[7] N. C. Gupta,[94] S. K. Gupta,[46] V. Gupta,[18] N. Gupte,[1]
J. Gurs,[98] N. Gutierrez,[176] N. Guttman,[6] F. Guzman,[131] D. Haba,[217] M. Haberland,[1] S. Haino,[218] E. D. Hall,[35]
E. Z. Hamilton,[99] G. Hammond,[87] M. Haney,[37] J. Hanks,[2] C. Hanna,[7] M. D. Hannam,[33] O. A. Hannuksela,[219]
A. G. Hanselman,[130] H. Hansen,[2] J. Hanson,[64] S. Hanumasagar,[57] R. Harada,[42] A. R. Hardison,[182]
S. Harikumar,[187] K. Haris,[37,72] I. Harley-Trochimczyk,[131] T. Harmark,[134] J. Harms,[44,45] G. M. Harry,[220]
I. W. Harry,[74] J. Hart,[105] B. Haskell,[96,221,222] C.-J. Haster,[213] K. Haughian,[87] H. Hayakawa,[50] K. Hayama,[223]
M. C. Heintze,[64] J. Heinze,[119] J. Heinzel,[35] H. Heitmann,[114] F. Hellman,[207] A. F. Helmling-Cornell,[78]
G. Hemming,[63] O. Henderson-Sapir,[116] M. Hendry,[87] I. S. Heng,[87] M. H. Hennig,[87] C. Henshaw,[57]
M. Heurs,[8,9] A. L. Hewitt,[224,225] J. Heynen,[15] J. Heyns,[35] S. Higginbotham,[33] S. Hild,[36,37] S. Hill,[87]

Y. Himemoto,[226] N. Hirata,[25] C. Hirose,[227] D. Hofman,[176] B. E. Hogan,[66] N. A. Holland,[37,108]
K. Holley-Bockelmann,[144] I. J. Hollows,[175] D. E. Holz,[130] L. Honet,[112] D. J. Horton-Bailey,[207] J. Hough,[87]
S. Hourihane,[11] N. T. Howard,[144] E. J. Howell,[73] C. G. Hoy,[74] C. A. Hrishikesh,[21] P. Hsi,[35] H.-F. Hsieh,[142]
H.-Y. Hsieh,[142] C. Hsiung,[228] S.-H. Hsu,[146] W.-F. Hsu,[110] Q. Hu,[87] H. Y. Huang,[141] Y. Huang,[7]
Y. T. Huang,[79] A. D. Huddart,[229] B. Hughey,[66] V. Hui,[31] S. Husa,[99] R. Huxford,[7] L. Iampieri,[39,38]
G. A. Iandolo,[36] M. Ianni,[22,21] G. Iannone,[132] J. Iascau,[78] K. Ide,[230] R. Iden,[217] A. Ierardi,[44,45] S. Ikeda,[147]
H. Imafuku,[42] Y. Inoue,[141] G. Iorio,[92] P. Iosif,[185,48] M. H. Iqbal,[34] J. Irwin,[87] R. Ishikawa,[230] M. Isi,[191,192]
K. S. Isleif,[231] Y. Itoh,[205,232] M. Iwaya,[204] B. R. Iyer,[24] C. Jacquet,[101] P.-E. Jacquet,[122] T. Jacquot,[41]
S. J. Jadhav,[233] S. P. Jadhav,[155] M. Jain,[133] T. Jain,[224] A. L. James,[11] K. Jani,[144] J. Janquart,[15]
N. N. Janthalur,[233] S. Jaraba,[234] P. Jaranowski,[235] R. Jaume,[99] W. Javed,[33] A. Jennings,[2] M. Jensen,[2]
W. Jia,[35] J. Jiang,[150] H.-B. Jin,[236,237] G. R. Johns,[123] N. A. Johnson,[46] M. C. Johnston,[213] R. Johnston,[87]
N. Johny,[8,9] D. H. Jones,[34] D. I. Jones,[210] R. Jones,[87] H. E. Jose,[78] P. Joshi,[7] S. K. Joshi,[80] G. Joubert,[56]
J. Ju,[238] L. Ju,[73] K. Jung,[239] J. Junker,[34] V. Juste,[112] H. B. Kabagoz,[64,35] T. Kajita,[240] I. Kaku,[205]
V. Kalogera,[97] M. Kalomenopoulos,[213] M. Kamiizumi,[50] N. Kanda,[232,205] S. Kandhasamy,[80]
G. Kang,[241] N. C. Kannachel,[6] J. B. Kanner,[11] S. A. KantiMahanty,[18] S. J. Kapadia,[80] D. P. Kapasi,[54]
M. Karthikeyan,[133] M. Kasprzack,[11] H. Kato,[152] T. Kato,[204] E. Katsavounidis,[35] W. Katzman,[64] R. Kaushik,[104]
K. Kawabe,[2] R. Kawamoto,[205] D. Keitel,[99] L. J. Kemperman,[116] J. Kennington,[7] F. A. Kerkow,[18]
R. Kesharwani,[80] J. S. Key,[242] R. Khadela,[8,9] S. Khadka,[90] S. S. Khadkikar,[7] F. Y. Khalili,[109] F. Khan,[8,9]
T. Khanam,[163] M. Khursheed,[104] N. M. Khusid,[191,192] W. Kiendrebeogo,[114,243] N. Kijbunchoo,[116] C. Kim,[244]
J. C. Kim,[245] K. Kim,[246] M. H. Kim,[238] S. Kim,[247] Y.-M. Kim,[246] C. Kimball,[97] K. Kimes,[54]
M. Kinnear,[33] J. S. Kissel,[2] S. Klimenko,[46] A. M. Knee,[115] E. J. Knox,[78] N. Knust,[8,9] K. Kobayashi,[204]
S. M. Koehlenbeck,[90] G. Koekoek,[37,36] K. Kohri,[248,249] K. Kokeyama,[33,250] S. Koley,[44,166] P. Kolitsidou,[119]
A. E. Koloniari,[251] K. Komori,[42] A. K. H. Kong,[142] A. Kontos,[252] L. M. Koponen,[119] M. Korobko,[98]
X. Kou,[18] A. Koushik,[23] N. Kouvatsos,[68] M. Kovalam,[73] T. Koyama,[152] D. B. Kozak,[11] S. L. Kranzhoff,[36,37]
V. Kringel,[8,9] N. V. Krishnendu,[119] S. Kroker,[253] A. Królak,[254,187] K. Kruska,[8,9] J. Kubisz,[255] G. Kuehn,[8,9]
S. Kulkarni,[216] A. Kulur Ramamohan,[34] Achal Kumar,[46] Anil Kumar,[233] Praveen Kumar,[178]
Prayush Kumar,[24] Rahul Kumar,[2] Rakesh Kumar,[94] J. Kume,[256,257,42] K. Kuns,[35] N. Kuntimaddi,[33]
S. Kuroyanagi,[208,258] S. Kuwahara,[42] K. Kwak,[239] K. Kwan,[34] S. Kwon,[42] G. Lacaille,[87] D. Laghi,[189,101]
A. H. Laity,[164] E. Lalande,[259] M. Lalleman,[23] P. C. Lalremruati,[260] M. Landry,[2] B. B. Lane,[35] R. N. Lang,[35]
J. Lange,[148] R. Langgin,[213] B. Lantz,[90] I. La Rosa,[99] J. Larsen,[200] A. Lartaux-Vollard,[41] P. D. Lasky,[6]
J. Lawrence,[165] M. Laxen,[64] C. Lazarte,[138] A. Lazzarini,[11] C. Lazzaro,[157,156] P. Leaci,[39,38] L. Leali,[18]
Y. K. Lecoeuche,[115] H. M. Lee,[261] H. W. Lee,[262] J. Lee,[79] K. Lee,[238] R.-K. Lee,[142] R. Lee,[35]
Sungho Lee,[246] Sunjae Lee,[238] Y. Lee,[141] I. N. Legred,[11] J. Lehmann,[8,9] L. Lehner,[183] M. Le Jean,[176,117]
A. Lemaître,[263] M. Lenti,[62,177] M. Leonardi,[75,76,264] M. Lequime,[40] N. Leroy,[41] M. Lesovsky,[11] N. Letendre,[31]
M. Lethuillier,[56] Y. Levin,[6] K. Leyde,[74] A. K. Y. Li,[11] K. L. Li,[265] T. G. F. Li,[110] X. Li,[149] Y. Li,[97] Z. Li,[87]
A. Lihos,[123] E. T. Lin,[142] F. Lin,[141] L. C.-C. Lin,[265] Y.-C. Lin,[142] C. Lindsay,[201] S. D. Linker,[181] A. Liu,[219]
G. C. Liu,[228] Jian Liu,[73] F. Llamas Villarreal,[165] J. Llobera-Querol,[99] R. K. L. Lo,[140] J.-P. Locquet,[110]
S. C. G. Loggins,[266] M. R. Loizou,[133] L. T. London,[68] A. Longo,[61,62] D. Lopez,[166] M. Lopez Portilla,[72]
A. Lorenzo-Medina,[178] V. Loriette,[41] M. Lormand,[64] G. Losurdo,[267,81] E. Lotti,[133] T. P. Lott IV,[57]
J. D. Lough,[8,9] H. A. Loughlin,[35] C. O. Lousto,[111] N. Low,[124] N. Lu,[34] L. Lucchesi,[81] H. Lück,[9,8,9]
D. Lumaca,[22] A. P. Lundgren,[268,269] A. W. Lussier,[259] R. Macas,[74] M. MacInnis,[35] D. M. Macleod,[33]
I. A. O. MacMillan,[11] A. Macquet,[41] K. Maeda,[152] S. Maenaut,[110] S. S. Magare,[80] R. M. Magee,[11]
E. Maggio,[1] R. Maggiore,[37,108] M. Magnozzi,[29,30] M. Mahesh,[98] M. Maini,[164] S. Majhi,[80] E. Majorana,[39,38]
C. N. Makarem,[11] D. Malakar,[106] J. A. Malaquias-Reis,[19] U. Mali,[190] S. Maliakal,[11] A. Malik,[104]
L. Mallick,[169,190] A.-K. Malz,[59] N. Man,[114] M. Mancarella,[100] V. Mandic,[18] V. Mangano,[171,156]
B. Mannix,[78] G. L. Mansell,[79] M. Manske,[10] M. Mantovani,[63] M. Mapelli,[92,93,270] C. Marinelli,[102]
F. Marion,[31] A. S. Markosyan,[90] A. Markowitz,[11] E. Maros,[11] S. Marsat,[101] F. Martelli,[61,62] I. W. Martin,[87]
R. M. Martin,[193] B. B. Martinez,[131] D. A. Martinez,[54] M. Martinez,[43,271] V. Martinez,[129] A. Martini,[75,76]
J. C. Martins,[19] D. V. Martynov,[119] E. J. Marx,[35] L. Massaro,[36,37] A. Masserot,[31] M. Masso-Reid,[87]
S. Mastrogiovanni,[38] T. Matcovich,[51] M. Matiushechkina,[8,9] L. Maurin,[209] N. Mavalvala,[35] N. Maxwell,[2]
T. May,[183] G. McCarrol,[64] R. McCarthy,[2] D. E. McClelland,[34] S. McCormick,[64] L. McCuller,[11] S. McEachin,[123]
C. McElhenny,[123] G. I. McGhee,[87] K. B. M. McGowan,[144] J. McIver,[115] A. McLeod,[73] I. McMahon,[189]
T. McRae,[34] R. McTeague,[87] D. Meacher,[10] B. N. Meagher,[79] R. Mechum,[111] Q. Meijer,[72] A. Melatos,[124]

C. S. Menoni,[137] F. Mera,[2] R. A. Mercer,[10] L. Mereni,[176] K. Merfeld,[163] E. L. Merilh,[64] J. R. Mérou,[99]
J. D. Merritt,[78] M. Merzougui,[114] C. Messick,[10] B. Mestichelli,[44] M. Meyer-Conde,[272] F. Meylahn,[8,9]
A. Mhaske,[80] A. Miani,[75,76] H. Miao,[273] C. Michel,[176] Y. Michimura,[42] H. Middleton,[119] D. P. Mihaylov,[105]
A. L. Miller,[37,72] S. J. Miller,[11] M. Millhouse,[57] E. Milotti,[185,48] V. Milotti,[92] Y. Minenkov,[22]
E. M. Minihan,[66] Ll. M. Mir,[43] L. Mirasola,[156,157] M. Miravet-Tenés,[138] C.-A. Miritescu,[43] A. Mishra,[24]
C. Mishra,[107] T. Mishra,[46] A. L. Mitchell,[37,108] J. G. Mitchell,[66] S. Mitra,[80] V. P. Mitrofanov,[109]
K. Mitsuhashi,[25] R. Mittleman,[35] O. Miyakawa,[50] S. Miyoki,[50] A. Miyoko,[66] G. Mo,[35] L. Mobilia,[61,62]
S. R. P. Mohapatra,[11] S. R. Mohite,[7] M. Molina-Ruiz,[207] M. Mondin,[181] M. Montani,[61,62] C. J. Moore,[224]
D. Moraru,[2] A. More,[80] S. More,[80] C. Moreno,[135] E. A. Moreno,[35] G. Moreno,[2] A. Moreso Serra,[83]
S. Morisaki,[42,204] Y. Moriwaki,[152] G. Morras,[208] A. Moscatello,[92] M. Mould,[35] B. Mours,[65]
C. M. Mow-Lowry,[37,108] L. Muccillo,[177,62] F. Muciaccia,[39,38] D. Mukherjee,[119] Samanwaya Mukherjee,[24]
Soma Mukherjee,[165] Subroto Mukherjee,[94] Suvodip Mukherjee,[13] N. Mukund,[35] A. Mullavey,[64] H. Mullock,[115]
J. Mundi,[220] C. L. Mungioli,[73] M. Murakoshi,[230] P. G. Murray,[87] D. Nabari,[75,76] S. L. Nadji,[8,9] A. Nagar,[28,274]
N. Nagarajan,[87] K. Nakagaki,[50] K. Nakamura,[25] H. Nakano,[275] M. Nakano,[11] D. Nanadoumgar-Lacroze,[43]
D. Nandi,[12] V. Napolano,[63] P. Narayan,[216] I. Nardecchia,[22] T. Narikawa,[204] H. Narola,[72] L. Naticchioni,[38]
R. K. Nayak,[260] L. Negri,[72] A. Nela,[87] C. Nelle,[78] A. Nelson,[131] T. J. N. Nelson,[64] M. Nery,[8,9] A. Neunzert,[2]
S. Ng,[54] L. Nguyen Quynh,[276] S. A. Nichols,[12] A. B. Nielsen,[277] Y. Nishino,[25,42] A. Nishizawa,[278]
S. Nissanke,[279,37] W. Niu,[7] F. Nocera,[63] J. Noller,[280] M. Norman,[33] C. North,[33] J. Novak,[117,234,281]
R. Nowicki,[144] J. F. Nuño Siles,[208] L. K. Nuttall,[74] K. Obayashi,[230] J. Oberling,[2] J. O'Dell,[229] E. Oelker,[35]
M. Oertel,[234,117,282,281] G. Oganesyan,[44,45] T. O'Hanlon,[64] M. Ohashi,[50] F. Ohme,[8,9] R. Oliveri,[117,282,281]
R. Omer,[18] B. O'Neal,[123] M. Onishi,[152] K. Oohara,[283] B. O'Reilly,[64] M. Orselli,[51,77] R. O'Shaughnessy,[111]
S. O'Shea,[87] S. Oshino,[50] C. Osthelder,[11] I. Ota,[12] D. J. Ottaway,[116] A. Ouzriat,[56] H. Overmier,[64]
B. J. Owen,[284] R. Ozaki,[230] A. E. Pace,[7] R. Pagano,[12] M. A. Page,[25] A. Pai,[195] L. Paiella,[44] A. Pal,[285]
S. Pal,[260] M. A. Palaia,[81,82] M. Pálfi,[203] P. P. Palma,[39,21,22] C. Palomba,[38] P. Palud,[20] H. Pan,[142] J. Pan,[73]
K. C. Pan,[142] P. K. Panda,[233] Shiksha Pandey,[7] Swadha Pandey,[35] P. T. H. Pang,[37,72] F. Pannarale,[39,38]
K. A. Pannone,[54] B. C. Pant,[104] F. H. Panther,[73] M. Panzeri,[61,62] F. Paoletti,[81] A. Paolone,[38,286]
A. Papadopoulos,[87] E. E. Papalexakis,[211] L. Papalini,[81,82] G. Papigkiotis,[251] A. Paquis,[41] A. Parisi,[77,51]
B.-J. Park,[246] J. Park,[287] W. Parker,[64] G. Pascale,[8,9] D. Pascucci,[95] A. Pasqualetti,[63] R. Passaquieti,[82,81]
L. Passenger,[6] D. Passuello,[81] O. Patane,[2] A. V. Patel,[141] D. Pathak,[80] A. Patra,[33] B. Patricelli,[82,81]
B. G. Patterson,[33] K. Paul,[107] S. Paul,[78] E. Payne,[11] T. Pearce,[33] M. Pedraza,[11] A. Pele,[11] F. E. Peña
Arellano,[288] X. Peng,[119] Y. Peng,[57] S. Penn,[289] M. D. Penuliar,[54] A. Perego,[75,76] Z. Pereira,[133]
C. Périgois,[290,93,92] G. Perna,[92] A. Perreca,[75,76,44] J. Perret,[20] S. Perriès,[56] J. W. Perry,[37,108] D. Pesios,[251]
S. Peters,[166] S. Petracca,[206] C. Petrillo,[77] H. P. Pfeiffer,[1] H. Pham,[64] K. A. Pham,[18] K. S. Phukon,[119]
H. Phurailatpam,[219] M. Piarulli,[101] L. Piccari,[39,38] O. J. Piccinni,[34] M. Pichot,[114] M. Piendibene,[82,81]
F. Piergiovanni,[61,62] L. Pierini,[38] G. Pierra,[38] V. Pierro,[291,132] M. Pietrzak,[96] M. Pillas,[166] F. Pilo,[81]
L. Pinard,[176] I. M. Pinto,[291,132,292,32] M. Pinto,[63] B. J. Piotrzkowski,[10] M. Pirello,[2] M. D. Pitkin,[224,87]
A. Placidi,[51] E. Placidi,[39,38] M. L. Planas,[99] W. Plastino,[212,22] C. Plunkett,[35] R. Poggiani,[82,81]
E. Polini,[35] J. Pomper,[81,82] L. Pompili,[1] J. Poon,[219] E. Porcelli,[37] E. K. Porter,[20] C. Posnansky,[7] R. Poulton,[63]
J. Powell,[155] G. S. Prabhu,[80] M. Pracchia,[166] B. K. Pradhan,[80] T. Pradier,[65] A. K. Prajapati,[94]
K. Prasai,[293] R. Prasanna,[233] P. Prasia,[80] G. Pratten,[119] G. Principe,[185,48] G. A. Prodi,[75,76] P. Prosperi,[81]
P. Prosposito,[21,22] A. C. Providence,[66] A. Puecher,[1] J. Pullin,[12] P. Puppo,[38] M. Pürrer,[164] H. Qi,[16]
J. Qin,[34] G. Quéméner,[174,117] V. Quetschke,[165] P. J. Quinonez,[66] N. Qutob,[57] R. Rading,[231] I. Rainho,[138]
S. Raja,[104] C. Rajan,[104] B. Rajbhandari,[111] K. E. Ramirez,[64] F. A. Ramis Vidal,[99] M. Ramos Arevalo,[165]
A. Ramos-Buades,[99,37] S. Ranjan,[57] K. Ransom,[64] P. Rapagnani,[39,38] B. Ratto,[66] A. Ravichandran,[133]
A. Ray,[97] V. Raymond,[33] M. Razzano,[82,81] J. Read,[54] T. Regimbau,[31] S. Reid,[55] C. Reissel,[35] D. H. Reitze,[11]
A. I. Renzini,[127,11] B. Revenu,[294,41] A. Revilla Peña,[83] R. Reyes,[181] L. Ricca,[15] F. Ricci,[39,38] M. Ricci,[38,39]
A. Ricciardone,[82,81] J. Rice,[79] J. W. Richardson,[211] M. L. Richardson,[116] A. Rijal,[66] K. Riles,[91] H. K. Riley,[33]
S. Rinaldi,[270] J. Rittmeyer,[98] C. Robertson,[229] F. Robinet,[41] M. Robinson,[2] A. Rocchi,[22] L. Rolland,[31]
J. G. Rollins,[11] A. E. Romano,[295] R. Romano,[3,4] A. Romero,[31] I. M. Romero-Shaw,[224] J. H. Romie,[64]
S. Ronchini,[7] T. J. Roocke,[116] L. Rosa,[4,32] T. J. Rosauer,[211] C. A. Rose,[57] D. Rosińska,[125] M. P. Ross,[53]
M. Rossello-Sastre,[99] S. Rowan,[87] S. K. Roy,[191,192] S. Roy,[15] D. Rozza,[127,128] P. Ruggi,[63] N. Ruhama,[239]
E. Ruiz Morales,[296,208] K. Ruiz-Rocha,[144] S. Sachdev,[57] T. Sadecki,[2] P. Saffarieh,[37,108] S. Safi-Harb,[169]
M. R. Sah,[13] S. Saha,[142] T. Sainrat,[65] S. Sajith Menon,[215,39,38] K. Sakai,[297] Y. Sakai,[272]

M. Sakellariadou,[68] S. Sakon,[7] O. S. Salafia,[159,128,127] F. Salces-Carcoba,[11] L. Salconi,[63] M. Saleem,[148]
F. Salemi,[39,38] M. Sallé,[37] S. U. Salunkhe,[80] S. Salvador,[174,173] A. Salvarese,[148] A. Samajdar,[72,37]
A. Sanchez,[2] E. J. Sanchez,[11] L. E. Sanchez,[11] N. Sanchis-Gual,[138] J. R. Sanders,[182] E. M. Sänger,[1]
F. Santoliquido,[44,45] F. Sarandrea,[28] T. R. Saravanan,[80] N. Sarin,[6] P. Sarkar,[8,9] A. Sasli,[251] P. Sassi,[51,77]
B. Sassolas,[176] R. Sato,[227] S. Sato,[152] Yukino Sato,[152] Yu Sato,[152] O. Sauter,[46] R. L. Savage,[2] T. Sawada,[50]
H. L. Sawant,[80] S. Sayah,[176] V. Scacco,[21,22] D. Schaetzl,[11] M. Scheel,[149] A. Schiebelbein,[190] M. G. Schiworski,[79]
P. Schmidt,[119] S. Schmidt,[72] R. Schnabel,[98] M. Schneewind,[8,9] R. M. S. Schofield,[78] K. Schouteden,[110]
B. W. Schulte,[8,9] B. F. Schutz,[33,8,9] E. Schwartz,[298] M. Scialpi,[299] J. Scott,[87] S. M. Scott,[34]
R. M. Sedas,[64] T. C. Seetharamu,[87] M. Seglar-Arroyo,[43] Y. Sekiguchi,[300] D. Sellers,[64] N. Sembo,[205]
A. S. Sengupta,[301] E. G. Seo,[87] J. W. Seo,[110] V. Sequino,[32,4] M. Serra,[38] A. Sevrin,[188] T. Shaffer,[2]
U. S. Shah,[57] M. A. Shaikh,[261] L. Shao,[302] A. K. Sharma,[99] Preeti Sharma,[12] Prianka Sharma,[104]
Ritwik Sharma,[18] S. Sharma Chaudhary,[106] P. Shawhan,[126] N. S. Shcheblanov,[303,263] E. Sheridan,[144]
Z.-H. Shi,[142] M. Shikauchi,[42] R. Shimomura,[304] H. Shinkai,[304] S. Shirke,[80] D. H. Shoemaker,[35]
D. M. Shoemaker,[148] R. W. Short,[2] S. ShyamSundar,[104] A. Sider,[158] H. Siegel,[191,192] N. Siemonsen,[305]
D. Sigg,[2] L. Silenzi,[36,37] L. Silvestri,[39,170] M. Simmonds,[116] L. P. Singer,[306] Amitesh Singh,[216] Anika Singh,[11]
D. Singh,[207] N. Singh,[99] S. Singh,[217,60] A. M. Sintes,[99] V. Sipala,[171,156] V. Skliris,[33] B. J. J. Slagmolen,[34]
D. A. Slater,[200] T. J. Slaven-Blair,[73] J. Smetana,[119] J. R. Smith,[54] L. Smith,[87,185,48] R. J. E. Smith,[6]
W. J. Smith,[144] S. Soares de Albuquerque Filho,[61] M. Soares-Santos,[189] K. Somiya,[217] I. Song,[142]
S. Soni,[35] V. Sordini,[56] F. Sorrentino,[29] H. Sotani,[307] F. Spada,[81] V. Spagnuolo,[37] A. P. Spencer,[87]
P. Spinicelli,[63] A. K. Srivastava,[94] F. Stachurski,[87] C. J. Stark,[123] D. A. Steer,[308] N. Steinle,[169]
J. Steinlechner,[36,37] S. Steinlechner,[36,37] N. Stergioulas,[251] P. Stevens,[41] M. StPierre,[164] M. D. Strong,[12]
A. Strunk,[2] A. L. Stuver,[103,*] M. Suchenek,[96] S. Sudhagar,[96] Y. Sudo,[230] N. Sueltmann,[98] L. Suleiman,[54]
K. D. Sullivan,[12] J. Sun,[241] L. Sun,[34] S. Sunil,[94] J. Suresh,[114] B. J. Sutton,[68] P. J. Sutton,[33] K. Suzuki,[217]
M. Suzuki,[204] B. L. Swinkels,[37] A. Syx,[117] M. J. Szczepańczyk,[309] P. Szewczyk,[125] M. Tacca,[37]
H. Tagoshi,[204] S. C. Tait,[11] K. Takada,[204] H. Takahashi,[272] R. Takahashi,[25] A. Takamori,[42] S. Takano,[310]
H. Takeda,[311,312] K. Takeshita,[217] I. Takimoto Schmiegelow,[44,45] M. Takou-Ayaoh,[79] C. Talbot,[130] M. Tamaki,[204]
N. Tamanini,[101] D. Tanabe,[141] K. Tanaka,[50] S. J. Tanaka,[230] S. Tanioka,[33] D. B. Tanner,[46] W. Tanner,[8,9]
L. Tao,[211] R. D. Tapia,[7] E. N. Tapia San Martín,[37] C. Taranto,[21,22] A. Taruya,[313] J. D. Tasson,[153]
J. G. Tau,[111] D. Tellez,[54] R. Tenorio,[99] H. Themann,[181] A. Theodoropoulos,[138] M. P. Thirugnanasambandam,[80]
L. M. Thomas,[11] M. Thomas,[64] P. Thomas,[2] J. E. Thompson,[210] S. R. Thondapu,[104] K. A. Thorne,[64]
E. Thrane,[6] J. Tissino,[44,45] A. Tiwari,[80] Pawan Tiwari,[44] Praveer Tiwari,[195] S. Tiwari,[189] V. Tiwari,[119]
M. R. Todd,[79] M. Toffano,[92] A. M. Toivonen,[18] K. Toland,[87] A. E. Tolley,[74] T. Tomaru,[25] V. Tommasini,[11]
T. Tomura,[50] H. Tong,[6] C. Tong-Yu,[141] A. Torres-Forné,[138,139] C. I. Torrie,[11] I. Tosta e Melo,[314]
E. Tournefier,[31] M. Trad Nery,[114] K. Tran,[123] A. Trapananti,[52,51] R. Travaglini,[168] F. Travasso,[52,51]
G. Traylor,[64] M. Trevor,[126] M. C. Tringali,[63] A. Tripathee,[91] G. Troian,[185,48] A. Trovato,[185,48] L. Trozzo,[4]
R. J. Trudeau,[11] T. Tsang,[33] S. Tsuchida,[315] L. Tsukada,[213] K. Turbang,[188,23] M. Turconi,[114]
C. Turski,[95] H. Ubach,[83,84] N. Uchikata,[204] T. Uchiyama,[50] R. P. Udall,[11] T. Uehara,[316] K. Ueno,[42]
V. Undheim,[277] L. E. Uronen,[219] T. Ushiba,[50] M. Vacatello,[81,82] H. Vahlbruch,[8,9] N. Vaidya,[11]
G. Vajente,[11] A. Vajpeyi,[6] J. Valencia,[99] M. Valentini,[108,37] S. A. Vallejo-Peña,[295] S. Vallero,[28] V. Valsan,[10]
M. van Dael,[37,317] E. Van den Bossche,[188] J. F. J. van den Brand,[36,108,37] C. Van Den Broeck,[72,37]
M. van der Sluys,[37,72] A. Van de Walle,[41] J. van Dongen,[37,108] K. Vandra,[103] M. VanDyke,[120]
H. van Haevermaet,[23] J. V. van Heijningen,[37,108] P. Van Hove,[65] J. Vanier,[259] M. VanKeuren,[105] J. Vanosky,[2]
N. van Remortel,[23] M. Vardaro,[36,37] A. F. Vargas,[124] V. Varma,[133] A. N. Vazquez,[90] A. Vecchio,[119]
G. Vedovato,[93] J. Veitch,[87] P. J. Veitch,[116] S. Venikoudis,[15] R. C. Venterea,[18] P. Verdier,[56] M. Vereecken,[15]
D. Verkindt,[31] B. Verma,[133] Y. Verma,[104] S. M. Vermeulen,[11] F. Vetrano,[61] A. Veutro,[38,39] A. Viceré,[61,62]
S. Vidyant,[79] A. D. Viets,[89] A. Vijaykumar,[190] A. Vilkha,[111] N. Villanueva Espinosa,[138] V. Villa-Ortega,[178]
E. T. Vincent,[57] J.-Y. Vinet,[114] S. Viret,[56] S. Vitale,[35] H. Vocca,[77,51] D. Voigt,[98] E. R. G. von Reis,[2]
J. S. A. von Wrangel,[8,9] W. E. Vossius,[231] L. Vujeva,[140] S. P. Vyatchanin,[109] J. Wack,[11] L. E. Wade,[105]
M. Wade,[105] K. J. Wagner,[111] L. Wallace,[11] E. J. Wang,[90] H. Wang,[217] J. Z. Wang,[91] W. H. Wang,[165]
Y. F. Wang,[1] G. Waratkar,[195] J. Warner,[2] M. Was,[31] T. Washimi,[25] N. Y. Washington,[11] D. Watarai,[42]
B. Weaver,[2] S. A. Webster,[87] N. L. Weickhardt,[98] M. Weinert,[8,9] A. J. Weinstein,[11] R. Weiss,[35,†] L. Wen,[73]
K. Wette,[34] J. T. Whelan,[111] B. F. Whiting,[46] C. Whittle,[11] E. G. Wickens,[74] D. Wilken,[8,9,9]
A. T. Wilkin,[211] B. M. Williams,[120] D. Williams,[87] M. J. Williams,[74] N. S. Williams,[1] J. L. Willis,[11]

B. Willke,[9,8,9] M. Wils,[110] L. Wilson,[105] C. W. Winborn,[106] J. Winterflood,[73] C. C. Wipf,[11] G. Woan,[87] J. Woehler,[36,37] N. E. Wolfe,[35] H. T. Wong,[141] I. C. F. Wong,[219,110] K. Wong,[190] T. Wouters,[72,37] J. L. Wright,[2] M. Wright,[87,72] B. Wu,[79] C. Wu,[142] D. S. Wu,[8,9] H. Wu,[142] K. Wu,[120] Q. Wu,[53] Y. Wu,[97] Z. Wu,[101] E. Wuchner,[54] D. M. Wysocki,[10] V. A. Xu,[207] Y. Xu,[99] N. Yadav,[28] H. Yamamoto,[11] K. Yamamoto,[152] T. S. Yamamoto,[42] T. Yamamoto,[50] R. Yamazaki,[230] T. Yan,[119] K. Z. Yang,[18] Y. Yang,[146] Z. Yarbrough,[12] J. Yebana,[99] S.-W. Yeh,[142] A. B. Yelikar,[144] X. Yin,[35] J. Yokoyama,[318,42] T. Yokozawa,[50] S. Yuan,[73] H. Yuzurihara,[50] M. Zanolin,[66] M. Zeeshan,[111] T. Zelenova,[63] J.-P. Zendri,[93] M. Zeoli,[15] M. Zerrad,[40] M. Zevin,[97] L. Zhang,[11] N. Zhang,[57] R. Zhang,[150] T. Zhang,[119] C. Zhao,[73] Yue Zhao,[162] Yuhang Zhao,[20] Z.-C. Zhao,[319] Y. Zheng,[106] H. Zhong,[18] H. Zhou,[79] H. O. Zhu,[73] Z.-H. Zhu,[319,320] A. B. Zimmerman,[148] L. Zimmermann,[56] M. E. Zucker,[35,11] and J. Zweizig[11]

(The LIGO Scientific Collaboration, the Virgo Collaboration, and the KAGRA Collaboration)

[1] *Max Planck Institute for Gravitational Physics (Albert Einstein Institute), D-14476 Potsdam, Germany*
[2] *LIGO Hanford Observatory, Richland, WA 99352, USA*
[3] *Dipartimento di Farmacia, Università di Salerno, I-84084 Fisciano, Salerno, Italy*
[4] *INFN, Sezione di Napoli, I-80126 Napoli, Italy*
[5] *University of Warwick, Coventry CV4 7AL, United Kingdom*
[6] *OzGrav, School of Physics & Astronomy, Monash University, Clayton 3800, Victoria, Australia*
[7] *The Pennsylvania State University, University Park, PA 16802, USA*
[8] *Max Planck Institute for Gravitational Physics (Albert Einstein Institute), D-30167 Hannover, Germany*
[9] *Leibniz Universität Hannover, D-30167 Hannover, Germany*
[10] *University of Wisconsin-Milwaukee, Milwaukee, WI 53201, USA*
[11] *LIGO Laboratory, California Institute of Technology, Pasadena, CA 91125, USA*
[12] *Louisiana State University, Baton Rouge, LA 70803, USA*
[13] *Tata Institute of Fundamental Research, Mumbai 400005, India*
[14] *Centre de Physique Théorique, Aix-Marseille Université,*
*Campus de Luminy, 163 Av. de Luminy, 13009 Marseille, France*
[15] *Université catholique de Louvain, B-1348 Louvain-la-Neuve, Belgium*
[16] *Queen Mary University of London, London E1 4NS, United Kingdom*
[17] *University of California, Davis, Davis, CA 95616, USA*
[18] *University of Minnesota, Minneapolis, MN 55455, USA*
[19] *Instituto Nacional de Pesquisas Espaciais, 12227-010 São José dos Campos, São Paulo, Brazil*
[20] *Université Paris Cité, CNRS, Astroparticule et Cosmologie, F-75013 Paris, France*
[21] *Università di Roma Tor Vergata, I-00133 Roma, Italy*
[22] *INFN, Sezione di Roma Tor Vergata, I-00133 Roma, Italy*
[23] *Universiteit Antwerpen, 2000 Antwerpen, Belgium*
[24] *International Centre for Theoretical Sciences, Tata Institute of Fundamental Research, Bengaluru 560089, India*
[25] *Gravitational Wave Science Project, National Astronomical Observatory of Japan,*
*2-21-1 Osawa, Mitaka City, Tokyo 181-8588, Japan*
[26] *Advanced Technology Center, National Astronomical Observatory of Japan,*
*2-21-1 Osawa, Mitaka City, Tokyo 181-8588, Japan*
[27] *Theoretisch-Physikalisches Institut, Friedrich-Schiller-Universität Jena, D-07743 Jena, Germany*
[28] *INFN Sezione di Torino, I-10125 Torino, Italy*
[29] *INFN, Sezione di Genova, I-16146 Genova, Italy*
[30] *Dipartimento di Fisica, Università degli Studi di Genova, I-16146 Genova, Italy*
[31] *Univ. Savoie Mont Blanc, CNRS, Laboratoire d'Annecy de Physique des Particules - IN2P3, F-74000 Annecy, France*
[32] *Università di Napoli "Federico II", I-80126 Napoli, Italy*
[33] *Cardiff University, Cardiff CF24 3AA, United Kingdom*
[34] *OzGrav, Australian National University, Canberra, Australian Capital Territory 0200, Australia*
[35] *LIGO Laboratory, Massachusetts Institute of Technology, Cambridge, MA 02139, USA*
[36] *Maastricht University, 6200 MD Maastricht, Netherlands*
[37] *Nikhef, 1098 XG Amsterdam, Netherlands*
[38] *INFN, Sezione di Roma, I-00185 Roma, Italy*
[39] *Università di Roma "La Sapienza", I-00185 Roma, Italy*
[40] *Aix Marseille Univ, CNRS, Centrale Med, Institut Fresnel, F-13013 Marseille, France*
[41] *Université Paris-Saclay, CNRS/IN2P3, IJCLab, 91405 Orsay, France*
[42] *University of Tokyo, Tokyo, 113-0033, Japan*
[43] *Institut de Física d'Altes Energies (IFAE), The Barcelona Institute of Science and Technology,*
*Campus UAB, E-08193 Bellaterra (Barcelona), Spain*
[44] *Gran Sasso Science Institute (GSSI), I-67100 L'Aquila, Italy*
[45] *INFN, Laboratori Nazionali del Gran Sasso, I-67100 Assergi, Italy*
[46] *University of Florida, Gainesville, FL 32611, USA*

[47]Dipartimento di Scienze Matematiche, Informatiche e Fisiche, Università di Udine, I-33100 Udine, Italy
[48]INFN, Sezione di Trieste, I-34127 Trieste, Italy
[49]Tecnologico de Monterrey, Escuela de Ingeniería y Ciencias, 64849 Monterrey, Nuevo León, Mexico
[50]Institute for Cosmic Ray Research, KAGRA Observatory, The University of Tokyo,
238 Higashi-Mozumi, Kamioka-cho, Hida City, Gifu 506-1205, Japan
[51]INFN, Sezione di Perugia, I-06123 Perugia, Italy
[52]Università di Camerino, I-62032 Camerino, Italy
[53]University of Washington, Seattle, WA 98195, USA
[54]California State University Fullerton, Fullerton, CA 92831, USA
[55]SUPA, University of Strathclyde, Glasgow G1 1XQ, United Kingdom
[56]Université Claude Bernard Lyon 1, CNRS, IP2I Lyon / IN2P3, UMR 5822, F-69622 Villeurbanne, France
[57]Georgia Institute of Technology, Atlanta, GA 30332, USA
[58]Chennai Mathematical Institute, Chennai 603103, India
[59]Royal Holloway, University of London, London TW20 0EX, United Kingdom
[60]Astronomical course, The Graduate University for Advanced Studies (SOKENDAI),
2-21-1 Osawa, Mitaka City, Tokyo 181-8588, Japan
[61]Università degli Studi di Urbino "Carlo Bo", I-61029 Urbino, Italy
[62]INFN, Sezione di Firenze, I-50019 Sesto Fiorentino, Firenze, Italy
[63]European Gravitational Observatory (EGO), I-56021 Cascina, Pisa, Italy
[64]LIGO Livingston Observatory, Livingston, LA 70754, USA
[65]Université de Strasbourg, CNRS, IPHC UMR 7178, F-67000 Strasbourg, France
[66]Embry-Riddle Aeronautical University, Prescott, AZ 86301, USA
[67]Dipartimento di Fisica "E.R. Caianiello", Università di Salerno, I-84084 Fisciano, Salerno, Italy
[68]King's College London, University of London, London WC2R 2LS, United Kingdom
[69]Korea Institute of Science and Technology Information, Daejeon 34141, Republic of Korea
[70]International College, Osaka University, 1-1 Machikaneyama-cho, Toyonaka City, Osaka 560-0043, Japan
[71]Accelerator Laboratory, High Energy Accelerator Research Organization (KEK),
1-1 Oho, Tsukuba City, Ibaraki 305-0801, Japan
[72]Institute for Gravitational and Subatomic Physics (GRASP),
Utrecht University, 3584 CC Utrecht, Netherlands
[73]OzGrav, University of Western Australia, Crawley, Western Australia 6009, Australia
[74]University of Portsmouth, Portsmouth, PO1 3FX, United Kingdom
[75]Università di Trento, Dipartimento di Fisica, I-38123 Povo, Trento, Italy
[76]INFN, Trento Institute for Fundamental Physics and Applications, I-38123 Povo, Trento, Italy
[77]Università di Perugia, I-06123 Perugia, Italy
[78]University of Oregon, Eugene, OR 97403, USA
[79]Syracuse University, Syracuse, NY 13244, USA
[80]Inter-University Centre for Astronomy and Astrophysics, Pune 411007, India
[81]INFN, Sezione di Pisa, I-56127 Pisa, Italy
[82]Università di Pisa, I-56127 Pisa, Italy
[83]Institut de Ciències del Cosmos (ICCUB), Universitat de Barcelona (UB),
c. Martí i Franquès, 1, 08028 Barcelona, Spain
[84]Departament de Física Quàntica i Astrofísica (FQA),
Universitat de Barcelona (UB), c. Martí i Franqués, 1, 08028 Barcelona, Spain
[85]Institut d'Estudis Espacials de Catalunya, c. Gran Capità, 2-4, 08034 Barcelona, Spain
[86]Dipartimento di Medicina, Chirurgia e Odontoiatria "Scuola Medica Salernitana",
Università di Salerno, I-84081 Baronissi, Salerno, Italy
[87]IGR, University of Glasgow, Glasgow G12 8QQ, United Kingdom
[88]HUN-REN Wigner Research Centre for Physics, H-1121 Budapest, Hungary
[89]Concordia University Wisconsin, Mequon, WI 53097, USA
[90]Stanford University, Stanford, CA 94305, USA
[91]University of Michigan, Ann Arbor, MI 48109, USA
[92]Università di Padova, Dipartimento di Fisica e Astronomia, I-35131 Padova, Italy
[93]INFN, Sezione di Padova, I-35131 Padova, Italy
[94]Institute for Plasma Research, Bhat, Gandhinagar 382428, India
[95]Universiteit Gent, B-9000 Gent, Belgium
[96]Nicolaus Copernicus Astronomical Center, Polish Academy of Sciences, 00-716, Warsaw, Poland
[97]Northwestern University, Evanston, IL 60208, USA
[98]Universität Hamburg, D-22761 Hamburg, Germany
[99]IAC3–IEEC, Universitat de les Illes Balears, E-07122 Palma de Mallorca, Spain
[100]Aix-Marseille Université, Université de Toulon, CNRS, CPT, Marseille, France
[101]Laboratoire des 2 Infinis - Toulouse (L2IT-IN2P3), F-31062 Toulouse Cedex 9, France
[102]Università di Siena, Dipartimento di Scienze Fisiche,
della Terra e dell'Ambiente, I-53100 Siena, Italy

[103]*Villanova University, Villanova, PA 19085, USA*
[104]*RRCAT, Indore, Madhya Pradesh 452013, India*
[105]*Kenyon College, Gambier, OH 43022, USA*
[106]*Missouri University of Science and Technology, Rolla, MO 65409, USA*
[107]*Indian Institute of Technology Madras, Chennai 600036, India*
[108]*Department of Physics and Astronomy, Vrije Universiteit Amsterdam, 1081 HV Amsterdam, Netherlands*
[109]*Lomonosov Moscow State University, Moscow 119991, Russia*
[110]*Katholieke Universiteit Leuven, Oude Markt 13, 3000 Leuven, Belgium*
[111]*Rochester Institute of Technology, Rochester, NY 14623, USA*
[112]*Université libre de Bruxelles, 1050 Bruxelles, Belgium*
[113]*Bar-Ilan University, Ramat Gan, 5290002, Israel*
[114]*Université Côte d'Azur, Observatoire de la Côte d'Azur, CNRS, Artemis, F-06304 Nice, France*
[115]*University of British Columbia, Vancouver, BC V6T 1Z4, Canada*
[116]*OzGrav, University of Adelaide, Adelaide, South Australia 5005, Australia*
[117]*Centre national de la recherche scientifique, 75016 Paris, France*
[118]*Univ Rennes, CNRS, Institut FOTON - UMR 6082, F-35000 Rennes, France*
[119]*University of Birmingham, Birmingham B15 2TT, United Kingdom*
[120]*Washington State University, Pullman, WA 99164, USA*
[121]*Cornell University, Ithaca, NY 14850, USA*
[122]*Laboratoire Kastler Brossel, Sorbonne Université, CNRS,*
*ENS-Université PSL, Collège de France, F-75005 Paris, France*
[123]*Christopher Newport University, Newport News, VA 23606, USA*
[124]*OzGrav, University of Melbourne, Parkville, Victoria 3010, Australia*
[125]*Astronomical Observatory Warsaw University, 00-478 Warsaw, Poland*
[126]*University of Maryland, College Park, MD 20742, USA*
[127]*Università degli Studi di Milano-Bicocca, I-20126 Milano, Italy*
[128]*INFN, Sezione di Milano-Bicocca, I-20126 Milano, Italy*
[129]*Université de Lyon, Université Claude Bernard Lyon 1,*
*CNRS, Institut Lumière Matière, F-69622 Villeurbanne, France*
[130]*University of Chicago, Chicago, IL 60637, USA*
[131]*University of Arizona, Tucson, AZ 85721, USA*
[132]*INFN, Sezione di Napoli, Gruppo Collegato di Salerno, I-80126 Napoli, Italy*
[133]*University of Massachusetts Dartmouth, North Dartmouth, MA 02747, USA*
[134]*Niels Bohr Institute, Copenhagen University, 2100 København, Denmark*
[135]*Universidad de Guadalajara, 44430 Guadalajara, Jalisco, Mexico*
[136]*Istituto di Astrofisica e Planetologia Spaziali di Roma, 00133 Roma, Italy*
[137]*Colorado State University, Fort Collins, CO 80523, USA*
[138]*Departamento de Astronomía y Astrofísica, Universitat de València, E-46100 Burjassot, València, Spain*
[139]*Observatori Astronòmic, Universitat de València, E-46980 Paterna, València, Spain*
[140]*Niels Bohr Institute, University of Copenhagen, 2100 Kóbenhavn, Denmark*
[141]*National Central University, Taoyuan City 320317, Taiwan*
[142]*National Tsing Hua University, Hsinchu City 30013, Taiwan*
[143]*OzGrav, Charles Sturt University, Wagga Wagga, New South Wales 2678, Australia*
[144]*Vanderbilt University, Nashville, TN 37235, USA*
[145]*University of Chinese Academy of Sciences / International Centre for Theoretical Physics Asia-Pacific, Bejing 100190, China*
[146]*Department of Electrophysics, National Yang Ming Chiao Tung University, 101 Univ. Street, Hsinchu, Taiwan*
[147]*Kamioka Branch, National Astronomical Observatory of Japan,*
*238 Higashi-Mozumi, Kamioka-cho, Hida City, Gifu 506-1205, Japan*
[148]*University of Texas, Austin, TX 78712, USA*
[149]*CaRT, California Institute of Technology, Pasadena, CA 91125, USA*
[150]*Northeastern University, Boston, MA 02115, USA*
[151]*Dipartimento di Ingegneria Industriale (DIIN),*
*Università di Salerno, I-84084 Fisciano, Salerno, Italy*
[152]*Faculty of Science, University of Toyama, 3190 Gofuku, Toyama City, Toyama 930-8555, Japan*
[153]*Carleton College, Northfield, MN 55057, USA*
[154]*University of Szeged, Dóm tér 9, Szeged 6720, Hungary*
[155]*OzGrav, Swinburne University of Technology, Hawthorn VIC 3122, Australia*
[156]*INFN Cagliari, Physics Department, Università degli Studi di Cagliari, Cagliari 09042, Italy*
[157]*Università degli Studi di Cagliari, Via Università 40, 09124 Cagliari, Italy*
[158]*Université Libre de Bruxelles, Brussels 1050, Belgium*
[159]*INAF, Osservatorio Astronomico di Brera sede di Merate, I-23807 Merate, Lecco, Italy*
[160]*Departamento de Matemáticas, Universitat de València, E-46100 Burjassot, València, Spain*
[161]*Montana State University, Bozeman, MT 59717, USA*
[162]*The University of Utah, Salt Lake City, UT 84112, USA*

[163]Johns Hopkins University, Baltimore, MD 21218, USA
[164]University of Rhode Island, Kingston, RI 02881, USA
[165]The University of Texas Rio Grande Valley, Brownsville, TX 78520, USA
[166]Université de Liège, B-4000 Liège, Belgium
[167]DIFA- Alma Mater Studiorum Università di Bologna, Via Zamboni, 33 - 40126 Bologna, Italy
[168]Istituto Nazionale Di Fisica Nucleare - Sezione di Bologna,
viale Carlo Berti Pichat 6/2 - 40127 Bologna, Italy
[169]University of Manitoba, Winnipeg, MB R3T 2N2, Canada
[170]INFN-CNAF - Bologna, Viale Carlo Berti Pichat, 6/2, 40127 Bologna BO, Italy
[171]Università degli Studi di Sassari, I-07100 Sassari, Italy
[172]INFN, Laboratori Nazionali del Sud, I-95125 Catania, Italy
[173]Université de Normandie, ENSICAEN, UNICAEN,
CNRS/IN2P3, LPC Caen, F-14000 Caen, France
[174]Laboratoire de Physique Corpusculaire Caen, 6 boulevard du maréchal Juin, F-14050 Caen, France
[175]The University of Sheffield, Sheffield S10 2TN, United Kingdom
[176]Université Claude Bernard Lyon 1, CNRS, Laboratoire des Matériaux Avancés (LMA),
IP2I Lyon / IN2P3, UMR 5822, F-69622 Villeurbanne, France
[177]Università di Firenze, Sesto Fiorentino I-50019, Italy
[178]IGFAE, Universidade de Santiago de Compostela, E-15782 Santiago de Compostela, Spain
[179]Dipartimento di Scienze Matematiche, Fisiche e Informatiche, Università di Parma, I-43124 Parma, Italy
[180]INFN, Sezione di Milano Bicocca, Gruppo Collegato di Parma, I-43124 Parma, Italy
[181]California State University, Los Angeles, Los Angeles, CA 90032, USA
[182]Marquette University, Milwaukee, WI 53233, USA
[183]Perimeter Institute, Waterloo, ON N2L 2Y5, Canada
[184]Corps des Mines, Mines Paris, Université PSL, 60 Bd Saint-Michel, 75272 Paris, France
[185]Dipartimento di Fisica, Università di Trieste, I-34127 Trieste, Italy
[186]Université Côte d'Azur, Observatoire de la Côte d'Azur, CNRS, Lagrange, F-06304 Nice, France
[187]National Center for Nuclear Research, 05-400 Świerk-Otwock, Poland
[188]Vrije Universiteit Brussel, 1050 Brussel, Belgium
[189]University of Zurich, Winterthurerstrasse 190, 8057 Zurich, Switzerland
[190]Canadian Institute for Theoretical Astrophysics,
University of Toronto, Toronto, ON M5S 3H8, Canada
[191]Stony Brook University, Stony Brook, NY 11794, USA
[192]Center for Computational Astrophysics, Flatiron Institute, New York, NY 10010, USA
[193]Montclair State University, Montclair, NJ 07043, USA
[194]HUN-REN Institute for Nuclear Research, H-4026 Debrecen, Hungary
[195]Indian Institute of Technology Bombay, Powai, Mumbai 400 076, India
[196]Centro de Física das Universidades do Minho e do Porto,
Universidade do Minho, PT-4710-057 Braga, Portugal
[197]Aix Marseille Univ, CNRS/IN2P3, CPPM, Marseille, France
[198]CNR-SPIN, I-84084 Fisciano, Salerno, Italy
[199]Scuola di Ingegneria, Università della Basilicata, I-85100 Potenza, Italy
[200]Western Washington University, Bellingham, WA 98225, USA
[201]SUPA, University of the West of Scotland, Paisley PA1 2BE, United Kingdom
[202]Barry University, Miami Shores, FL 33168, USA
[203]Eötvös University, Budapest 1117, Hungary
[204]Institute for Cosmic Ray Research, KAGRA Observatory, The University of Tokyo,
5-1-5 Kashiwa-no-Ha, Kashiwa City, Chiba 277-8582, Japan
[205]Department of Physics, Graduate School of Science,
Osaka Metropolitan University, 3-3-138 Sugimoto-cho,
Sumiyoshi-ku, Osaka City, Osaka 558-8585, Japan
[206]University of Sannio at Benevento, I-82100 Benevento,
Italy and INFN, Sezione di Napoli, I-80100 Napoli, Italy
[207]University of California, Berkeley, CA 94720, USA
[208]Instituto de Fisica Teorica UAM-CSIC, Universidad Autonoma de Madrid, 28049 Madrid, Spain
[209]Laboratoire d'Acoustique de l'Université du Mans, UMR CNRS 6613, F-72085 Le Mans, France
[210]University of Southampton, Southampton SO17 1BJ, United Kingdom
[211]University of California, Riverside, Riverside, CA 92521, USA
[212]Dipartimento di Ingegneria Industriale, Elettronica e Meccanica,
Università degli Studi Roma Tre, I-00146 Roma, Italy
[213]University of Nevada, Las Vegas, Las Vegas, NV 89154, USA
[214]University of Nottingham NG7 2RD, UK
[215]Ariel University, Ramat HaGolan St 65, Ari'el, Israel
[216]The University of Mississippi, University, MS 38677, USA

[217]*Graduate School of Science, Institute of Science Tokyo,*
*2-12-1 Ookayama, Meguro-ku, Tokyo 152-8551, Japan*
[218]*Institute of Physics, Academia Sinica, 128 Sec. 2, Academia Rd., Nankang, Taipei 11529, Taiwan*
[219]*The Chinese University of Hong Kong, Shatin, NT, Hong Kong*
[220]*American University, Washington, DC 20016, USA*
[221]*Dipartimento di Fisica, Università degli studi di Milano, Via Celoria 16, I-20133, Milano, Italy*
[222]*INFN, sezione di Milano, Via Celoria 16, I-20133, Milano, Italy*
[223]*Department of Applied Physics, Fukuoka University,*
*8-19-1 Nanakuma, Jonan, Fukuoka City, Fukuoka 814-0180, Japan*
[224]*University of Cambridge, Cambridge CB2 1TN, United Kingdom*
[225]*University of Lancaster, Lancaster LA1 4YW, United Kingdom*
[226]*College of Industrial Technology, Nihon University,*
*1-2-1 Izumi, Narashino City, Chiba 275-8575, Japan*
[227]*Faculty of Engineering, Niigata University, 8050 Ikarashi-2-no-cho,*
*Nishi-ku, Niigata City, Niigata 950-2181, Japan*
[228]*Department of Physics, Tamkang University, No. 151,*
*Yingzhuan Rd., Danshui Dist., New Taipei City 25137, Taiwan*
[229]*Rutherford Appleton Laboratory, Didcot OX11 0DE, United Kingdom*
[230]*Department of Physical Sciences, Aoyama Gakuin University,*
*5-10-1 Fuchinobe, Sagamihara City, Kanagawa 252-5258, Japan*
[231]*Helmut Schmidt University, D-22043 Hamburg, Germany*
[232]*Nambu Yoichiro Institute of Theoretical and Experimental Physics (NITEP),*
*Osaka Metropolitan University, 3-3-138 Sugimoto-cho,*
*Sumiyoshi-ku, Osaka City, Osaka 558-8585, Japan*
[233]*Directorate of Construction, Services & Estate Management, Mumbai 400094, India*
[234]*Observatoire Astronomique de Strasbourg, 11 Rue de l'Université, 67000 Strasbourg, France*
[235]*Faculty of Physics, University of Białystok, 15-245 Białystok, Poland*
[236]*National Astronomical Observatories, Chinese Academic of Sciences,*
*20A Datun Road, Chaoyang District, Beijing, China*
[237]*School of Astronomy and Space Science, University of Chinese Academy of Sciences,*
*20A Datun Road, Chaoyang District, Beijing, China*
[238]*Sungkyunkwan University, Seoul 03063, Republic of Korea*
[239]*Department of Physics, Ulsan National Institute of Science and Technology (UNIST),*
*50 UNIST-gil, Ulju-gun, Ulsan 44919, Republic of Korea*
[240]*Institute for Cosmic Ray Research, The University of Tokyo,*
*5-1-5 Kashiwa-no-Ha, Kashiwa City, Chiba 277-8582, Japan*
[241]*Chung-Ang University, Seoul 06974, Republic of Korea*
[242]*University of Washington Bothell, Bothell, WA 98011, USA*
[243]*Laboratoire de Physique et de Chimie de l'Environnement,*
*Université Joseph KI-ZERBO, 9GH2+3V5, Ouagadougou, Burkina Faso*
[244]*Ewha Womans University, Seoul 03760, Republic of Korea*
[245]*National Institute for Mathematical Sciences, Daejeon 34047, Republic of Korea*
[246]*Korea Astronomy and Space Science Institute, Daejeon 34055, Republic of Korea*
[247]*Department of Astronomy and Space Science, Chungnam National University,*
*9 Daehak-ro, Yuseong-gu, Daejeon 34134, Republic of Korea*
[248]*Institute of Particle and Nuclear Studies (IPNS),*
*High Energy Accelerator Research Organization (KEK),*
*1-1 Oho, Tsukuba City, Ibaraki 305-0801, Japan*
[249]*Division of Science, National Astronomical Observatory of Japan,*
*2-21-1 Osawa, Mitaka City, Tokyo 181-8588, Japan*
[250]*Nagoya University, Nagoya, 464-8601, Japan*
[251]*Department of Physics, Aristotle University of Thessaloniki, 54124 Thessaloniki, Greece*
[252]*Bard College, Annandale-On-Hudson, NY 12504, USA*
[253]*Technical University of Braunschweig, D-38106 Braunschweig, Germany*
[254]*Institute of Mathematics, Polish Academy of Sciences, 00656 Warsaw, Poland*
[255]*Astronomical Observatory, Jagiellonian University, 31-007 Cracow, Poland*
[256]*Department of Physics and Astronomy, University of Padova, Via Marzolo, 8-35151 Padova, Italy*
[257]*Sezione di Padova, Istituto Nazionale di Fisica Nucleare (INFN), Via Marzolo, 8-35131 Padova, Italy*
[258]*Department of Physics, Nagoya University, ES building,*
*Furocho, Chikusa-ku, Nagoya, Aichi 464-8602, Japan*
[259]*Université de Montréal/Polytechnique, Montreal, Quebec H3T 1J4, Canada*
[260]*Indian Institute of Science Education and Research,*
*Kolkata, Mohanpur, West Bengal 741252, India*
[261]*Seoul National University, Seoul 08826, Republic of Korea*

[262]*Department of Computer Simulation, Inje University,*
*197 Inje-ro, Gimhae, Gyeongsangnam-do 50834, Republic of Korea*
[263]*NAVIER, École des Ponts, Univ Gustave Eiffel, CNRS, Marne-la-Vallée, France*
[264]*Gravitational Wave Science Project, National Astronomical Observatory of Japan (NAOJ), Mitaka City, Tokyo 181-8588, Japan*
[265]*Department of Physics, National Cheng Kung University,*
*No.1, University Road, Tainan City 701, Taiwan*
[266]*St. Thomas University, Miami Gardens, FL 33054, USA*
[267]*Scuola Normale Superiore, I-56126 Pisa, Italy*
[268]*Institució Catalana de Recerca i Estudis Avançats, E-08010 Barcelona, Spain*
[269]*Institut de Física d'Altes Energies, E-08193 Barcelona, Spain*
[270]*Institut fuer Theoretische Astrophysik, Zentrum fuer Astronomie Heidelberg,*
*Universitaet Heidelberg, Albert Ueberle Str. 2, 69120 Heidelberg, Germany*
[271]*Institucio Catalana de Recerca i Estudis Avançats (ICREA),*
*Passeig de Lluís Companys, 23, 08010 Barcelona, Spain*
[272]*Research Center for Space Science, Advanced Research Laboratories, Tokyo City University,*
*3-3-1 Ushikubo-Nishi, Tsuzuki-Ku, Yokohama, Kanagawa 224-8551, Japan*
[273]*Tsinghua University, Beijing 100084, China*
[274]*Institut des Hautes Etudes Scientifiques, F-91440 Bures-sur-Yvette, France*
[275]*Faculty of Law, Ryukoku University, 67 Fukakusa Tsukamoto-cho,*
*Fushimi-ku, Kyoto City, Kyoto 612-8577, Japan*
[276]*Phenikaa Institute for Advanced Study (PIAS),*
*Phenikaa University, Yen Nghia, Ha Dong, Hanoi, Vietnam*
[277]*University of Stavanger, 4021 Stavanger, Norway*
[278]*Physics Program, Graduate School of Advanced Science and Engineering,*
*Hiroshima University, 1-3-1 Kagamiyama, Higashihiroshima City, Hiroshima 739-8526, Japan*
[279]*GRAPPA, Anton Pannekoek Institute for Astronomy and Institute for High-Energy Physics,*
*University of Amsterdam, 1098 XH Amsterdam, Netherlands*
[280]*University College London, London WC1E 6BT, United Kingdom*
[281]*Observatoire de Paris, 75014 Paris, France*
[282]*Laboratoire Univers et Théories, Observatoire de Paris, 92190 Meudon, France*
[283]*Graduate School of Science and Technology, Niigata University,*
*8050 Ikarashi-2-no-cho, Nishi-ku, Niigata City, Niigata 950-2181, Japan*
[284]*University of Maryland, Baltimore County, Baltimore, MD 21250, USA*
[285]*CSIR-Central Glass and Ceramic Research Institute, Kolkata, West Bengal 700032, India*
[286]*Consiglio Nazionale delle Ricerche - Istituto dei Sistemi Complessi, I-00185 Roma, Italy*
[287]*Department of Astronomy, Yonsei University,*
*50 Yonsei-Ro, Seodaemun-Gu, Seoul 03722, Republic of Korea*
[288]*Department of Physics, University of Guadalajara, Av. Revolucion 1500,*
*Colonia Olimpica C.P. 44430, Guadalajara, Jalisco, Mexico*
[289]*Hobart and William Smith Colleges, Geneva, NY 14456, USA*
[290]*INAF, Osservatorio Astronomico di Padova, I-35122 Padova, Italy*
[291]*Dipartimento di Ingegneria, Università del Sannio, I-82100 Benevento, Italy*
[292]*Museo Storico della Fisica e Centro Studi e Ricerche "Enrico Fermi", I-00184 Roma, Italy*
[293]*Kennesaw State University, Kennesaw, GA 30144, USA*
[294]*Subatech, CNRS/IN2P3 - IMT Atlantique - Nantes Université,*
*4 rue Alfred Kastler BP 20722 44307 Nantes CÉDEX 03, France*
[295]*Universidad de Antioquia, Medellín, Colombia*
[296]*Departamento de Física - ETSIDI, Universidad Politécnica de Madrid, 28012 Madrid, Spain*
[297]*Department of Electronic Control Engineering,*
*National Institute of Technology, Nagaoka College,*
*888 Nishikatakai, Nagaoka City, Niigata 940-8532, Japan*
[298]*Trinity College, Hartford, CT 06106, USA*
[299]*Dipartimento di Fisica e Scienze della Terra,*
*Università Degli Studi di Ferrara, Via Saragat, 1, 44121 Ferrara FE, Italy*
[300]*Faculty of Science, Toho University, 2-2-1 Miyama, Funabashi City, Chiba 274-8510, Japan*
[301]*Indian Institute of Technology, Palaj, Gandhinagar, Gujarat 382355, India*
[302]*Kavli Institute for Astronomy and Astrophysics, Peking University,*
*Yiheyuan Road 5, Haidian District, Beijing 100871, China*
[303]*Laboratoire MSME, Cité Descartes, 5 Boulevard Descartes,*
*Champs-sur-Marne, 77454 Marne-la-Vallée Cedex 2, France*
[304]*Faculty of Information Science and Technology, Osaka Institute of Technology,*
*1-79-1 Kitayama, Hirakata City, Osaka 573-0196, Japan*
[305]*Princeton University, Princeton, NJ 08544, USA*
[306]*NASA Goddard Space Flight Center, Greenbelt, MD 20771, USA*

[307] *Faculty of Science and Technology, Kochi University,*
*2-5-1 Akebono-cho, Kochi-shi, Kochi 780-8520, Japan*
[308] *Laboratoire de Physique de l'École Normale Supérieure, ENS, (CNRS,*
*Université PSL, Sorbonne Université, Université Paris Cité), F-75005 Paris, France*
[309] *Faculty of Physics, University of Warsaw, Ludwika Pasteura 5, 02-093 Warszawa, Poland*
[310] *Laser Interferometry and Gravitational Wave Astronomy,*
*Max Planck Institute for Gravitational Physics, Callinstrasse 38, 30167 Hannover, Germany*
[311] *The Hakubi Center for Advanced Research, Kyoto University,*
*Yoshida-honmachi, Sakyou-ku, Kyoto City, Kyoto 606-8501, Japan*
[312] *Department of Physics, Kyoto University, Kita-Shirakawa Oiwake-cho, Sakyou-ku, Kyoto City, Kyoto 606-8502, Japan*
[313] *Yukawa Institute for Theoretical Physics (YITP), Kyoto University,*
*Kita-Shirakawa Oiwake-cho, Sakyou-ku, Kyoto City, Kyoto 606-8502, Japan*
[314] *University of Catania, Department of Physics and Astronomy, Via S. Sofia, 64, 95123 Catania CT, Italy*
[315] *National Institute of Technology, Fukui College, Geshi-cho, Sabae-shi, Fukui 916-8507, Japan*
[316] *Department of Communications Engineering, National Defense Academy of Japan,*
*1-10-20 Hashirimizu, Yokosuka City, Kanagawa 239-8686, Japan*
[317] *Eindhoven University of Technology, 5600 MB Eindhoven, Netherlands*
[318] *Kavli Institute for the Physics and Mathematics of the Universe (Kavli IPMU), WPI,*
*The University of Tokyo, 5-1-5 Kashiwa-no-Ha, Kashiwa City, Chiba 277-8583, Japan*
[319] *Department of Astronomy, Beijing Normal University,*
*Xinjiekouwai Street 19, Haidian District, Beijing 100875, China*
[320] *School of Physics and Technology, Wuhan University,*
*Bayi Road 299, Wuchang District, Wuhan, Hubei, 430072, China*

We present the first directed searches for long-transient and continuous gravitational waves from ultralight vector boson clouds around known black holes (BHs). We use LIGO data from the first part of the fourth LIGO–Virgo–KAGRA observing run. The searches target two distinct types of BHs and use two new semicoherent methods: hidden Markov model (HMM) tracking for the remnant BHs of the mergers GW230814_230901 and GW231123_135430 (referred to as GW230814 and GW231123 in this study), and a dedicated method using the Band Sampled Data (BSD) framework for the galactic BH in the Cygnus X-1 binary system. Without finding evidence of a signal from vector bosons in the data, we estimate the mass range that can be constrained. For the HMM searches targeting the remnants from GW231123 and GW230814, we disfavor vector boson masses in the ranges $[0.94, 1.08]$ and $[2.75, 3.28] \times 10^{-13}$ eV, respectively, at 30% confidence, assuming a 1% false alarm probability. Although these searches are only marginally sensitive to signals from merger remnants at relatively large distances, future observations are expected to yield more stringent constraints with high confidence. For the BSD search targeting the BH in Cygnus X-1, we exclude vector boson masses in the range $[0.85, 1.59] \times 10^{-13}$ eV at 95% confidence, assuming an initial BH spin larger than 0.5.

## I. INTRODUCTION

Ultralight bosons are a class of theoretical particles proposed in certain extensions of the Standard Model, and their discovery could address numerous unresolved questions in particle physics and cosmology (e.g., the nature of dark matter [1–4] or the strong charge-parity-problem [5–7]). Theories predict different subclasses of ultralight bosons based on spin, including scalar (spin-0) [5–9], vector (spin-1) [10–16], and tensor (spin-2) [17–22] fields. Assuming only gravitational coupling, the superradiance mechanism provides a means by which ultralight bosons may form bound states around rotating black holes (BHs) and grow into macroscopic clouds, producing quasi-monochromatic, long-duration gravitational wave (GW) signals that may be observable by ground-based detectors [23–40].

Ultralight vector bosons with mass $m_V$ can extract rotational energy from a BH through the superradiance mechanism if the following condition is satisfied:

$$0 < \omega_V < m\Omega_H, \tag{1}$$

where $\omega_V \approx m_V c^2/\hbar$ is the angular frequency of the boson field, $m$ is the azimuthal quantum number, and $\Omega_H$ is the angular frequency of the BH's outer horizon. Bound states can therefore grow exponentially in time with an instability growth rate that is maximized when the boson's Compton wavelength $\lambda$ is comparable to the BH's horizon radius $r_g$. For a superradiantly unstable state, the instability extracts energy and angular momentum fluxes from the BH at the horizon into the bosonic field, with the change in mass directly related to the change in angular momentum. If we assume the primary interaction of the ultralight bosons is gravitational, this results in compound field amplification and the growth of a macroscopic cloud that may extract as much as $\sim 10\%$ of the BH's initial mass [23, 37, 41–48].

---

[*] Deceased, September 2024.
[†] Deceased, August 2025.

This exchange of energy and angular momentum continues until Eq. (1) is saturated ($\omega_V = m\Omega_H$), or in other words, until the BH has been spun down so much that superradiance can no longer occur. At this point, the cloud begins to deplete through GW emission, which occurs at roughly twice the boson cloud oscillation frequency, with a small positive frequency drift as the magnitude of the bosons' binding energy to the BH decreases [30, 37–39, 49–52]. For stellar and intermediate-mass BHs and bosons with masses within the range $\sim 10^{-14}$–$10^{-11}$ eV [26, 29], this emission frequency falls in the sensitive band of ground-based GW detectors. Thus, current and future ground-based GW detector networks [53–59] offer a unique way to search for these ultralight bosons. If no detection is made, we are able to place constraints on the existence of ultralight bosons within the above mass range.

Many observational studies have already been designed and implemented to search for ultralight scalar bosons, and, in the absence of a detection, constrain their existence. Although a handful of studies have derived constraints on vector bosons as well, the vector signal morphology has only recently been accurately modeled via numerical calculations in both the relativistic and non-relativistic regimes,[1] enabling more accurate predictions of the signal morphology and more robust constraints on the boson mass [39]. Constraints are placed on the existence of ultralight scalar [26, 29, 32, 60–62] and vector [30, 32, 62, 63] particles using BH spin measurements. In some cases, however, these constraints are limited by systematic uncertainties in the inferred BH spins and masses, which depend on modelling assumptions and observational systematics [64–66]. Searches for continuous gravitational waves (CWs) that target either the galactic center or the entire sky are used to constrain scalars and, based on assumptions about the BH population (e.g., mass distribution, spins, and ages) and their impact on the formation and evolution of boson clouds, they disfavor the scalar boson mass range of $\sim 10^{-13}$–$10^{-12}$ eV [67–70]; Ref. [71] also briefly considered vector boson condensates in the near-zero frequency-derivative regime, estimating the distance reach for vector signals in the mass range of $\sim 10^{-14}$–$10^{-13}$ eV around BHs with a fixed spin. Using the null results from searches for a stochastic GW background generated by a population of BHs with scalar [72, 73] and vector [74] clouds, boson masses $\sim 10^{-13}$ eV have been disfavored for both scalars and vectors, based on assumptions regarding the BH population and spin distributions. A directed search targeting the BH in the X-ray binary Cygnus X-1 excludes scalars in the mass range of $\sim [0.6, 1] \times 10^{-12}$ eV, with the constraint depending on the assumed BH age, which sets the timescale for boson cloud decay [75, 76]. Although the results from some of these studies overlap with the parameter space of interest in this paper, their interpretations rely on several assumptions and carry certain caveats, including uncertainties in BH population and spin distributions, as well as BH evolution history and estimated ages (see discussion above). As a result, we cannot yet rule out the possibility that an ultralight boson exists within the disfavored mass ranges listed above.

In addition to indirect searches, ground-based interferometers are used as particle detectors for the direct detection of ultralight scalars in Refs. [77–79] and vectors in Refs. [80, 81]. Looking to the future, the existence of a scalar cloud could impact the inspiral of binary BHs, and this may soon be detectable for certain boson masses and field strengths [33, 82, 83].

In this study, we present the results from the first directed searches for GW signals from ultralight vector boson clouds (VBCs) around selected known BHs, performed using data from the first part of the fourth observing run (O4a) of the LIGO Scientific Collaboration, Virgo Collaboration, and KAGRA Collaboration (LVK). We use two semicoherent methods to target vector boson signals produced by two different categories of astrophysical sources: i) using methods outlined in Refs. [84, 85] based on a hidden Markov model (HMM), we undertake the first ever directed searches for GWs from VBCs around compact binary merger remnant BHs [86–88], and ii) using a new method based on the so-called Band Sampled Data (BSD) framework [89], we search for GWs from a VBC around the BH in the known binary system Cygnus X-1. Each method is tailored to track signals from a different type of source; while merger remnants are isolated and are expected to emit signals with rapidly evolving frequencies, Cygnus X-1 is a binary system with a BH that would emit a nearly monochromatic signal and has uncertain orbital parameters that must be accounted for. For a more in-depth discussion of these sources and their differences, see Sec. II C.

One benefit of targeting known BHs—whether they are remnants from previous GW observations or identified via X-ray emissions—is that more robust constraints can be derived. In contrast to the broader searches mentioned above, which rely on assumptions about the underlying BH population, directed searches benefit from more complete information about the target BHs. In particular, uncertainties in the BH age and spin—which can strongly influence the resulting constraints—are reduced or eliminated when the source is well-characterized. For young merger remnants, very few hypotheses are needed on the history and evolution of the BHs since their formation. On the other hand, targeting a galactic BH like Cygnus X-1 is beneficial due to its proximity [90]. In addition, because the system is much older [91], any signal observable during O4a must correspond to an emission process that occurs over much longer timescales and produces a more slowly evolving signal (i.e., like a traditional CW), and

---

[1] In the relativistic regime, the BH and the superradiant cloud are approximately the same size, whereas in the non-relativistic regime, the cloud is much larger than the BH.

hence the search can be run across the full O4a dataset.[2]

The organization of the paper is as follows. In Sec. II, we identify the target BHs and describe the common evolution features of the expected GW signals, along with target-specific parameters relevant to the searches. In Sec. III, we outline the two search methods used in this study, each optimized for different signal durations. Sec. IV details the search configurations and setup for each method, with distinctions between merger remnants and persistent sources highlighted throughout. In Sec. V, we present the search results and explain the candidate follow-up procedures, again addressing each target in turn. Then, in Sec. VI, we estimate the range of vector boson masses that can be disfavored given that no signal is detected. We summarize our findings and conclude in Sec. VII. While the discussion is organized thematically to emphasize the shared methodological framework and signal properties, each source is discussed at every stage of the analysis to maintain clarity and completeness.

## II. TARGET SOURCES

In this section, we give an overview of the BHs targeted by the two search pipelines, as well as their expected GW signal parameters, which can be predicted using a combination of analytic [30, 92–95] and numerical [32, 36–39, 96] methods. We generate the signal parameters using the waveform model `SuperRad`, which models the dynamics, oscillation frequency, and GW emission of ultralight boson clouds with high accuracy [52, 97].

### A. Merger remnant black holes

For the HMM search, we target two binary merger remnant BHs from O4a [88]: the remnants of the GW230814_230901 [98] and GW231123_135430 [99] mergers (henceforth referred to as GW230814 and GW231123, respectively). The estimated median parameters for each remnant are shown in Table I, where $M_i$ and $\chi_i$ are the mass and dimensionless spin of the BH before superradiance has occurred, $D_{\rm L}$ is the luminosity distance, $\iota$ is the inclination angle, and RA and Dec are the right ascension and declination of the BH. The remnants from these two events are chosen in particular because, for each BH, we find that the median estimated luminosity distance is less than the furthest reachable distance (see Fig. 9 in Ref. [84]) for a BH with the same median mass and spin. Note, because we use an earlier version of the parameter estimates (which were the most recent and accurate estimates available at the time of this study), the values shown in Table I vary slightly from those reported in Refs. [88] and [99]. However, these differences are minor and have no noticeable impact on the analyses or conclusions, as the searches are relatively insensitive to small deviations in the parameter estimates.[3]

The parameter estimates used in this study have been generated with the `NRSur7dq4` waveform model [100]. This model has been chosen because it interpolates between numerical relativity data without making additional waveform modeling assumptions, and it typically performs well for signals from higher-mass sources like GW231123 [99]. In standard astrophysical formation scenarios of binary systems, the high spin for the primary constituent BH favored by the analysis of GW231123 [99] is in tension with the existence of a vector boson with mass that would give the loudest signal for the remnant BH [63]. Nonetheless, in general there is value in targeting remnants for a direct and independent search that is not subject to astrophysical uncertainties such as the age of the binary, spin modification through accretion, and systematic uncertainties in waveform inference [63], thereby providing a complementary and more direct probe of boson signals.

### B. Cygnus X-1

In the BSD-based search, we target the BH in the Cygnus X-1 system, with parameters listed in Table I taken from a recent study [90]. Cygnus X-1 is a binary system with an orbital period $P = 5.599829 \pm 0.000016$ days [101]. Several of its orbital parameters are constrained through X-ray observations and are summarized in Table II. In particular, the projected semi-major axis is defined as $a_{\rm p} = a\sin(\iota)/c$, with $a$ the semi-major axis, $\iota$ the inclination angle, and $c$ the speed of light,[4] which represents the time needed for the wave to cross the system along the line of sight. The age of the BH is estimated to be $6.2 \pm 1.8 \times 10^6$ yrs [91].

The signal's frequency varies in time due to the change of the binding energy of the cloud to the BH as it depletes. Thus, the frequency drift happens on the same timescale as the cloud annihilation, $\tau_{\rm GW}$. This timescale also represents the decay of the signal amplitude over time, and a

---

[2] While merger remnants could produce similarly long-lived GW emission if the bosons with appropriate masses exist, the growth time of the corresponding clouds would far exceed the O4a time frame.

[3] For GW230814, the posterior distributions of the BH properties from the preliminary version of the parameter estimation are consistent with those reported in Ref. [88]. For GW231123, the posterior distributions show minor differences compared to those presented in Ref. [99]. In particular, the distribution of $D_L$ in Ref. [99] is more tightly constrained than the preliminary version used in this study; nonetheless, the two distributions remain consistent at the 90% confidence level. Since we adopt the broader $D_L$ distribution, our results can be considered conservative.

[4] Following the considerations described in Ref. [90], we assume that the BH spin axis is aligned with the orbital angular momentum. We therefore do not distinguish between the orbital and BH spin inclination.

Table I. Estimated median parameters for the remnant BHs from the GW230814 and GW231123 mergers and for the galactic BH Cygnus X-1.

| Source | $M_i$ $[M_\odot]$ | $\chi_i$ | $D_\mathrm{L}$ [Mpc] | $\cos\iota$ | RA [rad] | Dec [rad] |
|---|---|---|---|---|---|---|
| Remnant from GW230814 | $58.9^{+1.8}_{-1.8}$[a] | $0.68^{+0.01}_{-0.02}$ | $301^{+171}_{-138}$ | $0.03^{+0.74}_{-0.67}$ | $3.21^{+2.62}_{-2.95}$[b] | $0.04^{+1.02}_{-1.08}$[b] |
| Remnant from GW231123 | $219.8^{+22.6}_{-46.2}$[a] | $0.85^{+0.05}_{-0.18}$ | $2054^{+2960}_{-1280}$ | $0.45^{+0.45}_{-1.23}$ | $3.37^{+1.67}_{-0.59}$[b] | $0.38^{+0.40}_{-0.63}$[b] |
| BH in Cygnus X-1 | $21.2^{+2.2}_{-2.3}$ | 0.95[d] | $0.00222^{+0.00018}_{-0.00017}$ | $0.887^{+0.005}_{-0.006}$ | 5.22883712[c] | 0.61438355[c] |

[a] We use $M_i$ and $\chi_i$ to represent the mass and dimensionless spin of the BH before superradiance occurs, i.e., the final BH mass ($M_f$) and spin ($\chi_f$) used in the compact binary coalescence parameter estimation. The reason we do not use $M_f$ and $\chi_f$ here is to avoid confusion with the final BH mass and spin after superradiance occurs.

[b] See Fig. 1.

[c] At reference epoch MJD 56198.

[d] The spin of Cygnus X-1 is debated in the literature. In our analysis, we treat the final spin of the BH as a free parameter and assume a nominal initial spin of $\chi_i = 0.95$. The impact of the initial spin on the derived constraints is discussed in Sec. VI.

Table II. Orbital parameters for Cygnus X-1.

| Parameter | Symbol | Value | Ref. |
|---|---|---|---|
| Orbital Period [days] | $P$ | 5.599829(16) | [101] |
| Proj. Semi-major Axis [s][a] | $a_\mathrm{p}$ | $36.88^{+4.02}_{-3.65}$ | [90] |
| Eccentricity [-] | $e$ | $0.0188^{+0.0028}_{-0.0026}$ | [90] |
| Arg. of periastron [deg] | $\omega$ | $306.6^{+6.6}_{-6.3}$ | [90] |

[a] We define the projected semi-major axis as the delay $a_\mathrm{p} = a\sin(\iota)/c$, with $a$ the semi-major axis, $\iota$ the inclination angle, and $c$ the speed of light ($a_\mathrm{p}$ is given in units of light-seconds).

detectable signal should therefore evolve over a timescale comparable to the BH's age, $\tau_\mathrm{GW} \lesssim t_\mathrm{age}$. Given the system's age, any detectable signal is therefore expected to exhibit high stability over the observation period, $\mathcal{O}(1\,\mathrm{yr})$, with only small variations in the emission frequency over time. This expectation is supported by simulations using the `SuperRad` waveform model, showing that the signal frequency drift remains within $\mathcal{O}(10^{-12})\ \mathrm{Hz\,s^{-1}}$ across the entire parameter space, which is well below the frequency resolution of the analysis. Consequently, we assume a monochromatic emission for the whole duration of O4a, and we neglect frequency derivatives typically included in standard Taylor expansions (e.g., [102, 103]).

In the literature, several studies report an extreme spin ($\geq 0.95$) for the BH in Cygnus X-1 [104–108]. These results disfavor the existence of a VBC since a significant part of the rotational energy of the BH would have been extracted through superradiance, so such a high spin could not be measured after superradiance took place. However, these measurements are impacted by systematic uncertainties and may depend on the accretion model. This is reflected by a disagreement in the literature with other studies allowing spin values between 0.5 and 0.9 [109–114], some even compatible with a spin below 0.2 [115, 116]. In the Cygnus X-1 search, we ignore this tension by treating the measurable final spin of the BH after superradiance as a free parameter. To estimate the VBC properties, we adopt an initial spin value $\chi_i = 0.95$, as shown in Table I. In Sec. VI, we derive constraints on the possible boson mass for different assumed values of $\chi_i$.

## C. GW signal parameters

Using the `SuperRad` waveform model [52, 97] and the values for $M_i$ and $\chi_i$ shown in Table I, we find the optimal vector mass—that is, the mass $m_V^\mathrm{opt}$ that optimizes superradiant instability for a given BH, producing the maximum GW strain amplitude attainable by the system at a reference epoch $t_\mathrm{ref}$. For the remnants from GW230814 and GW231123, $t_\mathrm{ref}$ is fixed at the time when the VBC reaches its full size [84], corresponding to the time $t_\mathrm{sat}$ when Eq. (1) is saturated. In the case of Cygnus X-1, we consider the start of the O4a period as the reference time. The values of $m_V^\mathrm{opt}$ are shown for each source in the second column of Table III. Then, based on these values and the median BH parameters, we use `SuperRad` (for the fastest growing, initially dominant mode $m = 1$) to estimate the GW signal parameters for each BH. The parameters, also listed in Table III, are defined as follows. The values $\tau_\mathrm{growth}^\mathrm{det}$ and $\tau_\mathrm{GW}^\mathrm{det}$ are the VBC growth and depletion timescales in the detector frame. The parameter $\tau_\mathrm{growth}^\mathrm{det}$ represents the timescale over which the VBC grows to its full size, and it is the inverse of the growth rate (see Eq. 4 in Ref. [84]). The parameter $\tau_\mathrm{GW}^\mathrm{det}$ is the GW emission timescale (i.e., the time over which the signal amplitude decreases by a factor of two), and it depends on the mass of the VBC and the radiated power at saturation. The parameters $h_0^\mathrm{eff}$, $f_\mathrm{GW}^\mathrm{det}$, and $\dot{f}_\mathrm{GW}^\mathrm{det}$ are, respectively, the GW strain amplitude (i.e., $h_0$ scaled by the orientation angle $\iota$ of the BH as shown: $h_0^\mathrm{eff} = h_0\, 2^{-1/2}\{[(1+\cos^2\iota)/2]^2 + \cos^2\iota\}^{1/2}$ [117]), the GW emission frequency, and the frequency drift, each evaluated in the detector frame at the reference time ($t = t_\mathrm{ref}$). We use the following definitions to simplify our notation: $f_\mathrm{GW}^\mathrm{det}(t_\mathrm{ref}) \equiv f_0$ and $\dot{f}_\mathrm{GW}^\mathrm{det}(t_\mathrm{ref}) \equiv \dot{f}_0$.

Since vector bound states carry spin angular momentum, they can still grow via superradiance even with zero orbital angular momentum number ($\ell = 0$). As a result, vector bound states can be concentrated closer to the BH, leading to clouds that grow and deplete more rapidly and radiate at much higher power than their scalar counterparts [30, 36, 38–40]. Here, we provide a depiction of how the signal frequency evolves once the VBC is saturated, independent of the specific target being searched. At $t_{\rm sat}$, the VBC is oscillating around the BH with angular frequency $\omega_V = m\Omega_H$ [38]. Then, the initial frequency of the GW emission in the source frame depends on this angular frequency: $f_{\rm GW}(t_{\rm sat}) = \omega_V/\pi$. The evolution of $f_{\rm GW}$ in the source frame can be approximated as [52]

$$f_{\rm GW}(t) = f_\infty - \frac{|f_{\rm shift}|}{1 + (t - t_{\rm sat})/\tau_{\rm GW}}, \tag{2}$$

where $\tau_{\rm GW}$ is the source frame GW emission timescale, $f_\infty$ is the asymptotic frequency at late times ($t - t_{\rm sat} \gg \tau_{\rm GW}$) and $f_{\rm shift}$ is the negative shift of $f_{\rm GW}$ away from $f_\infty$ as a result of the self-gravity of the VBC at $t_{\rm sat}$ [52, 84, 97], i.e., we have $f_{\rm GW}(t_{\rm sat}) = f_\infty - |f_{\rm shift}|$. While Eq. (2) provides a useful illustration of how the emission frequency evolves over time, the frequencies and their time derivatives shown in Table III are computed with greater accuracy using `Superrad`, which incorporates higher-order relativistic corrections [97]. Note that the signal characteristics differ between the merger remnants and Cygnus X-1, as the depletion timescales $\tau_{\rm GW}$ considered are different by orders of magnitude.

As is clear from Tables I and III, the characteristics of these target BHs are quite different. While the merger remnants are young, isolated BHs that are expected to emit short-duration, more rapidly evolving signals, Cygnus X-1 is a binary system with a much older BH that is expected to emit a long-duration, approximately monochromatic signal. Hence, we use two different search methods, each designed to exploit a different aspect of VBC signals: HMM is a flexible, less model-dependent method that is well-suited for signals with larger frequency drifts and greater uncertainties (see Sec. III A), whereas the Binary BSD-VBC search technique is designed for signals with negligible frequency drifts from sources whose orbital motion must be taken into account (see Sec. III B).

In the case of BHs from merger remnants with $D_{\rm L} \sim \mathcal{O}({\rm Gpc})$, we take into consideration the non-negligible impact of redshift on the GW emission frequency and timescale. The frequency in the detector frame scales as $f_{\rm GW}^{\rm det} = f_{\rm GW}\,(1+z)^{-1}$, and correspondingly, the frequency derivative in the detector frame scales as $\dot{f}_{\rm GW}^{\rm det} = \dot{f}_{\rm GW}\,(1+z)^{-2}$ (where $\dot{f}_{\rm GW}$ is the frequency drift in the source frame). In a similar vein, the GW emission timescale is modified as $\tau_{\rm GW}^{\rm det} = \tau_{\rm GW}\,(1+z)$. For an in-depth discussion of how these redshift corrections affect the searches, see Sec. IV in Ref. [84].

## III. METHODS

In this paper, we use two semicoherent search methods: the HMM tracking method (Sec. III A) and the Binary BSD-VBC method (Sec. III B). Although both methods are based on previous work on traditional CW searches targeting individual spinning neutron stars with nonaxisymmetries [69, 89, 117, 118], this section describes how they have been tailored to searches for vector boson signals.

### A. HMM method: Merger remnants

The HMM tracking technique is useful for detecting signals with wandering frequencies. It models the frequency evolution probabilistically as a Markov chain of transitions between discrete, unobservable ("hidden") frequency states over a number of discrete time steps, and it connects these hidden states with observable data through an emission probability. HMM tracking has been used in various searches for continuous or long-transient GW signals [49, 75, 117–127]. This method is beneficial for two main reasons: i) it is computationally efficient, which is important for this study because vector boson signals live in a large, multi-dimensional parameter space, and ii) it is more capable of accounting for both the detector noise fluctuations and any uncertainties that may be present in the predicted signal waveform than other, more model-dependent CW semicoherent search techniques (see Ref. [128]).

Reference [49] was the first to propose using an HMM-based method for follow-up searches targeting slowly-evolving scalar boson clouds around BH merger remnants. Building upon the work of Isi et al. [49], Ref. [84] implemented a modified HMM search pipeline capable of tracking signals from VBCs that occur over shorter timescales [$\sim \mathcal{O}$(days-months)], making it well-suited for targets such as newly formed merger remnants. The pipeline is an efficient semicoherent search method combining the HMM tracking scheme with a frequency-domain matched filter ($\mathcal{F}$-statistic), which quantifies the likelihood that a signal, parameterized by its frequency and associated time derivatives, is present in the data [129]. Previous studies have shown that this pipeline is sensitive enough to potentially detect signals from VBCs using data from current-generation detectors [84].

In the following two subsections, we summarize the HMM search pipeline described in Ref. [84], as well as the process of choosing search configurations for a given system, explained in Ref. [85]. Section III A 1 is meant to give a high-level overview of the HMM algorithm; for a more detailed explanation, see Refs. [117, 118].

#### 1. *Search pipeline*

The search pipeline combines the HMM tracking technique with an $\mathcal{F}$-statistic, computed over discrete time segments. The $\mathcal{F}$-statistic takes as its input short Fourier transforms (SFTs) of the relevant time series data collected by each GW detector [130]. Note that for the simulated data used in various places throughout the study, we create these SFTs by injecting synthetic signal

Table III. Estimated GW signal parameters for the remnant BHs from the GW230814 and GW231123 mergers and the BH in Cygnus X-1 using the median BH parameters and their respective $m_V^{\rm opt}$ values.

| Source | $m_V^{\rm opt}$ $[10^{-13}$ eV] | $\tau_{\rm growth}^{\rm det}$ | $\tau_{\rm GW}^{\rm det}$ | $h_0^{\rm eff}$ $[10^{-24}]$ | $f_0$ [Hz] | $\dot{f}_0$ $[{\rm Hz\,s^{-1}}]$ |
|---|---|---|---|---|---|---|
| Remnant from GW230814 | 3.805 | 7.8 h | 28 h | 0.341 | 170.4 | $6.2 \times 10^{-7}$ |
| Remnant from GW231123 | 1.652 | 2.3 h | 2.5 h | 1.69 | 51.2 | $9.4 \times 10^{-6}$ |
| BH in Cygnus X-1 | 1.040 | 560 y | $7.5 \times 10^6$ y | 1.75 | 50.3 | $1.6 \times 10^{-19}$ |

waveforms generated by the waveform model `SuperRad` into Gaussian noise using the simulateCW Python module in the LALPulsar library of LALSuite [131, 132].

For this pipeline, we compute the $\mathcal{F}$-statistic coherently over time segments of length $T_{\rm coh}$. These coherent segments are then incoherently combined using an HMM, which is solved via the Viterbi algorithm [133]. The Viterbi algorithm efficiently finds the most probable path of the signal evolution (also known as the Viterbi path) in the frequency-time plane with $N_Q$ frequency bins of width $\delta f$ and $N_T$ time segments of length $T_{\rm coh}$ (see detailed formulation and descriptions in, e.g., Refs. [117, 118]). The value $T_{\rm coh}$ (and correspondingly $\delta f$) are bounded by the predicted signal's maximum frequency derivative $\dot{f}_{\rm max}$ such that i) the signal may be thought of as monochromatic across a single time segment and ii) the signal can increase at most one frequency bin between each time segment. The frequency bin width $\delta f$ is fixed to $1/(2T_{\rm coh})$. Given that the maximum spin-up of the signal across the full search duration $T_{\rm obs} = T_{\rm coh}N_T$ must satisfy $\dot{f}_{\rm max}T_{\rm coh} \leq \delta f$, we have the following upper bound on $T_{\rm coh}$:

$$T_{\rm coh} \leq (2\dot{f}_{\rm max})^{-1/2}. \tag{3}$$

Because increasing $T_{\rm coh}$ generally improves the search sensitivity [117], in these searches we fix $T_{\rm coh}$ to its largest possible value to maximize sensitivity for a given source model configuration (see Section III A 2). The frequency drift is at its maximum when the VBC reaches saturation at a time $t_{\rm sat}$. Thus, for a given system, we compute $\dot{f}_{\rm max}$ using `SuperRad` and then set $T_{\rm coh} = (2\dot{f}_{\rm max})^{-1/2}$. This ensures that the signal will not evolve outside HMM's tracking capabilities.

The Viterbi path returned by the search pipeline has an associated detection statistic that quantifies its significance. There are different ways to define the detection statistic (see, for example, the Viterbi score in, e.g., Ref. [117], or the log likelihood of the optimal path, $\mathcal{L}$, in, e.g., Ref. [134]). For the searches in this paper, we use $\mathcal{L}$ divided by the number of coherent segments $N_T$ [84], written as

$$\bar{\mathcal{L}} \equiv \mathcal{L}/N_T. \tag{4}$$

We use the log likelihood-based detection statistic $\mathcal{L}$ rather than, e.g., the Viterbi score because $\mathcal{L}$ has been shown to be more reliable for short duration searches [120, 123, 125, 126, 134], whereas the Viterbi score is only reliable in the regime $N_Q \gg N_T$, appropriate for very long-duration searches [49, 75, 117]. In addition, normalizing $\mathcal{L}$ by $N_T$ makes it applicable across the many different search configurations used in this analysis.

### 2. *Configurations*

Given a target BH, we start by finding $m_V^{\rm opt}$. We then define a range of vector masses the pipeline *may* be sensitive to, $m_V \in [0.6, 1.1]m_V^{\rm opt}$,[5] given the BH we consider, and we choose some number of evenly spaced $m_V$ values from within this range [85]. We must then select a set of search configurations $\{t_{\rm start},\, T_{\rm SFT},\, T_{\rm coh},\, T_{\rm obs}\}$, where $t_{\rm start}$ is the GPS start time of the search (corresponding to when the VBC has reached saturation) and $T_{\rm SFT}$ is the SFT length, to sufficiently cover this parameter space. These configuration parameters are chosen based on the predicted signal evolution, which in turn depends on the given system parameters $\{M_i,\, \chi_i,\, D_{\rm L},\, m_V\}$. As demonstrated in Ref. [85], because we use the flexible HMM search technique, even a single set of search configuration parameters can recover signals generated by systems with a range of parameters. Still, we require more than one configuration to provide adequate coverage of the full parameter space. In principle, if we had unlimited computational resources, we would search using a series of optimized configurations tailored to each possible signal to maximize the sensitivity. In practice, however, we must limit the number of configurations sampled in order to balance search sensitivity with computational cost. The configurations used in this analysis are therefore chosen to span the relevant parameter space with sufficient coverage, while keeping the total cost tractable. The resulting sensitivity, accounting for the finite sampling of configurations, is quantitatively evaluated through simulations in Sec. VI A The process of choosing a set of configurations is explained in detail in Appendix A of Ref. [85] and summarized here.

We first impose several limits on the allowed search configurations to ensure computational feasibility: We require the SFT length to lie within 15 sec $\leq T_{\rm SFT} \leq$ 30 min (they need not be fixed to the standard $T_{\rm SFT} =$ 30 min

---

[5] As shown in Ref. [84], these searches are in fact more sensitive to some sub-optimal vector masses than the optimal mass because, for a given BH, sub-optimal masses produce longer-lived GW emission, allowing us to extend the $T_{\rm coh}$ used in the search.

used in most CW searches) and the coherent length within 1 min $\leq T_{\mathrm{coh}} \leq$ 10 day. The ratio $T_{\mathrm{coh}}/T_{\mathrm{SFT}}$ must be an integer value of at least four; that is, each detector must contribute a minimum of four SFTs per $T_{\mathrm{coh}}$ segment. Finally, we set $T_{\mathrm{obs}} = \tau_{\mathrm{GW}}^{\mathrm{det}}$ but require that it must not exceed 180 days to minimize the computational cost of the search for sub-optimally matched boson masses [84]. The search computing cost for an average system scales roughly with the duration of the signal, ranging from approximately $\mathcal{O}$(minutes)–$\mathcal{O}$(hours) on a single-core computer. To cover the full parameter space for a given remnant BH (i.e., a $\sim$ 50–100 Hz bandwidth using 11 different search configurations), the total cost of the search is approximately $\mathcal{O}(10^2)$ core-hours. Deriving the final sensitivity across the full parameter space via simulations (using the same configurations) typically takes $\mathcal{O}(10^4)$ core-hours per target.

Following the guidelines outlined in Ref. [85], we randomly draw 200 posterior samples from the remnant BH's multidimensional posterior distribution. For each sample BH and each value of $m_V$ we consider in the search, we find the optimal search configuration. We then independently draw 11 values from each of these three distributions at the following percentiles: 2, 10, 20, 30, 40, 50, 60, 70, 80, 90, and 98. This forms 11 search configurations with which we will run the search (see Tables IV and V for the sets of configurations used in this work). For most systems drawn from the remnant's posterior distribution, more than one of these configurations should be able to recover the signal, making this spacing a conservative choice.

## B. Binary BSD-VBC method: Cygnus X-1

The Binary BSD-VBC pipeline developed in this work builds on the BSD framework [89], which provides a compact and flexible format to manipulate and analyze calibrated strain data. Thanks to its modularity, the BSD framework has been applied to various CW searches—both fully coherent [135, 136] and semicoherent [67, 69, 80, 102, 120, 137, 138]—including the all-sky search for scalar boson clouds using data from the LVK's third observing run [67].

The Binary BSD-VBC method adapts and extends these pipelines to target CW signals emitted by VBCs around BHs in known binary systems. The main case study is Cygnus X-1, whose orbital parameters are well constrained by X-ray observations [90, 91, 101]. Details of the specific implementation for this source are given in Sec. IV B.

### 1. *Search pipeline*

In this search, data are analyzed in sub-bands of 1 Hz overlapped by 0.5 Hz using the BSD format. The files contain a complex time series downsampled to 1 Hz and covering the full O4a.

The search pipeline follows a two-step approach based on standard BSD tools. The first step aims to increase the signal coherence by coherently removing the Doppler modulation caused by the combined motion of the source and the detector. The data is demodulated for a chosen target coherence time, $T_{\mathrm{coh}}$, and a given set of parameters $\mathbf{\Lambda} = \{f_0, \mathrm{RA}, \mathrm{Dec}, a_{\mathrm{p}}, t_{\mathrm{asc}}, \Omega, e, \omega\}$, where $f_0$ is the emission frequency, $t_{\mathrm{asc}}$ is the time of ascending node, $\Omega$ is the orbital angular frequency related to the orbital period $P$ as $\Omega = 2\pi/P$, $e$ is the orbital eccentricity, and $\omega$ is the argument of periapse. The correction is performed using the standard *heterodyne* method implemented in the BSD framework [89] and outlined in Appendix A 2. The heterodyne procedure produces a new time series where, for a proper choice of $\mathbf{\Lambda}$, a signal can be considered monochromatic up to the frequency resolution $\delta f_0 = 1/T_{\mathrm{coh}}$.

The second step consists of a standard semicoherent search for the demodulated signal. A collection of significant peaks in the time-frequency plane, known as the *peakmap*, is generated using the method detailed in Ref. [139]. Under proper demodulation, the signal appears in the peakmap as a line of constant frequency, with all its power contained in the same frequency bin of width $\delta f_0 = 1/T_{\mathrm{coh}}$. To identify the signal, the peakmap is projected onto the frequency axis to produce a histogram of peak counts per frequency bin.

The significance of the number of peaks in each frequency bin is evaluated by the robust Critical Ratio (CR) statistic [103], defined in Appendix A 3. Candidates are then selected by uniformly dividing the 1 Hz band into 50 sub-bands of 0.02 Hz and choosing the frequency bin with the highest CR statistic within each sub-band.

### 2. *Configurations*

We adopt a signal model, described in Appendix A 1, where the frequency modulation is entirely defined by a set of modulation parameters $\mathbf{\Lambda}$. The sampling of parameters $\mathbf{\Lambda}$ must ensure adequate coverage of the parameter space to avoid significant loss in the detection sensitivity. At the same time, the computational cost of the analysis scales with the number of templates, which must therefore be kept to a minimum. The number of templates needed to cover a parameter space is discussed in Sec. A 4.

The dimensionality of the parameter space to be covered can be reduced based on the considerations that we discuss below. These assumptions are not generally valid and must be validated for a given source and search setup. In particular, their validity for the Cygnus X-1 search is discussed in Sec. IV B. We have verified, through injection-and-recovery of simulated signals,[6] that our search setup and simplified phase model can recover VBC signals emitted from Cygnus X-1. The injections were performed in simulated data that mimics the detectors' noise profile.

The unknown signal frequency $f_0$ can be accounted for using a correction strategy similar to the sub-band method presented in Ref. [69]. Taking advantage of the BSD format, our analysis considers frequency sub-bands of 1 Hz each. In place of the unknown signal frequency, we correct the timeseries via the heterodyne procedure using the sub-band's central frequency, $f_c$. Using an incorrect signal frequency results in a residual frequency modulation of the amplitude, $\Delta f$, which can be neglected as long as it is fully contained within a single frequency bin, i.e., $2\Delta f < 1/T_{\mathrm{coh}}$, thereby limiting the value of $T_{\mathrm{coh}}$. We note that although the template frequencies are spaced by 0.5 Hz, this spacing does not affect the search frequency resolution, $\delta f_0 = 1/T_{\mathrm{coh}}$, which is determined by the coherence time $T_{\mathrm{coh}}$ used to create the peakmap.

The search targets a system whose sky position is known with high precision; we therefore fix RA and Dec to the central value of their respective electromagnetic estimates. For the orbital parameters, we further assume that the angular frequency $\Omega$, eccentricity $e$, and argument of periastron $\omega$ are well-constrained from electromagnetic observations, allowing the use of single central values of $\Omega$, $e$, and $\omega$ for the heterodyne correction. Similar to the emission frequency, a parameter is considered to be well-constrained for a given coherence time $T_{\mathrm{coh}}$ if, while using the central value of the parameter, the residual modulation in the heterodyned data is fully contained in a single frequency bin of the peakmap.

Using the simplified model presented above, a given 1 Hz band is analyzed by sampling a collection of heterodyne parameters $\mathbf{\Lambda}_i = \{f_c, \mathrm{RA}_c, \mathrm{Dec}_c, a_{\mathrm{p},i}, t_{\mathrm{asc},i}, \Omega_c, e_c, \omega_c\}$, where the subscript $c$ indicates that we take a fixed central value for the parameter. The sampling of these parameters is performed to cover the two-dimensional plane ($a_{\mathrm{p}}$, $t_{\mathrm{asc}}$). The time of ascending node $t_{\mathrm{asc}}$ is bounded by the orbital period as $t_{\mathrm{asc}} \in [-P/2, P/2]$, and the range of $a_{\mathrm{p}}$ is constrained by electromagnetic observations of the source. The parameter-space metric of the binary phase evolution has been evaluated and tested in Ref. [140]. In particular, we consider here the short-segment regime $T_{\mathrm{coh}} \ll P$ of the metric, which is satisfied by our search setup (see Sec. IV B) and by the orbital period of Cygnus X-1 reported in Table II. To cover the parameter space ($a_{\mathrm{p}} - t_{\mathrm{asc}}$), we use a restricted version of the binary phase metric. Following the discussion in Ref. [140], the resolutions in $a_{\mathrm{p}}$ and $t_{\mathrm{asc}}$, while allowing for a maximal loss in signal-to-noise ratio of 10%, are

$$\delta a_{\mathrm{p}} = \frac{\sqrt{0.6}}{\pi \Omega T_{\mathrm{coh}} f_0} \qquad \delta t_{\mathrm{asc}} = \frac{\sqrt{0.6}}{\pi \Omega^2 a_{\mathrm{p}} T_{\mathrm{coh}} f_0}. \tag{5}$$

These resolutions are used to construct a square lattice $\mathbb{Z}_2$, as described in Refs. [140, 141]. Details on the grid construction can be found in Appendix A 4.

Typically, an analysis satisfying these limitations would take $< \mathcal{O}(10^5)$ core-hours to cover the reduced parameter space, such as that of Cygnus X-1. In the absence of detection, constraints can be derived very efficiently using the method outlined in Sec. VI B 1, and the computation time needed to derive these constraints is negligible compared to the analysis time.

### 3. *Candidate selection and coincidences*

For each 1 Hz band, the search is repeated for all templates $\{\mathbf{\Lambda}_i\}_{i=1}^{N}$. As presented above, for each template, we uniformly select the 50 most significant frequency bins. Combining the results across all templates, we obtain a list of candidates, from which we select a subset of the most significant ones. Specifically, for each frequency bin of width $\delta f_0 = 1/T_{\mathrm{coh}}$, we select the two candidates with the highest CR values. In this way, and for the coherence time $T_{\mathrm{coh}} = 1000$ s used in the BSD search, a maximum of 2000 candidates are selected for each 1 Hz band. This step reduces the number of candidates to a manageable level. We note that the selection of high CR candidates does not impact the upper limits set by this search. Indeed, as presented in Sec. VI B 1, the upper limits are estimated using a semi-analytic approach that considers only the loudest candidate in each 1 Hz band analyzed; weaker candidates discarded during the candidate selection are irrelevant for the upper limits estimation.

Then, candidates are filtered to keep only those with a CR above a threshold. Similar to Ref. [120], the threshold is chosen for each 1 Hz band as the mean CR plus two standard deviations of the CR distribution of the candidates, corresponding to a false alarm probability $P_{\mathrm{fa}} \approx 5\%$ for this first step of selection. The CR distribution is built by excluding candidates associated with known instrumental lines (see Sec. V B). We then identify pairs of candidates coincident between the Hanford and Livingston detectors. Candidates are considered coincidental if they are on the same or adjacent frequency bins. Furthermore, coincident candidates must have compatible orbital parameters, i.e.,

$$d_{\mathrm{metric}} = \sqrt{\left(\frac{\Delta a_{\mathrm{p}}}{\delta a_{\mathrm{p}}}\right)^2 + \left(\frac{\Delta t_{\mathrm{asc}}}{\delta t_{\mathrm{asc}}}\right)^2} < 3, \tag{6}$$

where $\Delta a_{\mathrm{p}}$ and $\Delta t_{\mathrm{asc}}$ denote the differences between the parameters of the candidates in each detector.

Coincident pairs of candidates, referenced hereafter as stage-2 candidates, are further analyzed in the follow-up procedure presented in Sec. V B.

---

[6] The templates used in this search are placed according to the binary phase metric introduced in Ref. [140], which was derived from noise-free mismatch studies. The analysis of injected signals in simulated noise discussed in this section aims to validate the reduced phase model and the search setup for detecting signals in realistic, noisy data.

## IV. SEARCH SETUP

In this section, we provide details on the parameters and configurations used to run the HMM and BSD searches. We use data taken by the two Advanced LIGO detectors, Hanford and Livingston [53], during O4a, which ran from 15:00 UTC on May 24, 2023 to 16:00 UTC on January 16, 2024 [56, 142–144]. The HMM searches analyze data spanning two different time segments (corresponding to the weeks following both the GW230814 and GW231123 binary merger events), whereas the BSD search uses the full O4a data, for which the duty factors are 67% and 69% for Hanford and Livingston, respectively. All the data used in this paper, acquired when the detectors were in science observing mode, are online calibrated (i.e., low-latency C00 frames), and analysis-ready (channel names: `H1:GDS-CALIB_STRAIN_CLEAN_AR` and `L1:GDS-CALIB_STRAIN_CLEAN_AR`) [143, 145–151]. Calibration uncertainties in the strain data can affect boson parameter estimates (if a signal is detected) and influence constraints or sensitivity estimates (if not). In O4a, the 1-$\sigma$ frequency- and time-dependent uncertainties are $\lesssim 10\%$ in magnitude and $\lesssim 10$ deg in phase and differ between LIGO sites [145]. However, their overall impact is subdominant to noise fluctuations. We therefore do not explicitly include calibration uncertainties in our analysis. The HMM searches take as input SFTs generated after applying a glitch gating procedure [152]. The BSD are generated from the Short FFT Database (SFDB) [139], and cleaned using the double-gating procedure described in Refs. [89, 153].

### A. HMM searches: Merger remnants

#### 1. *GW230814*

Recalling Sec. II C and Table III, for the remnant BH from GW230814, we find $m_V^{\rm opt} = 3.805 \times 10^{-13}$ eV. Thus, the interesting vector mass range $[0.6, 1.1]\, m_V^{\rm opt}$ (see Sec. III A 2) becomes $[2.283, 4.185] \times 10^{-13}$ eV for this search. Each boson mass within this range, if it exists, would emit GWs at a different frequency, so we have a corresponding frequency range of [97, 196] Hz across which we run the search, divided into 1 Hz sub-bands.

When choosing which sky position(s) to target, it may seem reasonable to simply target the median RA and Dec listed in the table. However, because the estimated posterior distribution of the RA for this system is bimodal, the median is not representative of the data (see top panel of Fig. 1).[7] Instead, we choose the optimal sky positions empirically by drawing a joint random sample of 100 RA and Dec values from the BH posterior distribution, injecting them into Gaussian noise, and attempting to recover them using a grid of sky positions. The spacing of this grid reflects the size of the effective point spread function (EPSF) shown in Fig. 2, in which a signal has been injected at RA, Dec = [3.854, 0.370] rad and then recovered using a grid of sky positions offset from this sky position. Overall, the sky positions that recover the largest number of randomly sampled injections are RA, Dec = [1.088, -0.387], [1.388, -0.387], [3.254, 0.370], and [3.554, 0.370] rad. We target all four sky positions in

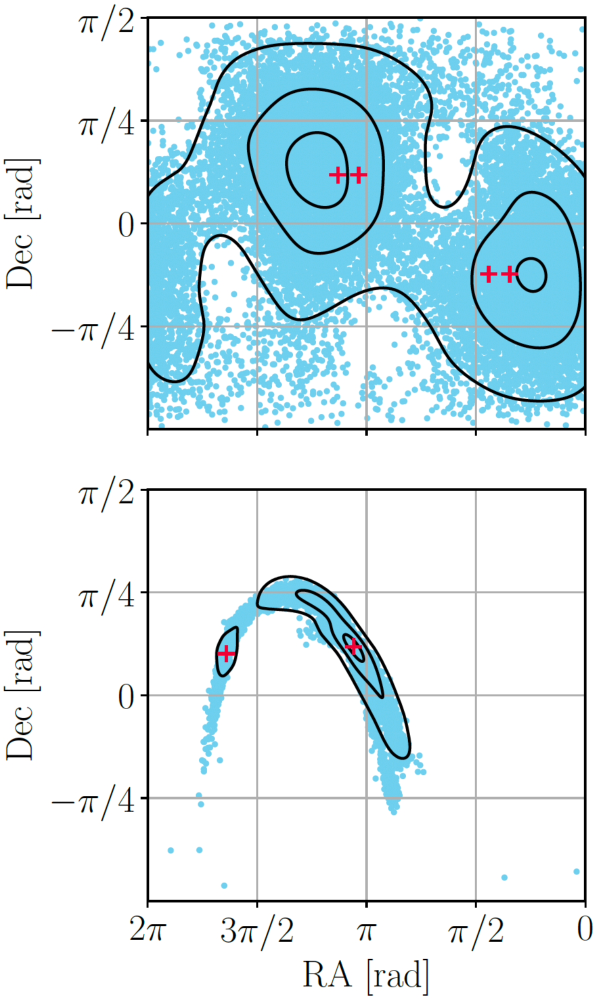

Figure 1. Joint RA and Dec posterior distribution for the merger remnants from GW230814 (top) and GW231123 (bottom). The black contours show the 90%, 50%, and 10% confidence intervals. The red crosses indicate the sky positions targeted in the search for each remnant.

---

[7] GW230814 was observed only by the Livingston detector, so the remnant's poorly constrained sky location aligns with the detector's antenna pattern.

the search to obtain better coverage over the whole sky.[8] They are marked with red crosses in the top panel of Fig. 1. The search is not particularly sensitive to sky localization for short-duration signals with $T_{\rm obs} \lesssim 1$ day, although the low sky resolution does lead to degraded sensitivity [84]. For longer signals with $T_{\rm obs} \gtrsim 1$ day, however, a mismatch in sky position can still cause a marginal signal to be missed. This uncertainty due to poorly-constrained sky localization is incorporated into the sensitivity estimates we present in Sec. VI A.

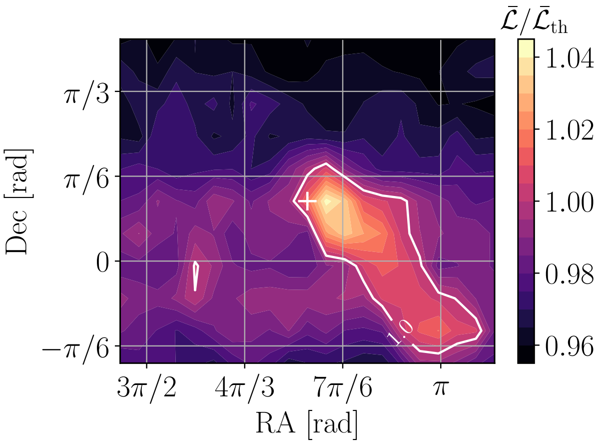

Figure 2. Colored contour of $\bar{\mathcal{L}}/\bar{\mathcal{L}}_{\rm th}$ as a function of RA and Dec for a synthetic signal injected at [3.854, 0.370] rad, shown with a white cross marker. The signal was generated using the median BH remnant parameters from the GW230814 merger shown in Table I and using $m_V = 2.283 \times 10^{-13}$ eV. The bright EPSF enclosed within the white contour signifies the region of the sky with $\bar{\mathcal{L}} > \bar{\mathcal{L}}_{\rm th}$ where the signal has been recovered.

Using the method outlined in Appendix A of Ref. [85] (and summarized in Sec. III A 2 above) for choosing search configurations, we use 11 different configurations in the search, shown in Table IV. In particular, we choose a set of $T_{\rm coh}$ values to cover the full range of $\dot{f}_{\rm max}$ values that may occur for the system: $\sim \mathcal{O}[10^{-9}, 10^{-6}]$ Hz s$^{-1}$. Across all 11 configurations, we run the search on detector data spanning the GPS times [1376111180, 1385937626] s. Gaps are present in the available data from Hanford and Livingston during this time period, resulting from both scheduled maintenance and unexpected lock loss due to various environmental disturbances. In particular, although the duty factor is ∼ 70% for each detector during the analysis time of GW230814, many of the data gaps lie within roughly two days post-merger, when the signal is expected to be strongest. While the HMM search pipeline is designed to accommodate data gaps, the less data that is available, the less sensitive the search becomes. This decreased sensitivity is reflected in the eventual estimated vector mass range that is disfavored by targeting this remnant (see Sec. VI A).

### 2. *GW231123*

As in the previous section, we refer to Table III for the optimal boson mass corresponding to the remnant BH from GW231123: $m_V^{\rm opt} = 1.652 \times 10^{-13}$ eV. Thus, for the search we consider the range $m_V = [0.901, 1.502] \times 10^{-13}$ eV and the corresponding frequency band [21, 73] Hz, split into 1 Hz sub-bands.

Once again, the RA posterior distribution shows some bimodality, but because the sky position is significantly more well-constrained than GW230814 [i.e., the 90% confidence interval is constrained to $\mathcal{O}(10^3)$ deg$^2$], for the search we simply target the two local maxima marked by red crosses in the bottom panel of Fig. 1, located at RA, Dec = [3.329, 0.372] and [5.153, 0.318] rad. These two local maxima are tested using the same method described above for GW230814, and we find that they provide sufficient coverage across the 90% credible region of the sky position.

We start by identifying 11 potential search configurations at the same percentiles used for GW230814. However, two configurations cannot be used in the search, as their GPS start times (1602835969 and 2785340449 for the 90th and 98th percentiles, respectively) do not fall within the fourth observing run (O4).[9] Thus, we limit the number of configurations used in the search to only the first 9, shown in Table V. Again, we choose the set of $T_{\rm coh}$ values to cover the potential $\dot{f}_{\rm max}$ range $\sim \mathcal{O}[10^{-15}, 10^{-5}]$ Hz s$^{-1}$ for this system. Gaps are again present in the data available from both detectors, limiting the search sensitivity; while the duty factor for Hanford is 68% across the relevant time frame, for Livingston it is only 51%.

## B. BSD search: Cygnus X-1

Using the median values for the parameters of Cygnus X-1 reported in Table I, we find the boson mass $m_V^{\rm opt} = 1.040 \times 10^{-13}$ eV produces the signal with the maximum strain amplitude at the start of O4a. Taking into account the uncertainties in the BH parameters, we estimate the signal amplitudes corresponding to boson masses around $m_V^{\rm opt}$ using the `SuperRad` model. Then, comparing these values to the minimum detectable strain given

---

[8] It is particularly valuable to target multiple sky positions (when the true sky position is not well constrained) for the configurations that use longer $T_{\rm coh}$ values. This is because searches with longer coherent segments are more sensitive to Doppler modulation effects and thus the assumed sky position, so there is a larger chance of missing a GW signal if an incorrect sky position is used.

[9] These times correspond to a non-optimal region of the parameter space where the VBC grows and dissipates very slowly and thus it will be $\mathcal{O}$(years) before the GW emission reaches its peak.

Table IV. Search configuration parameters and the percentiles at which they are drawn for the BH remnant from the GW230814 merger. These percentiles, taken from the distribution of search configurations generated for 200 randomly sampled BH posteriors × 11 values of $m_V$, are chosen so that the configurations used in the search adequately cover the remnant's full posterior distribution.

| Percentile | $T_{\rm SFT}$ [m] | $T_{\rm coh}$ [m] | $T_{\rm obs}$ [m] | GPS start time [s] |
|---|---|---|---|---|
| 2 | 2.85 | 11.4 | 991.8 | 1376111180 |
| 10 | 3.4 | 13.6 | 1278.4 | 1376115080 |
| 20 | 3.9 | 15.6 | 1653.6 | 1376119160 |
| 30 | 4.55 | 18.2 | 2311.4 | 1376124380 |
| 40 | 5.75 | 23.0 | 3519.0 | 1376134280 |
| 50 | 7.45 | 29.8 | 5632.2 | 1376148320 |
| 60 | 10.45 | 41.8 | 9823.0 | 1376172680 |
| 70 | 15.05 | 60.2 | 17759.0 | 1376211140 |
| 80 | 24.4 | 97.6 | 36990.4 | 1376285360 |
| 90 | 26.85 | 161.1 | 79583.4 | 1376412320 |
| 98 | 27.65 | 248.85 | 155780.1 | 1376590820 |

Table V. Search configuration parameters and the percentiles at which they are drawn for the BH remnant from the GW231123 merger. These percentiles, taken from the distribution of search configurations generated for 200 randomly sampled BH posteriors × 11 values of $m_V$, are chosen so that the configurations used in the search adequately cover the remnant's full posterior distribution.

| Percentile | $T_{\rm SFT}$ [m] | $T_{\rm coh}$ [m] | $T_{\rm obs}$ [m] | GPS start time [s] |
|---|---|---|---|---|
| 2 | 0.6 | 2.4 | 84.0 | 1384788409 |
| 10 | 1.0 | 4.0 | 172.0 | 1384792009 |
| 20 | 1.45 | 5.8 | 301.6 | 1384796449 |
| 30 | 2.25 | 9.0 | 630.0 | 1384804309 |
| 40 | 3.55 | 14.2 | 1235.4 | 1384816729 |
| 50 | 6.0 | 24.0 | 2424.0 | 1384837489 |
| 60 | 9.4 | 37.6 | 4587.2 | 1384866949 |
| 70 | 14.35 | 57.4 | 9011.8 | 1384911769 |
| 80 | 26.2 | 157.2 | 42601.2 | 1385145169 |

in Eq. (67) of Ref. [103], we select the frequency band $f_0 \in [24.5, 125.5]$ Hz as the range of frequencies where a signal could be detected. Therefore, the search spans 202 distinct 1 Hz bands, overlapped by 50%.

We fix the coherence time to $T_{\rm coh} = 1000$ s for all frequency bands investigated. This value is motivated by multiple factors. Demodulating the data using the central frequency of the band rather than the real—unknown—frequency of the signal leads to a residual modulation of the signal. Our choice of $T_{\rm coh}$ ensures that, for any signal present in the band, the residual modulation $\Delta f$ is smaller than the size of a frequency bin, i.e. $2\Delta f < 1/T_{\rm coh}$. Similarly, this coherence time ensures that the uncertainties in the eccentricity parameters of Cygnus X-1's orbit, reported in Table II, are fully covered by a template using the central values of the parameters. At the same time, a coherence time $T_{\rm coh} = 1000$ s keeps the analysis time to a realistic level with $\mathcal{O}(60\,000)$ core-hours being needed to analyze the parameter space of Cygnus X-1 in both LIGO detectors.

Following the grid construction method presented in Sec. III B 2, for each band we define a set of parameter points $\{\mathbf{\Lambda}_i\}_{i=1}^{N}$ covering the uncertainties in the orbital parameters of Cygnus X-1 reported in Table II. The time of superior conjunction $T_0$ of Cygnus X-1 has been estimated in Ref. [101], but the extrapolation of this value to estimate the time of ascending node $t_{\rm asc}$ at the O4a period leads to significant uncertainties compared to our search resolution. We choose an agnostic approach where the range of all possible values $t_{\rm asc} \in [-P/2, P/2]$ has been covered by the search. The number of templates per band ranges from $N = 1\,960$ at 24.5 Hz to $N = 43\,416$ at 125.5 Hz, in agreement with Eq. (A12). Combining the number of templates used in all the bands, the search uses 3 687 225 templates.

The search is performed with bands overlapping by 0.5 Hz to avoid cropping signals close to the band edges during BSD creation. Each band is searched independently, and each produces its own set of stage-2 candidates, which are selected following the discussion in Sec. III B 3.

## V. CANDIDATE FOLLOW-UP

In this section, we outline the follow-up procedures used to eliminate any search candidates whose origins are not astrophysical. See Tables VI and VII for the numbers of candidates that remain from the HMM and BSD searches after each veto procedure described in the following sections.

### A. HMM searches: Merger remnants

For GW230814, we run the search over 99 individual 1 Hz bands, 11 search configurations, and 4 sky positions. This is 4356 iterations in total. Similarly, for GW231123, we have 52 1 Hz bands, 9 search configurations, and 2 sky positions, yielding 936 search iterations. For each 1 Hz band, we require the detection statistic $\bar{\mathcal{L}}$ to exceed a threshold $\bar{\mathcal{L}}_{\rm th}$ corresponding to a 1% false alarm probability ($P_{\rm fa}$).[10] The value of $\bar{\mathcal{L}}_{\rm th}$, which varies for each $T_{\rm coh}$ used in the searches, is obtained empirically as follows: For a given value of $T_{\rm coh}$, we run 300 searches in pure Gaussian noise (with Amplitude Spectral Density (ASD) $= 4 \times 10^{-24}$ Hz$^{-1/2}$) at a randomly chosen 1 Hz frequency band, and we define $\bar{\mathcal{L}}_{\rm th}$ as the value of $\bar{\mathcal{L}}$ that lies at the 99th percentile of these results.

---

[10] The 1% false alarm probability corresponds to each configuration in each 1 Hz band.

After implementing this initial threshold cut, we have 421 and 285 signal candidates across all configurations for GW230814 and GW231123, respectively. However, many candidates actually appear to be the same candidates picked up by different configurations (e.g., for GW230814, a candidate at $\sim 102.1$ Hz is identified for nearly every value of $T_{\rm coh}$ and at every sky position). We expect a large fraction of these first-pass candidates to be simply the result of noise artifacts (e.g., power line harmonics, thermally excited mirror suspension violin modes [143, 154]) and non-Gaussianities in the interferometric data. We use the known-line [155] and single-interferometer veto techniques described in Appendix B 1 (which are commonly used in CW searches) to help distinguish candidates of this nature from a true astrophysical signal [134]. We manually inspect any candidates that survive these initial vetoes by assessing their consistency with the signal model, scrutinizing the spectrograms, identifying clear characteristics of noise (such as a candidate occurring in only one detector due to short-period artifacts and failing to meet the stringent criteria of the single-interferometer veto), etc. For a detailed description, see Appendix B 1. Table VI shows the candidates that remain for each merger remnant after each veto. After manual inspection, no signal candidates remain.

Table VI. Number of candidates remaining from the search targeting the remnants from the GW230814 and GW231123 mergers after each veto has been applied.

| | Remaining candidates | |
|---|---|---|
| Stage | GW230814 | GW231123 |
| Initial candidates | 421 | 285 |
| Known-line veto | 44 | 209 |
| Single-interferometer veto | 19 | 101 |
| Manual inspection | 0 | 0 |

### B. BSD search: Cygnus X-1

From the BSD-based search, we identify 27 stage-2 candidates that pass the selection process described in Sec. III B 3. We follow up these candidates using the vetoing procedure described in Appendix B 2, corresponding to an overall false alarm probability $P_{\rm fa} < 0.1\%$. The list of candidates is first filtered by removing those associated with known instrumental lines [155], reducing the list to eight candidates. During the creation of candidate pairs (see Sec. III B 3), the same candidate could be matched to multiple coincident candidates in the other detector. To remove this redundancy, we cluster all pairs that share a common candidate, reducing the number of independent candidates to six. We then apply standard vetoes adapted from previous BSD-based searches (e.g., [69, 120]), which are based on the consistency of the candidates with the parameters of Cygnus X-1 and with the expected behavior of the detection statistic. Three candidates pass these vetoes and are further inspected. All three are consistent with artifacts produced by non-Gaussianities in the detector. More details on the follow-up procedure are given in Appendix B 2. Table VII summarizes the number of candidates remaining after each veto.

Table VII. Number of candidates remaining from the Cygnus X-1 search after each veto has been applied.

| | Remaining candidates |
|---|---|
| Stage | Cygnus X-1 |
| Initial candidates | 27 |
| Known-line veto | 8 |
| Clustering | 6 |
| Astrophysical consistency veto | 5 |
| Statistical consistency check | 3 |
| Manual inspection | 0 |

## VI. CONSTRAINTS

In this section, we estimate the vector boson mass range that can be constrained given the absence of a confident detection in the searches described above.

### A. HMM searches: Merger remnants

After applying the veto procedures described in Sec. V A, all candidates from the HMM searches are eliminated. In this section, we investigate the confidence with which we disfavor the existence of a given vector boson mass range. We adopt an empirical approach in which synthetic signals are injected into simulated Gaussian noise configured to match the real data, with ASDs derived from detector data at the corresponding times and frequencies, and with data gaps reproduced to reflect those present during the analysis period. We marginalize the detection probabilities over the BH parameter uncertainties to reduce potential biases in the sensitivity estimates. We make a common assumption when interpreting the search results: the vector field interacts only gravitationally, with no additional interactions or couplings to the Standard Model. See Sec. IV of Ref. [85] for details on how this assumption can be partially lifted.

In Ref. [85], a framework is developed for constraining the boson mass that marginalizes over the parameter uncertainties typical to a binary merger remnant detected gravitationally. We start by drawing a number $N_{\rm BH}$ of random samples from the BH posterior distribution with parameters $\boldsymbol{\theta}_i$. Then, for a given boson mass, we generate a synthetic GW signal for each sample BH and inject the signal into a number $N_{\rm noise}$ of random Gaussian noise simulations. We evaluate the recovery rate across all sampled systems and noise realizations as shown [85]:

$$P_{\rm det}(m_V) = \frac{1}{N_{\rm BH} N_{\rm noise}} \sum_{i=1}^{N_{\rm BH}} N_{\rm det}(\boldsymbol{\theta}_i; m_V), \tag{7}$$

where $N_{\rm det}(\boldsymbol{\theta}_i; m_V)$ is the number of recovered ($\bar{\mathcal{L}} > \bar{\mathcal{L}}_{\rm th}$) signals out of $N_{\rm noise}$ noise realizations for a given vector mass $m_V$ and set of BH parameters $\theta_i$. This value $P_{\rm det}(m_V)$ can be interpreted as the confidence to which the existence of the vector boson with mass $m_V$ can be excluded given that no signal is detected in the searches.

In Fig. 3 we show the confidence with which we disfavor the vector mass using this procedure for GW230814 (left panel) and GW231123 (right panel), where, following the guidelines in Ref. [85], we have used $N_{\rm BH} = 200$ and $N_{\rm noise} = 10$. We run the simulations across all configurations used in the real searches (i.e., {RA, Dec} and $\{T_{\rm SFT},\ T_{\rm coh},\ T_{\rm obs},\ t_{\rm start}\}$). The synthetic signal is considered recovered if at least one configuration returns an above-threshold detection statistic. The orange, blue, and purple lines in the figure indicate a 1%, 5%, and 10% $P_{\rm fa}$ threshold, respectively. $P_{\rm det}$ indicates the confidence with which one can disfavor a vector mass range given the null search results (i.e., if some range of data points lie above a given $P_{\rm det}$ value, that mass range is disfavored with $P_{\rm det}$ confidence). While the searches targeting the remnant from GW230814 and GW231123 are not sensitive enough to constrain the vector mass at high confidence, the following is an example of how we would estimate the boson mass range that can be constrained: We disfavor the vector mass ranges $[2.75, 3.28] \times 10^{-13}$ and $[0.94, 1.08] \times 10^{-13}$ eV for GW230814 and GW231123, respectively, with 30% confidence for $P_{\rm fa} = 1\%$.

These results show that we are approaching the sensitivity required to place robust constraints on the vector boson mass. As the detectors continue to undergo improvements in subsequent observing runs, we anticipate a growing number of high-SNR events, which will enable increasingly sensitive searches and stronger constraints across a wide range of the mass parameter space. In addition, once the vector mass can be constrained with higher confidence, the results can be mapped to other interaction models [85].

## B. BSD search: Cygnus X-1

Among the 27 stage-2 candidates obtained from the BSD search, none pass the follow-up procedure. In the absence of a plausible signal candidate, we set upper limits on the strain amplitude of CWs emitted by a VBC surrounding Cygnus X-1. In the following subsections, we outline the procedure used to estimate these upper limits and describe how they are subsequently translated into constraints on the mass of a hypothetical ultralight vector boson.

### 1. *Upper limits and Sensitivity*

In this section, we estimate upper limits on the strain amplitude $h_0$, defined as the maximum amplitude above which the presence of a CW signal can be excluded at a given confidence level. The limits are computed using a conservative semi-analytical method previously applied in Refs. [67, 69, 102]. The method evaluates the upper limits in each 1 Hz frequency band using the analytical relation [67, 69, 102]

$$h_{\rm UL}^{95\%} \approx \frac{\mathcal{B}}{N^{1/4}} \sqrt{\frac{S_n(f)}{T_{\rm coh}}} \sqrt{{\rm CR}_{\rm max} + 1.645}, \tag{8}$$

where $N \sim T_{\rm obs}/T_{\rm coh}$ is the number of segments used to construct the peakmap, the value 1.645 is computed from Eq.(67) in Ref. [103] fixing the confidence level to 95%, $S_n^{1/2}(f)$ is the detector average ASD, and ${\rm CR}_{\rm max}$ is the maximum CR value observed in the band. The coefficient $\mathcal{B}$ accounts for the average detector response to the source sky position and signal polarization and depends on the peak selection threshold. For this search and the sky position of Cygnus X-1, we evaluate $\mathcal{B} \approx 3.37$ in Livingston and $\mathcal{B} \approx 3.30$ in Hanford. The computation of these factors is detailed in Appendix A 5 following the discussions in Refs. [69, 103, 157]. The final upper limit placed in each band is taken as the less constraining limits of the two detectors.

We have verified that this semi-analytical approach yields conservative upper limits compared to those obtained with a classical frequentist approach based on simulated signal injections, while requiring fewer computational resources. This verification was performed on ten 1 Hz frequency bands, randomly selected within the search frequency range, using simulated data that reproduces the detectors' noise levels. The validation complements previous checks carried out for other observing runs of the LIGO and Virgo detectors and for similar BSD-based methods [69, 158].

In Fig. 4, we show the joint upper limits at a 95% confidence level, reporting in each frequency band the worst-case estimate between the two detectors. We also report the boson masses corresponding to the frequency axis, assuming the central astrophysical parameters of Cygnus X-1 reported in Table I.

We quantify the performance of the search using the *sensitivity depth* [159], defined as

$$\mathcal{D}^{95\%} = \frac{\sqrt{S_n(f)}}{h_{\rm UL}^{95\%}}. \tag{9}$$

This quantity has become a key figure for assessing the performance of a CW search configuration, independent of the noise level [102, 160–162]. For the BSD search, we report a sensitivity depth of 37.22 $\text{Hz}^{-1/2}$ in the band centered on 50.5 Hz corresponding to the optimal boson mass for Cygnus X-1 (see Table III). The average depth over all the analyzed bands is 35.15 $\text{Hz}^{-1/2}$ and is more

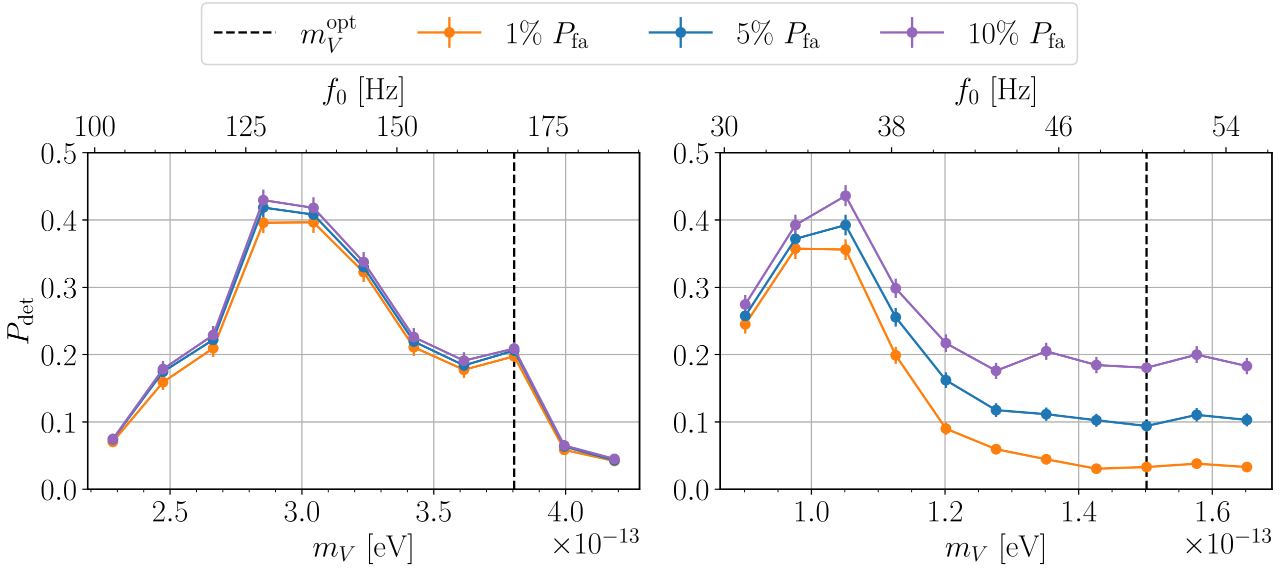

Figure 3. The detection probability $P_{\rm det}$ as a function of $m_V$ (bottom axis) and the corresponding GW frequency $f_0$ in the detector frame (top axis) with a 1% (orange), 5% (blue), and 10% (purple) false alarm probability for the remnant BHs from the GW230814 (left) and GW231123 (right) mergers. A redshift correction has been applied to obtain $f_0$ in the detector frame using the median $D_L$ value for each remnant (as reported in Table I). The vertical dashed lines mark the optimal boson masses $m_V^{\rm opt}$ for the remnants with median parameters also shown in Table I. The error bars represent the $1\sigma$ beta-binomial uncertainty in $P_{\rm det}$ [156].

or less constant in all the bands, excluding the one with significant noise disturbances.

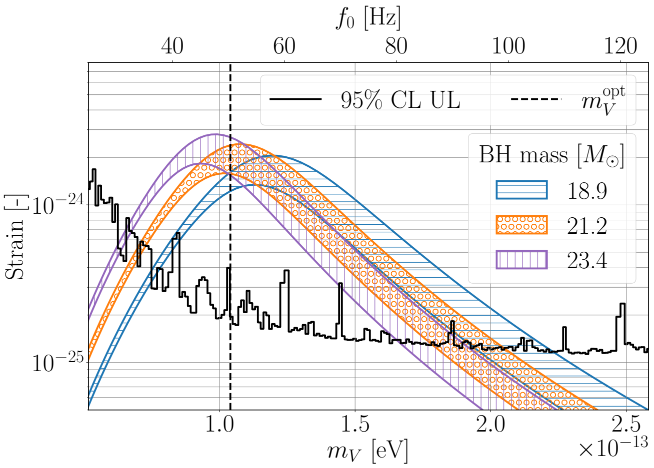

Figure 4. Upper limit estimates at a 95% confidence level (black curve) as a function of frequency (top axis) and the corresponding boson mass assuming the central values for the mass and age of Cygnus X-1 (bottom axis). The hashed regions correspond to the predicted strain amplitude from a VBC around Cygnus X-1, assuming the central value (orange, circles), 5th percentile (blue, horizontal lines), and 95th percentile (purple, vertical lines) of the BH mass posterior distribution from [90]. We assume the BH initial spin to be $\chi_i = 0.95$ and the hashed regions account for uncertainties in the BH age and distance.

### 2. *Constraints*

The upper limits obtained in the previous section can be used to constrain the existence of ultralight vector bosons by comparing them to the expected strain amplitude of a signal emitted by a VBC in Cygnus X-1. The amplitude is estimated assuming the central value, the 5th, and the 95th percentiles of the BH mass posterior distribution reported in Ref. [90]. We also consider the uncertainties in the BH age and distance and assume the BH spin before the superradiant instability to be $\chi_i = 0.95$. The amplitude is then evaluated at different boson masses (i.e., at different frequencies) using the `SuperRad` model [52, 97]. The simulated strain amplitudes are shown in Fig. 4, along with the upper limits derived in the previous section.

By comparing the upper limits with the expected strain amplitude, we can exclude the presence of a signal emitted by a VBC in Cygnus X-1 in every frequency band in the range 41.25–80 Hz, with the exception of the narrow band 69.75–70.25 Hz. The absence of a signal in these bands excludes the existence of an ultralight vector boson with a mass in the range $[0.85, 1.65] \times 10^{-13}$ eV (excluding the band $[1.44, 1.45] \times 10^{-13}$ eV).

These exclusion regions are obtained under the assumption that the initial spin of the BH was $\chi_i = 0.95$. This assumption can be relaxed by computing the exclusion region for different initial spin values. As the assumed initial spin decreases, the expected amplitude decreases accordingly. Nevertheless, based on `SuperRad` simulations, for any value $\chi_i > 0.5$, our upper limits can constrain the existence of a signal between 41.25 and 77.25 Hz, corresponding to boson masses within the range $[0.85, 1.59] \times 10^{-13}$ eV (with the same excluded band as before). For spin values $\chi_i < 0.5$, the lower expected amplitude narrows down the constrained frequency range. At $\chi_i = 0.2$, we are still able to constrain frequencies in the range 50.25–77.25 Hz and boson masses $[1.03, 1.59] \times 10^{-13}$ eV. For lower initial spins $\chi_i < 0.2$, the expected signal amplitude decreases rapidly, and the region of parameter space that can be meaningfully constrained correspondingly narrows and eventually vanishes. All of these exclusion intervals are computed at a 95% confidence and using the least constraining values for the BH age, distance, and mass.

## VII. CONCLUSION

In this paper, we carry out the first directed searches for long-duration, quasi-monochromatic GWs from VBCs around known BHs. We analyze data from the first part of the LVK's fourth observing run, and we use two semi-coherent CW search methods, HMM tracking and the Binary BSD-VBC pipeline. Having found no evidence of a GW signal, we estimate the range of ultralight vector boson masses that can be constrained. From the HMM search, we disfavor the vector mass ranges $[0.94, 1.08]$ and $[2.75, 3.28] \times 10^{-13}$ eV at 30% confidence ($P_{\text{fa}} = 1\%$). While the present search sensitivity is limited because we target remnant BHs with SNR values $\lesssim 40$—and thus the confidence level remains statistically insignificant—future searches targeting higher SNR events are expected to yield high-confidence constraints. Meanwhile, the BSD-based search excludes the mass range $[0.85, 1.59] \times 10^{-13}$ eV at 95% confidence, assuming an initial spin value $\chi_i > 0.5$ for Cygnus X-1.

As the BSD search demonstrates, we are now able to set constraints on the existence of ultralight vector bosons by targeting known galactic BHs. Although the constraints obtained from Cygnus X-1 cover only a narrow range of masses, future improvements in detector sensitivity will enhance these constraints. The boson mass ranges that can be constrained also highly depend upon the BH parameters. Therefore, running similar searches targeting other known galactic BHs could extend the exclusion region.

The first HMM search targeting binary merger remnants demonstrates that we are approaching the required sensitivity to place high-confidence constraints on a range of vector masses. Targeting young merger remnants allows us to set independent constraints with minimal assumptions about the BH's history and evolution since formation. Several contributing factors will improve the sensitivity of this type of search: in particular, both increased detector sensitivity and improved search methodologies. Future observing runs and next-generation GW detectors will offer enhanced sensitivity, enabling the detection of numerous binary mergers in the high-SNR regime [57–59, 88]. These high-SNR events will yield remnant BHs with masses and spins that are more accurately and precisely measured. For HMM-based searches, improved posteriors on these parameters will directly translate into tighter constraints on the vector boson mass. In addition, future searches can incorporate modifications to the analysis pipelines to further improve search sensitivity (e.g., extending the HMM-based analysis in suitable cases to track time derivatives of the signal frequency within the $\mathcal{F}$-statistic, as demonstrated in Ref. [127]).

Observational studies have indirectly constrained the existence of ultralight vector bosons either from BH spin measurements [30, 32], by reinterpreting the results of GW searches [71], or from searches for a stochastic GW background [74]. A recent analysis using the GW231123 and GW190517 constituent BHs disfavors a vector mass range of $[0.11, 18] \times 10^{-13}$ eV assuming a BH age of $10^5$ yrs [63]. In other searches, the interaction of ultralight vectors with ground-based GW detectors has been directly constrained [80, 81]. While each approach involves its own assumptions and limitations, the results presented in this paper provide independent constraints obtained from directed searches that, consistent with previous studies, disfavor the existence of vector bosons with masses of $\sim 1 \times 10^{-13}$ eV.

## VIII. ACKNOWLEDGMENTS

This material is based upon work supported by NSF's LIGO Laboratory, which is a major facility fully funded by the National Science Foundation. The authors also gratefully acknowledge the support of the Science and Technology Facilities Council (STFC) of the United Kingdom, the Max-Planck-Society (MPS), and the State of Niedersachsen/Germany for support of the construction of Advanced LIGO and construction and operation of the GEO 600 detector. Additional support for Advanced LIGO was provided by the Australian Research Council. The authors gratefully acknowledge the Italian Istituto Nazionale di Fisica Nucleare (INFN), the French Centre National de la Recherche Scientifique (CNRS) and the Netherlands Organization for Scientific Research (NWO) for the construction and operation of the Virgo detector and the creation and support of the EGO consortium. The authors also gratefully acknowledge research support from these agencies as well as by the Council of Scientific and Industrial Research of India, the Department of Science and Technology, India, the Science & Engineering Research Board (SERB), India, the Ministry of Human Resource Development, India, the Spanish Agencia Estatal de Investigación (AEI), the Spanish Ministerio de Ciencia, Innovación y Universidades, the European Union NextGenerationEU/PRTR (PRTR-C17.I1), the ICSC - CentroNazionale di Ricerca in High Performance Computing, Big Data and Quantum Computing, funded by the European Union NextGenerationEU, the Comunitat Autonòma de les Illes Balears through the Conselleria d'Educació i Universitats, the Conselleria d'Innovació, Universitats, Ciència i Societat Digital de la Generalitat Valenciana and the CERCA Programme Generalitat de Catalunya, Spain, the Polish National Agency for Academic Exchange, the National Science Centre of Poland and the European Union - European Regional Development Fund; the Foundation for Polish Science (FNP), the Polish Ministry of Science and Higher Education, the Swiss National Science Foundation (SNSF), the Russian Science Foundation, the European Commission, the European Social Funds (ESF), the European Regional Development Funds (ERDF), the Royal Society, the Scottish Funding Council, the Scottish Universities Physics Alliance, the Hungarian Scientific Research Fund (OTKA), the French Lyon Institute of Origins (LIO), the Belgian Fonds de la Recherche Scientifique (FRS-FNRS), Actions de Recherche Concertées (ARC) and Fonds Wetenschappelijk Onderzoek Vlaanderen (FWO), the supercomputing facilities of the Université catholique de Louvain (CISM/UCL) and the Consortium des Équipements de Calcul Intensif en Fédération Wallonie Bruxelles (CÉCI), Belgium, the Paris Île-de-France Region, the National Research, Development and Innovation Office of Hungary (NKFIH), the National Research Foundation of Korea, the Natural Sciences and Engineering Research Council of Canada (NSERC), the Canadian Foundation for Innovation (CFI), the Brazilian Ministry of Science, Technology, and Innovations, the International Center for Theoretical Physics South American Institute for Fundamental Research (ICTP-SAIFR), the Research Grants Council of Hong Kong, the National Natural Science Foundation of China (NSFC), the Israel Science Foundation (ISF), the US-Israel Binational Science Fund (BSF), the Leverhulme Trust, the Research Corporation, the National Science and Technology Council (NSTC), Taiwan, the United States Department of Energy, and the Kavli Foundation. The authors gratefully acknowledge the support of the NSF, STFC, INFN and CNRS for provision of computational resources.

This work was supported by MEXT, the JSPS Leading-edge Research Infrastructure Program, JSPS Grant-in-Aid for Specially Promoted Research 26000005, JSPS Grant-in-Aid for Scientific Research on Innovative Areas 2402: 24103006, 24103005, and 2905: JP17H06358, JP17H06361 and JP17H06364, JSPS Core-to-Core Program A. Advanced Research Networks, JSPS Grants-in-Aid for Scientific Research (S) 17H06133 and 20H05639, JSPS Grant-in-Aid for Transformative Research Areas (A) 20A203: JP20H05854, the joint research program of the Institute for Cosmic Ray Research, University of Tokyo, the National Research Foundation (NRF), the Computing Infrastructure Project of the Global Science experimental Data hub Center (GSDC) at KISTI, the Korea Astronomy and Space Science Institute (KASI), the Ministry of Science and ICT (MSIT) in Korea, Academia Sinica (AS), the AS Grid Center (ASGC) and the National Science and Technology Council (NSTC) in Taiwan under grants including the Science Vanguard Research Program, the Advanced Technology Center (ATC) of NAOJ, and the Mechanical Engineering Center of KEK.

Additional acknowledgements for support of individual authors may be found in the following document: `https://dcc.ligo.org/LIGO-M2300033/public`. For the purpose of open access, the authors have applied a Creative Commons Attribution (CC BY) license to any Author Accepted Manuscript version arising. We request that citations to this article use 'A. G. Abac *et al.* (LIGO-Virgo-KAGRA Collaboration), ...' or similar phrasing, depending on journal convention.

## Appendix A: Details on BSD search pipeline

### 1. Signal phase

The phase evolution of a monochromatic signal emitted by a source in a binary system is, in the detector frame, given by

$$\Phi(t) = 2\pi f_0 t + \Delta\phi(t), \tag{A1}$$

where $f_0$ is the signal frequency. The phase modulation due to the combined motion of the source and the detector is given by

$$\Delta\phi(t) = 2\pi f_0 \left[ \frac{\mathbf{r}\cdot\hat{\mathbf{n}}}{c} - \frac{R\big(t + \frac{\mathbf{r}\cdot\hat{\mathbf{n}}}{c}\big)}{c} \right], \tag{A2}$$

with $\mathbf{r}$ the position vector of the detector relative to the Solar-System Barycenter (SSB), and $\hat{\mathbf{n}}$ the unit vector pointing from the SSB to the source. The Rømer delay, $R$, can be expressed in a low-eccentricity orbit approximation (consistent with the nearly circular orbit of Cygnus X-1), neglecting an irrelevant constant term [140]:

$$\begin{aligned}\frac{R(t)}{c} = a_\mathrm{p} \Bigg[ & \sin(\psi(t)) + \frac{e\cos(\omega)}{2}\sin(2\psi(t)) \\ & - \frac{e\sin(\omega)}{2}\cos(2\psi(t)) \Bigg],\end{aligned} \tag{A3}$$

where $a_\mathrm{p}$ is the projected semi-major axis, $e$ is the orbital eccentricity, and $\omega$ is the argument of periapse. The function $\psi$ is the mean orbital phase measured from the time of ascending node $t_\mathrm{asc}$, defined as

$$\psi(t) = \Omega(t - t_\mathrm{asc}), \tag{A4}$$

with $\Omega$ the orbital angular frequency.

### 2. Heterodyne correction

The procedure of the heterodyne correction of BSD is presented in Ref. [89]. It consists of multiplying the data by a complex phase factor $\exp(-i\,\Delta\phi(t))$ to correct Doppler-induced variations. The phase $\Delta\phi(t)$ is computed from Eq. (A2) assuming a set of parameters $\mathbf{\Lambda}$ to compensate for the delays in the signal arrival time from the motion of the source and the detector. The modulation also depends on the unknown signal frequency. Taking advantage of the BSD framework and the downsampling of the data into 1 Hz bands, we substitute for $f_0$ a reference value fixed at the central frequency. By doing so, we ensure that the error in frequency is bounded by $|f_0 - f_{0,\mathrm{ref}}| \leq 0.5$ Hz.

### 3. Detection statistic

The CR statistic is estimated on a peakmap by projecting the peakmap on the frequency axis and producing the distribution of number of peaks per frequency bin $n(f)$. We then use a robust estimator defined as [103]

$$\mathrm{CR}(f) = \frac{n(f) - \bar{n}}{\sigma}, \tag{A5}$$

where $\bar{n}$ is the median of the number of peaks per frequency bin, and the dispersion parameter $\sigma$ is defined by

$$\sigma = \frac{\mathrm{median}(|n(f) - \bar{n}|)}{0.6745}. \tag{A6}$$

The normalization factor $\sigma$ ensures that if $n$ follows a normal distribution, then $\sigma$ is the standard deviation.

### 4. Template placement

For the placement of templates to cover the $a_\mathrm{p}, t_\mathrm{asc}$ parameter space, we use a restricted version of the binary search metric described in Ref. [140]. We use the metric in the semicoherent short-segment regime, where $T_\mathrm{coh} \ll P$,

$$g_{a_\mathrm{p}a_\mathrm{p}} = \frac{1}{6}(\pi\Omega T_\mathrm{coh} f_0)^2, \tag{A7}$$

$$g_{t_\mathrm{asc}t_\mathrm{asc}} = \frac{1}{6}\left(\pi\Omega^2 T_\mathrm{coh} f_0 a_\mathrm{p}\right)^2. \tag{A8}$$

The resolution in an orbital parameter $i$ is then given by [140][11]

$$\delta_i = \sqrt{0.1[g^{-1}]^{ii}}, \tag{A9}$$

where $g^{-1}$ is the inverse metric, and the factor 0.1 corresponds to a maximal loss of signal-to-noise ratio of 10%. Explicitly, we get for the two remaining orbital parameters $a_\mathrm{p}$ and $t_\mathrm{asc}$:

$$\delta a_\mathrm{p} = \frac{\sqrt{0.6}}{\pi\Omega T_\mathrm{coh} f_0}, \tag{A10}$$

$$\delta t_\mathrm{asc} = \frac{\sqrt{0.6}}{\pi\Omega^2 a_\mathrm{p} T_\mathrm{coh} f_0}. \tag{A11}$$

Constructing a template grid with varying resolution across the parameter space can be challenging. To simplify this, we adopt a conservative strategy by fixing all the variable parameters to values that maximize grid density. Specifically, we use the maximum frequency $f_{0,\,\mathrm{max}}$ within the 1 Hz band, and the maximum value of the projected semi-major axis $a_\mathrm{p,max}$ within the range to be covered. Fixing the resolutions as $\delta a_\mathrm{p}(f_{0,\,\mathrm{max}})$ and $\delta t_\mathrm{asc}(f_{0,\,\mathrm{max}}, a_\mathrm{p,max})$ over the entire parameter space ensures an overcoverage of the search parameter space. With this simplification, the template grid is constructed using a standard square lattice $\mathbb{Z}_2$, as described in Refs. [140, 141].

With this placement strategy, the number of templates needed to cover the parameter space is given by [140]

$$N \approx \left\lceil \frac{\mathcal{R}_{a_\mathrm{p}}}{\sqrt{2}\delta a_\mathrm{p}} \right\rceil \left\lceil \frac{\mathcal{R}_{t_\mathrm{asc}}}{\sqrt{2}\delta t_\mathrm{asc}} \right\rceil, \tag{A12}$$

where $\mathcal{R}_{a_\mathrm{p}}$ and $\mathcal{R}_{t_\mathrm{asc}}$ are the sizes of the dimensions to be covered.

### 5. Upper limits formula

The average prefactor $\mathcal{B}$ in Eq. 8 is computed by reproducing the derivation of Eq.(67) in Ref. [103] and according to the correction detailed in Ref. [157]. The general expression of $\mathcal{B}$ is a function of time, the signal polarization angle $\psi$, the source sky-position (RA, Dec), and the source inclination angle $\iota$. It can be expressed as

$$\mathcal{B} = \sqrt{\frac{\pi}{2.4308\left\langle (F_+A_+ + F_\times A_\times)^2\right\rangle_t}}\left(\frac{p_0(1-p_0)}{p_1^2}\right)^{1/4} \tag{A13}$$

where the factor $\frac{\pi}{2.4308}$ is taken from Eq. B18 in Ref. [103], and $p_0$ and $p_1$ are functions of the peak selection threshold $\theta_\mathrm{thr}$ [103, 157]. For $\theta_\mathrm{thr} = 2.5$, we have $p_0 = 0.075$ and $p_1 = 0.096$, using the updated definition of $p_1$ shown in Ref. [157]. The two beam pattern functions $F_+$ and $F_\times$ are defined in Ref. [129], and the polarization amplitudes are given by $A_+ = \frac{1+\cos^2\iota}{2}$ and $A_\times = \cos\iota$ [103].

For the BSD search, we evaluate the expression of $\mathcal{B}$ for the sky-position of Cygnus X-1, and by averaging over the inclination angle error range [90] and the polarization angle $\psi \in [-\pi/4, \pi/4]$. Using properties of the beam pattern function [69], we can write

$$\left\langle (F_+A_+ + F_\times A_\times)^2\right\rangle_{t,\psi,\cos\iota}\Big|_\mathrm{Dec} = \left\langle F_\times^2\right\rangle_{t,\psi}\Big|_\mathrm{Dec}\left\langle A_+^2 + A_\times^2\right\rangle_{\cos\iota}. \tag{A14}$$

We compute $\left\langle A_+^2 + A_\times^2\right\rangle_{\cos\iota} = 1.582$, and, following the development in Ref. [69], $\left\langle F_\times^2\right\rangle_{t,\psi}\Big|_\mathrm{Dec} = 0.197$ in Livingston and 0.206 in Hanford. Injecting these values in Eq. A13 gives $\mathcal{B} \approx 3.37$ in Livingston and $\mathcal{B} \approx 3.30$ in Hanford.

---

[11] Note that a factor 2 is missing compared to Ref. [140]. In the present work, these resolutions are used to compute the distance from a template placed on the parameter space rather than the total extent of this template.

## Appendix B: Follow-up vetoes

As detailed in this section, we only veto candidates that we are confident are caused by noise artifacts. The safety of the vetoes used prior to the final manual inspection has been verified in previous analyses employing HMM- and BSD-based techniques, using Monte Carlo simulations in clean frequency bands (see, e.g., Refs. [69, 120, 121]). However, if a GW signal is present in the data but overlaps with a noise artifact, it is deemed "contaminated" and will be vetoed. In other words, we do not yet have a sufficiently reliable method to separate signals from overlapping, unidentified noise artifacts. Consequently, the false dismissal probability cannot be easily quantified for the vetoes discussed here with the presence of noise artifacts.

### 1. HMM searches: Merger remnants

#### a. *Known-line veto*

The first veto we use in the HMM search involves comparing the frequency path of each signal candidate against all known instrumental lines present in either the Hanford or Livingston detector to see if there is any overlap [155]. We increase the width of the Viterbi path $\delta f \approx 10^{-6} f_i + 8\,\delta f_{\mathrm{SFT}}$, where $f_i$ is a given frequency anywhere along the path and $\delta f_{\mathrm{SFT}}$ is the SFT frequency bin width. The first part accounts for the Doppler modulation due to Earth's sidereal motion, and the second part accounts for the additional data used in the $\mathcal{F}$-statistic calculation. We consider candidates with a wide range of sky positions, start times, and total durations. Because most search timescales are much shorter than a year, we conservatively choose not to factor in Earth's orbital Doppler modulation in this initial veto. The few longer-duration candidates (with $T_{\mathrm{obs}} >$ a few months) that could have been vetoed if Earth's orbital Doppler modulation had been included are addressed in later steps.

#### b. *Single-interferometer veto*

Next we use a technique that vetoes candidates caused by noise artifacts in a single detector that are not yet well understood or identified in the official release of O4a known instrumental lines. The detailed criteria are as follows: We run the search with each interferometer individually. Then, a signal candidate can be vetoed as an unknown instrumental line if the detection statistic in one detector is below threshold while the other is greater than the detection statistic from the combined detector search, and if the Viterbi paths of the latter two searches overlap.

#### c. *Manual inspection*

Because the previous two veto procedures are designed for following up long-duration CW search candidates, they are not always able to effectively identify candidates from a short-duration search. Thus, there are many candidates that still remain at this stage. We visually inspect each candidate using a variety of approaches designed to distinguish signals from noise artifacts, typically applying multiple checks to each candidate for confirmation. These approaches are listed here. We note that if a true GW signal overlaps with a noise artifact, it would be deemed contaminated and vetoed. Since these short-duration searches are particularly susceptible to transient detector noise, injection-based estimation of the false dismissal probability for the manually vetoed candidates is infeasible in practice.

1. We relax certain criteria of the single interferometer veto based on close inspection; for example, we veto any candidate whose detection statistic is below threshold in one detector and anomalously high in the other (e.g., $\bar{\mathcal{L}} \gtrsim 100$), regardless of the detection statistic from the original combined search.

2. We compare the frequency drift of the candidate across $T_{\mathrm{obs}}$ against the expected frequency drift of a real signal. If the candidate frequency remains within a single bin for at least three quarters of the total duration, *and* if it is not identified by at least one other configuration with a larger value of $T_{\mathrm{coh}}$ (which is by design more sensitive to signals with smaller frequency drifts), then it is unlikely to be a real signal. For example, one candidate from GW231123 has an apparent $\dot{f}_0 < 10^{-8}$ Hz s$^{-1}$, but the expected frequency drift optimized for $T_{\mathrm{coh}} =$ 14.2 m is $\dot{f}_0 \sim 7 \times 10^{-7}$ Hz s$^{-1}$. This veto criterion is typically applied in conjunction with at least one other veto as a cross-check.

3. We assess whether the detection statistic of a given candidate is consistent with expectations for a signal from the remnant BH given its distance estimate. If the statistic is significantly larger than expected (e.g., $\bar{\mathcal{L}} \gtrsim 100$), we can veto the candidate as a loud but unidentified noise artifact. This veto is applied only in conjunction with at least one other veto. For example, if the detection statistic combining two detectors is significantly larger than expected for the target's distance, it is usually accompanied by the candidate being much louder in one detector than in the other, in which case the candidate is also vetoed according to the first manual inspection criterion described above.

4. We examine the signal candidate in the spectrogram from each interferometer in the relevant frequency band and time segment to determine whether it overlaps with any visible noise artifacts.

5. Finally, if two candidates with the same frequency path are found using two different search configurations—in other words, if the same candidate is identified in two different searches—and if one of them has been vetoed by any of the above criteria, we consider the other likely to have arisen from the same artifacts. This veto criterion is typically applied in conjunction with other manual inspections as a cross-check.

### 2. BSD search: Cygnus X-1

For the BSD search, the 27 stage-2 candidates have been filtered by removing those associated with known instrumental lines [155] and clustering candidates that shared a common candidate. Six candidates remained after this filtering and are listed in Table VIII. The values reported in the table correspond to the averages of the template parameters between the two detectors, and the quoted uncertainties are obtained by propagating the template resolutions given in Eqs. A10 and A11. As discussed in Sec. III B 2, the other parameters, $\{\mathrm{RA}, \mathrm{Dec}, P, e, \omega\}$, are fixed to the central values listed in Tables I and II, and are therefore identical for all the candidates.

Given the small number of surviving candidates, we conducted the following tests and visually inspected the results for each. Although we did not formally estimate the false dismissal probability, the validity and safety of each veto have been confirmed by applying the follow-up procedure to simulated signals with parameters similar to those of the six candidates. The tests, adapted from previous BSD-based searches (e.g., [69, 120]), are grouped into three categories: (i) consistency of the candidate with its astrophysical parameters, (ii) consistency of the detection statistic with different search configurations, and (iii) a manual inspection where we associated some candidates to artifacts caused by non-Gaussianities in the detector. These tests are described in detail below.

Table VIII. Parameters of the candidates from the BSD search, averaged between the two detectors. For each candidate, we indicate the test by which it was vetoed.

| $f_0$ [Hz] | $a_\mathrm{p}$ [s] | $t_\mathrm{asc}$ [s] | Veto |
|---|---|---|---|
| 32.751 | $38.84 \pm 0.82$ | $5\,600 \pm 1\,700$ | Stat. |
| 37.131 | $36.09 \pm 0.73$ | $188\,100 \pm 1\,600$ | Manual |
| 41.176 | $36.79 \pm 0.66$ | $-4\,383 \pm 1\,400$ | Astro. |
| 41.627 | $38.60 \pm 0.65$ | $-11\,800 \pm 1\,300$ | Stat. |
| 53.890 | $40.62 \pm 0.50$ | $204\,700 \pm 950$ | Manual |
| 96.114 | $38.10 \pm 0.28$ | $223\,790 \pm 570$ | Manual |

#### a. *Known-line veto*

Similar to the HMM method, we veto any candidate whose frequency evolution crosses a known instrumental line in either the Hanford or Livingston detector [155]. For a candidate observed at a frequency $f_0$, we estimate the modulation range as $f_0 \pm \delta f$, where $\delta f$ is the modulation size computed with the parameters of the candidate, $\delta f = \max_t \left(\frac{\mathrm{d}\Delta\phi(\mathrm{t})}{\mathrm{d}t}\right)$, where $\Delta\phi(t)$ is the phase modulation defined in Eq. A2.

#### b. *Clustering*

During the coincident candidate selection process, we consider all possible pairs of candidates from both detectors. Some redundancy is therefore possible in the list of candidates. Indeed, from the eight candidates passing the known-line veto, two candidates are repeated twice, in association with two different (but similar) candidates in the second detectors. We therefore cluster these two sets of candidates and follow them up conjointly. The number of unique candidates is reduced to six.

#### c. *Astrophysical consistency veto*

The second step of the follow-up procedure involves assessing the consistency of each candidate with an astrophysical signal through two key checks. Any candidate failing at least one of these tests is discarded from further analysis.

1. **Frequency refinement.** Since the search demodulates the data using the central frequency of each 1 Hz band, a real signal may not be perfectly corrected if its true frequency differs from this reference. To refine the analysis, we re-run a localized search using the candidate recovered frequency as the reference frequency for demodulation. A genuine signal must persist with similar or improved significance under this correction.

2. **Unmodulated test.** As the search is directed toward a signal emitted from Cygnus X-1, the significance of an astrophysical signal should decrease when using parameters incompatible with the target. In particular, we try to recover the candidate without performing the heterodyne correction. A candidate persisting with comparable significance in this configuration cannot be of astrophysical origin and is therefore vetoed.

#### d. *Statistical consistency check*

1. **Sensitivity vetoes.** For a true signal, the detection statistic should scale with the sensitivity of each

detector. We check this by normalizing the CR with the median ASD of the 1 Hz band, $\sqrt{S_n}$. We then require

$$\frac{\mathrm{CR}_1}{\sqrt{S_{n_1}}} < 3\frac{\mathrm{CR}_2}{\sqrt{S_{n_2}}}, \tag{B1}$$

where detector 1 is less sensitive and detector 2 is more sensitive. The factor 3 is a conservative choice and indeed none of the candidate was vetoed by this check.

2. **Cumulative and Uniformity veto.** A genuine astrophysical CW signal should persist throughout the observation run, and we expect: (i) steadily increasing significance as more data are included, and (ii) the candidate to be present in any subset of the data.

   We first examined cumulative behavior by computing the CR and signal-to-noise ratio (SNR) over data segments whose durations increased in 30-day steps, for both detectors and for data with and without heterodyne correction. We compared the corrected and uncorrected results, looking for behavior inconsistent with the presence of a signal. One candidate was vetoed because the uncorrected data yielded higher significance for most of the run. A second candidate showed a sharp increase during the first month, indicating the presence of non-stationary noise.

   To verify the persistence across subsets, we analyzed one-month segments with various start times, again for both detectors and both data types. Some variation is expected due to varying duty cycles or noise levels, so results were interpreted with tolerance. For the second suspect candidate identified in the cumulative test, corrected and uncorrected data gave similar CR values except in the first month, where the corrected data produced a much higher CR. This confirmed the non-persistent nature of the candidate, and it was vetoed.

#### e. *Manual inspection*

Finally, we manually inspect the three remaining candidates. For each, we investigate the spectra of the corrected and uncorrected data using two different frequency resolutions: $5.5 \times 10^{-4}$ and $1.1 \times 10^{-5}$ Hz, corresponding to coherence times of 30 min and 1 day, respectively. In all three candidates' bands, we observe strong non-Gaussian noise profiles. Such non-Gaussianities are known to produce artifacts in specific frequency bins during peakmap peak selection [139], and, coincidentally, all the remaining candidates are present in one of these frequency bins. By slightly modifying the resolution of the background estimation used to compute the equalized spectra [139], we force the artifact-affected bins to be moved away from the candidate bins. This modified setup ensures that the candidates' frequency bins were not contaminated by the peakmap creation artifacts. We tested several such configurations, and in all cases the CR of each candidate dropped well below the selection threshold. For each of the three candidates, we have assessed the impact of these modified configurations on a simulated signal injection. The injections were done with the same orbital parameters as the candidates. We have chosen the injection amplitudes from Eq. (8) by replacing $\mathrm{CR}_{\mathrm{max}}$ with the threshold value in band as defined in Sec. III B 3. We observed that all the injections remained detectable in all configurations considered. On this basis, and given that candidates are not significant, in the sense discussed in Sec. III B 3, in unaffected configurations, we vetoed all remaining candidates.

## REFERENCES

[1] G. Bertone and T. M. P. Tait, Nature **562**, 51 (2018).
[2] G. Bertone and D. Hooper, Rev. Mod. Phys. **90**, 045002 (2018).
[3] E. Oks, New Astronomy Reviews **93**, 101632 (2021).
[4] M. Baryakhtar, L. Rosenberg, and G. Rybka, Reports on Progress in Physics **88**, 106901 (2025).
[5] R. D. Peccei and H. R. Quinn, Phys. Rev. Lett. **38**, 1440 (1977).
[6] R. D. Peccei and H. R. Quinn, Phys. Rev. D **16**, 1791 (1977).
[7] S. Weinberg, Phys. Rev. Lett. **40**, 223 (1978).
[8] A. Arvanitaki, S. Dimopoulos, S. Dubovsky, N. Kaloper, and J. March-Russell, Phys. Rev. D **81**, 123530 (2010).
[9] F. F. Freitas, C. A. Herdeiro, A. P. Morais, A. Onofre, R. Pasechnik, E. Radu, N. Sanchis-Gual, and R. Santos, Journal of Cosmology and Astroparticle Physics **2021**, 047 (2021).
[10] B. Holdom, Physics Letters B **166**, 196 (1986).
[11] M. Goodsell, J. Jaeckel, J. Redondo, and A. Ringwald, Journal of High Energy Physics **2009**, 027 (2009).
[12] J. Jaeckel and A. Ringwald, Annual Review of Nuclear and Particle Science **60**, 405 (2010).
[13] R. Essig *et al.*, in *Snowmass 2013: Snowmass on the Mississippi* (2013) arXiv:1311.0029 [hep-ph].
[14] L. Hui, J. P. Ostriker, S. Tremaine, and E. Witten, Phys. Rev. D **95**, 043541 (2017).
[15] P. Agrawal, N. Kitajima, M. Reece, T. Sekiguchi, and F. Takahashi, Physics Letters B **801**, 135136 (2020).
[16] M. Fabbrichesi, E. Gabrielli, and G. Lanfranchi, *The physics of the dark photon* (Springer International Publishing, 2021).
[17] T. Clifton, P. G. Ferreira, A. Padilla, and C. Skordis, Phys. Rept. **513**, 1 (2012).
[18] E. Babichev, L. Marzola, M. Raidal, A. Schmidt-May, F. Urban, H. Veermäe, and M. v. Strauss, Journal of Cosmology and Astroparticle Physics **2016**, 016 (2016).
[19] E. Babichev, L. Marzola, M. Raidal, A. Schmidt-May, F. Urban, H. Veermäe, and M. von Strauss, Phys. Rev. D **94**, 084055 (2016).
[20] K. Aoki and S. Mukohyama, Phys. Rev. D **94**, 024001 (2016).

[21] K. Aoki and K.-i. Maeda, Phys. Rev. D **97**, 044002 (2018).

[22] Y. Manita, K. Aoki, T. Fujita, and S. Mukohyama, Phys. Rev. D **107**, 104007 (2023).

[23] A. Arvanitaki and S. Dubovsky, Phys. Rev. D **83**, 044026 (2011).

[24] H. Yoshino and H. Kodama, Progress of Theoretical and Experimental Physics **2014** (2014), 10.1093/ptep/ptu029, 043E02.

[25] H. Yoshino and H. Kodama, Progress of Theoretical and Experimental Physics **2015** (2015), 10.1093/ptep/ptv067, 061E01.

[26] A. Arvanitaki, M. Baryakhtar, and X. Huang, Phys. Rev. D **91**, 084011 (2015).

[27] A. Arvanitaki, M. Baryakhtar, S. Dimopoulos, S. Dubovsky, and R. Lasenby, Phys. Rev. D **95**, 043001 (2017).

[28] R. Brito, S. Ghosh, E. Barausse, E. Berti, V. Cardoso, I. Dvorkin, A. Klein, and P. Pani, Phys. Rev. Lett. **119**, 131101 (2017).

[29] R. Brito, S. Ghosh, E. Barausse, E. Berti, V. Cardoso, I. Dvorkin, A. Klein, and P. Pani, Phys. Rev. D **96**, 064050 (2017).

[30] M. Baryakhtar, R. Lasenby, and M. Teo, Phys. Rev. D **96**, 035019 (2017).

[31] K. H. M. Chan and O. A. Hannuksela, Phys. Rev. D **109**, 023009 (2024).

[32] V. Cardoso, Óscar J.C. Dias, G. S. Hartnett, M. Middleton, P. Pani, and J. E. Santos, Journal of Cosmology and Astroparticle Physics **2018**, 043 (2018).

[33] D. Baumann, H. S. Chia, and R. A. Porto, Phys. Rev. D **99**, 044001 (2019).

[34] O. A. Hannuksela, K. W. K. Wong, R. Brito, E. Berti, and T. G. F. Li, Nature Astronomy **3**, 447 (2019).

[35] J. Zhang and H. Yang, Phys. Rev. D **99**, 064018 (2019).

[36] W. E. East, Phys. Rev. D **96**, 024004 (2017).

[37] W. E. East and F. Pretorius, Phys. Rev. Lett. **119**, 041101 (2017).

[38] W. E. East, Phys. Rev. Lett. **121**, 131104 (2018).

[39] N. Siemonsen and W. E. East, Phys. Rev. D **101**, 024019 (2020).

[40] R. Brito, V. Cardoso, and P. Pani, Lect. Notes Phys. **906**, pp.1 (2020), arXiv:1501.06570 [gr-qc].

[41] R. Penrose, Nuovo Cimento Rivista Serie **1**, 252 (1969).

[42] W. H. Press and S. A. Teukolsky, Nature (London) **238**, 211 (1972).

[43] Y. B. Zel'Dovich, Soviet Journal of Experimental and Theoretical Physics Letters **14**, 180 (1971).

[44] A. A. Starobinskii, Soviet Phys JETP **37**, 28 (1973).

[45] S. Detweiler, Phys. Rev. D **22**, 2323 (1980).

[46] J. D. Bekenstein, Phys. Rev. D **7**, 949 (1973).

[47] S. R. Dolan, Phys. Rev. D **76**, 084001 (2007).

[48] C. A. Herdeiro, E. Radu, and N. M. Santos, Physics Letters B **824**, 136835 (2022).

[49] M. Isi, L. Sun, R. Brito, and A. Melatos, Phys. Rev. D **99**, 084042 (2019).

[50] M. Baryakhtar, M. Galanis, R. Lasenby, and O. Simon, Phys. Rev. D **103**, 095019 (2021).

[51] N. Siemonsen, C. Mondino, D. Egaña Ugrinovic, J. Huang, M. Baryakhtar, and W. E. East, Phys. Rev. D **107**, 075025 (2023).

[52] T. May, W. E. East, and N. Siemonsen, Phys. Rev. D **111**, 044062 (2025).

[53] J. Aasi *et al.*, Classical and Quantum Gravity **32**, 074001 (2015).

[54] F. Acernese *et al.*, Classical and Quantum Gravity **32**, 024001 (2014).

[55] T. Akutsu *et al.*, Progress of Theoretical and Experimental Physics **2021**, 05A101 (2020), https://academic.oup.com/ptep/article-pdf/2021/5/05A101/37974994/ptaa125.pdf.

[56] W. Jia *et al.*, Science **385**, 1318 (2024), https://www.science.org/doi/pdf/10.1126/science.ado8069.

[57] B. P. Abbott *et al.*, Living Reviews in Relativity **23**, 3 (2020).

[58] M. Punturo *et al.*, *Proceedings, 14th workshop on gravitational wave data analysis (GWDAW-14): Rome, Italy, January 26-29, 2010*, Classical and Quantum Gravity **27**, 194002 (2010).

[59] M. Evans, R. X. Adhikari, C. Afle, S. W. Ballmer, S. Biscoveanu, S. Borhanian, D. A. Brown, Y. Chen, R. Eisenstein, A. Gruson, A. Gupta, E. D. Hall, R. Huxford, B. Kamai, R. Kashyap, J. S. Kissel, K. Kuns, P. Landry, A. Lenon, G. Lovelace, L. McCuller, K. K. Y. Ng, A. H. Nitz, J. Read, B. S. Sathyaprakash, D. H. Shoemaker, B. J. J. Slagmolen, J. R. Smith, V. Srivastava, L. Sun, S. Vitale, and R. Weiss, arXiv e-prints (2021), arXiv:2109.09882 [astro-ph.IM].

[60] K. K. Y. Ng, S. Vitale, O. A. Hannuksela, and T. G. F. Li, Phys. Rev. Lett. **126**, 151102 (2021).

[61] A. Caputo, G. Franciolini, and S. J. Witte, "Superradiance Constraints from GW231123," (2025), arXiv:2507.21788 [hep-ph].

[62] A. G. Abac *et al.* (LIGO Scientific Collaboration, Virgo Collaboration, and KAGRA Collaboration), The Astrophysical Journal Letters **993**, L21 (2025).

[63] P. S. Aswathi, W. E. East, N. Siemonsen, L. Sun, and D. Jones, Phys. Rev. D **112**, 123048 (2025).

[64] A. Mummery, J. Jiang, A. Ingram, A. Fabian, and J. Rule, Mon. Not. Roy. Astron. Soc. **544**, 2880 (2025), arXiv:2505.13119 [astro-ph.HE].

[65] C. S. Reynolds, Nature Astron. **3**, 41 (2019), arXiv:1903.11704 [astro-ph.HE].

[66] J. E. McClintock, R. Narayan, and J. F. Steiner, Space Sci. Rev. **183**, 295 (2014), arXiv:1303.1583 [astro-ph.HE].

[67] R. Abbott *et al.* (The LIGO Scientific Collaboration, the Virgo Collaboration, and the KAGRA Collaboration), Phys. Rev. D **105**, 102001 (2022).

[68] C. Palomba *et al.*, Phys. Rev. Lett. **123**, 171101 (2019).

[69] R. Abbott *et al.* (KAGRA, LIGO Scientific, VIRGO), Phys. Rev. D **106**, 042003 (2022).

[70] S. J. Zhu, M. Baryakhtar, M. A. Papa, D. Tsuna, N. Kawanaka, and H.-B. Eggenstein, Phys. Rev. D **102**, 063020 (2020).

[71] V. Dergachev and M. A. Papa, Phys. Rev. Lett. **123**, 101101 (2019).

[72] L. Tsukada, T. Callister, A. Matas, and P. Meyers, Phys. Rev. D **99**, 103015 (2019).

[73] C. Yuan, Y. Jiang, and Q.-G. Huang, Phys. Rev. D **106**, 023020 (2022).

[74] L. Tsukada, R. Brito, W. E. East, and N. Siemonsen, Phys. Rev. D **103**, 083005 (2021).

[75] L. Sun, R. Brito, and M. Isi, Phys. Rev. D **101**, 063020 (2020).

[76] S. Collaviti, L. Sun, M. Galanis, and M. Baryakhtar, Classical and Quantum Gravity **42**, 025006 (2024).

[77] S. Vermeulen, P. Relton, H. Grote, V. Raymond, C. Affeldt, F. Bergamin, A. Bisht, M. Brinkmann, K. Danzmann, S. Doravari, V. Kringel, J. Lough, H. Lück, M. Mehmet, N. Mukund Menon, S. Nadji, E. Schreiber, B. Sorazu, K. Strain, and H. Wittel, Nature **600**, 424 (2021).

[78] A. S. Göttel, A. Ejlli, K. Karan, S. M. Vermeulen, L. Aiello, V. Raymond, and H. Grote, Phys. Rev. Lett. **133**, 101001 (2024).

[79] L. Aiello, J. W. Richardson, S. M. Vermeulen, H. Grote, C. Hogan, O. Kwon, and C. Stoughton, Phys. Rev. Lett. **128**, 121101 (2022).

[80] R. Abbott *et al.* (LIGO Scientific Collaboration, Virgo Collaboration, and KAGRA Collaboration), Phys. Rev. D **105**, 063030 (2022).

[81] A. G. Abac *et al.* (LIGO Scientific, Virgo, and KAGRA Collaborations), Phys. Rev. D **110**, 042001 (2024).

[82] Q. Yang, L.-W. Ji, B. Hu, Z.-J. Cao, and R.-G. Cai, Research in Astronomy and Astrophysics **18**, 065 (2018).

[83] S. Choudhary, N. Sanchis-Gual, A. Gupta, J. C. Degollado, S. Bose, and J. A. Font, Phys. Rev. D **103**, 044032 (2021).

[84] D. Jones, L. Sun, N. Siemonsen, W. E. East, S. M. Scott, and K. Wette, Phys. Rev. D **108**, 064001 (2023).

[85] D. Jones, N. Siemonsen, L. Sun, W. E. East, A. L. Miller, K. Wette, and O. J. Piccinni, Phys. Rev. D **111**, 063028 (2025).

[86] A. G. Abac *et al.* (LIGO Scientific Collaboration, Virgo Collaboration, and KAGRA Collaboration), The Astrophysical Journal Letters **995**, L18 (2025).

[87] The LIGO Scientific Collaboration and the Virgo Collaboration and the KAGRA Collaboration, "GWTC-4.0: Methods for Identifying and Characterizing Gravitational-wave Transients," (2025), arXiv:2508.18081 [gr-qc].

[88] The LIGO Scientific Collaboration and The Virgo Collaboration and the KAGRA Collaboration, "GWTC-4.0: Updating the Gravitational-Wave Transient Catalog with Observations from the First Part of the Fourth LIGO-Virgo-KAGRA Observing Run," (2025), arXiv:2508.18082 [gr-qc].

[89] O. J. Piccinni, P. Astone, S. D'Antonio, S. Frasca, G. Intini, P. Leaci, S. Mastrogiovanni, A. Miller, C. Palomba, and A. Singhal, Classical and Quantum Gravity **36**, 015008 (2018).

[90] J. C. A. Miller-Jones, A. Bahramian, J. A. Orosz, I. Mandel, L. Gou, T. J. Maccarone, C. J. Neijssel, X. Zhao, J. Ziółkowski, M. J. Reid, P. Uttley, X. Zheng, D.-Y. Byun, R. Dodson, V. Grinberg, T. Jung, J.-S. Kim, B. Marcote, S. Markoff, M. J. Rioja, A. P. Rushton, D. M. Russell, G. R. Sivakoff, A. J. Tetarenko, V. Tudose, and J. Wilms, Science **371**, 1046 (2021).

[91] T.-W. Wong, F. Valsecchi, T. Fragos, and V. Kalogera, The Astrophysical Journal **747**, 111 (2012).

[92] J. G. Rosa and S. R. Dolan, Phys. Rev. D **85**, 044043 (2012).

[93] P. Pani, V. Cardoso, L. Gualtieri, E. Berti, and A. Ishibashi, Phys. Rev. D **86**, 104017 (2012).

[94] V. P. Frolov, P. Krtouš, D. Kubizňák, and J. E. Santos, Phys. Rev. Lett. **120**, 231103 (2018).

[95] D. Baumann, H. S. Chia, J. Stout, and L. ter Haar, JCAP **12**, 006 (2019).

[96] S. R. Dolan, Phys. Rev. D **98**, 104006 (2018).

[97] N. Siemonsen, T. May, and W. E. East, Phys. Rev. D **107**, 104003 (2023), arXiv:2211.03845 [gr-qc].

[98] The LIGO Scientific Collaboration and The Virgo Collaboration and the KAGRA Collaboration, "GW230814: investigation of a loud gravitational-wave signal observed with a single detector," (2025), arXiv:2509.07348 [gr-qc].

[99] A. G. Abac *et al.* (LIGO Scientific Collaboration, Virgo Collaboration, and KAGRA Collaboration), The Astrophysical Journal Letters **993**, L25 (2025).

[100] V. Varma, S. E. Field, M. A. Scheel, J. Blackman, D. Gerosa, L. C. Stein, L. E. Kidder, and H. P. Pfeiffer, Phys. Rev. Res. **1**, 033015 (2019).

[101] C. Brocksopp, A. Tarasov, V. Lyuty, and P. Roche, Astronomy and Astrophysics **343** (1999).

[102] R. Abbott *et al.* (LIGO Scientific Collaboration, Virgo Collaboration, and KAGRA Collaboration), Phys. Rev. D **106**, 102008 (2022).

[103] P. Astone, A. Colla, S. D'Antonio, S. Frasca, and C. Palomba, Phys. Rev. D **90**, 042002 (2014).

[104] L. Gou, J. E. McClintock, M. J. Reid, J. A. Orosz, J. F. Steiner, R. Narayan, J. Xiang, R. A. Remillard, K. A. Arnaud, and S. W. Davis, The Astrophysical Journal **742**, 85 (2011).

[105] X. Zhao, L. Gou, Y. Dong, X. Zheng, J. F. Steiner, J. C. A. Miller-Jones, A. Bahramian, J. A. Orosz, and Y. Feng, The Astrophysical Journal **908**, 117 (2021).

[106] L. Gou, J. E. McClintock, R. A. Remillard, J. F. Steiner, M. J. Reid, J. A. Orosz, R. Narayan, M. Hanke, and J. García, The Astrophysical Journal **790**, 29 (2014).

[107] M. Axelsson, R. P. Church, M. B. Davies, A. J. Levan, and F. Ryde, Monthly Notices of the Royal Astronomical Society **412**, 2260 (2011), https://academic.oup.com/mnras/article-pdf/412/4/2260/3334647/mnras0412-2260.pdf.

[108] D. J. Walton, J. A. Tomsick, K. K. Madsen, V. Grinberg, D. Barret, S. E. Boggs, F. E. Christensen, M. Clavel, W. W. Craig, A. C. Fabian, F. Fuerst, C. J. Hailey, F. A. Harrison, J. M. Miller, M. L. Parker, F. Rahoui, D. Stern, L. Tao, J. Wilms, and W. Zhang, The Astrophysical Journal **826**, 87 (2016).

[109] R. Duro, T. Dauser, V. Grinberg, I. Miškovičová, J. Rodriguez, J. Tomsick, M. Hanke, K. Pottschmidt, M. A. Nowak, S. Kreykenbohm, M. Cadolle Bel, A. Bodaghee, A. Lohfink, C. S. Reynolds, E. Kendziorra, M. G. F. Kirsch, R. Staubert, and J. Wilms, Astronomy and Astrophysics **589**, A14 (2016), arXiv:1602.08756 [astro-ph.HE].

[110] A. A. Zdziarski, S. Banerjee, S. Chand, G. Dewangan, R. Misra, M. Szanecki, and A. Niedźwiecki, The Astrophysical Journal **962**, 101 (2024).

[111] T. Kawano, C. Done, S. Yamada, H. Takahashi, M. Axelsson, and Y. Fukazawa, Publications of the Astronomical Society of Japan **69**, 36 (2017), https://academic.oup.com/pasj/article-pdf/69/2/36/54678093/pasj_69_2_36.pdf.

[112] J. A. Tomsick, M. A. Nowak, M. Parker, J. M. Miller, A. C. Fabian, F. A. Harrison, M. Bachetti, D. Barret, S. E. Boggs, F. E. Christensen, W. W. Craig, K. Forster, F. Fürst, B. W. Grefenstette, C. J. Hailey, A. L. King, K. K. Madsen, L. Natalucci, K. Pottschmidt, R. R. Ross, D. Stern, D. J. Walton, J. Wilms, and W. W. Zhang, The Astrophysical Journal **780**, 78 (2013).

[113] H. Krawczynski and B. Beheshtipour, The Astrophysical Journal **934**, 4 (2022).

[114] H. Krawczynski, General Relativity and Gravitation **50**, 100 (2018), arXiv:1806.10347 [astro-ph.HE].

[115] J. M. Miller, C. S. Reynolds, A. C. Fabian, G. Miniutti, and L. C. Gallo, The Astrophysical Journal **697**, 900 (2009).

[116] A. A. Zdziarski, S. Chand, S. Banerjee, M. Szanecki, A. Janiuk, P. Lubiński, A. Niedźwiecki, G. Dewangan, and R. Misra, The Astrophysical Journal Letters **967**, L9 (2024).

[117] L. Sun, A. Melatos, S. Suvorova, W. Moran, and R. J. Evans, Phys. Rev. D **97**, 043013 (2018).

[118] S. Suvorova, L. Sun, A. Melatos, W. Moran, and R. J. Evans, Phys. Rev. D **93**, 123009 (2016).

[119] L. Sun and A. Melatos, Phys. Rev. D **99**, 123003 (2019).

[120] R. Abbott *et al.*, The Astrophysical Journal **921**, 80 (2021).

[121] B. P. Abbott *et al.* (LIGO Scientific Collaboration and Virgo Collaboration), Phys. Rev. D **95**, 122003 (2017).

[122] B. P. Abbott *et al.* (LIGO Scientific Collaboration and Virgo Collaboration), Phys. Rev. D **100**, 122002 (2019).

[123] M. Millhouse, L. Strang, and A. Melatos, Phys. Rev. D **102**, 083025 (2020).

[124] D. Jones and L. Sun, Physical Review D **103** (2021).

[125] D. Beniwal, P. Clearwater, L. Dunn, A. Melatos, and D. Ottaway, Phys. Rev. D **103**, 083009 (2021).

[126] R. Abbott *et al.* (LIGO Scientific Collaboration, Virgo Collaboration, and KAGRA Collaboration), Phys. Rev. D **105**, 022002 (2022).

[127] A. M. Knee, H. Du, E. Goetz, J. McIver, J. B. Carlin, L. Sun, L. Dunn, L. Strang, H. Middleton, and A. Melatos, Phys. Rev. D **109**, 062008 (2024).

[128] K. Riles, Living Reviews in Relativity **26**, 3 (2023).

[129] P. Jaranowski, A. Królak, and B. F. Schutz, Phys. Rev. D **58**, 063001 (1998).

[130] C. Cutler and B. F. Schutz, Physical Review D **72** (2005), 10.1103/physrevd.72.063006.

[131] LIGO Scientific Collaboration and Virgo Collaboration and KAGRA Collaboration, "LVK Algorithm Library - LALSuite," Free software (GPL) (2018).

[132] K. Wette, SoftwareX **12**, 100634 (2020).

[133] A. Viterbi, IEEE Transactions on Information Theory **13**, 260 (1967).

[134] R. Abbott *et al.* (LIGO Scientific Collaboration, Virgo Collaboration, and KAGRA Collaboration), Phys. Rev. D **106**, 062002 (2022).

[135] R. Abbott *et al.*, The Astrophysical Journal Letters **902**, L21 (2020).

[136] R. Abbott *et al.*, The Astrophysical Journal **935**, 1 (2022).

[137] O. J. Piccinni, P. Astone, S. D'Antonio, S. Frasca, G. Intini, I. La Rosa, P. Leaci, S. Mastrogiovanni, A. Miller, and C. Palomba, Phys. Rev. D **101**, 082004 (2020).

[138] B. P. Abbott *et al.* (LIGO Scientific Collaboration and Virgo Collaboration), Phys. Rev. D **100**, 024004 (2019).

[139] P. Astone, S. Frasca, and C. Palomba, Classical and Quantum Gravity **22**, S1197 (2005).

[140] P. Leaci and R. Prix, Phys. Rev. D **91**, 102003 (2015).

[141] K. Wette, Phys. Rev. D **90**, 122010 (2014).

[142] E. Capote *et al.*, Phys. Rev. D **111**, 062002 (2025).

[143] S. Soni *et al.*, Classical and Quantum Gravity **42**, 085016 (2025).

[144] D. Ganapathy *et al.* (LIGO O4 Detector Collaboration), Phys. Rev. X **13**, 041021 (2023).

[145] The LIGO Scientific, Virgo, and KAGRA Collaborations, "LIGO Virgo KAGRA Calibration Uncertainty (O4)," (2025).

[146] M. Wade, J. Betzwieser, D. Bhattacharjee, L. Dartez, E. Goetz, J. Kissel, L. Sun, A. Viets, M. Carney, E. Makelele, and L. Wade, Classical and Quantum Gravity **42**, 215016 (2025).

[147] L. Sun, E. Goetz, J. S. Kissel, J. Betzwieser, S. Karki, A. Viets, M. Wade, D. Bhattacharjee, V. Bossilkov, P. B. Covas, L. E. H. Datrier, R. Gray, S. Kandhasamy, Y. K. Lecoeuche, G. Mendell, T. Mistry, E. Payne, R. L. Savage, A. J. Weinstein, S. Aston, A. Buikema, C. Cahillane, J. C. Driggers, S. E. Dwyer, R. Kumar, and A. Urban, Classical and Quantum Gravity **37**, 225008 (2020).

[148] A. D. Viets, M. Wade, A. L. Urban, S. Kandhasamy, J. Betzwieser, D. A. Brown, J. Burguet-Castell, C. Cahillane, E. Goetz, K. Izumi, S. Karki, J. S. Kissel, G. Mendell, R. L. Savage, X. Siemens, D. Tuyenbayev, and A. J. Weinstein, Classical and Quantum Gravity **35**, 095015 (2018).

[149] A. D. Viets, *Optimizing Advanced LIGO's scientific output with fast, accurate, clean calibration*, Phd thesis, University of Wisconsin-Milwaukee, Milwaukee, WI (2019).

[150] G. Vajente, Y. Huang, M. Isi, J. C. Driggers, J. S. Kissel, M. J. Szczepańczyk, and S. Vitale, Phys. Rev. D **101**, 042003 (2020).

[151] The LIGO Scientific, Virgo, and KAGRA Collaborations, "Open Data from LIGO, Virgo, and KAGRA through the first part of the fourth observing run," (2025).

[152] D. Davis, A. Neunzert, E. Goetz, K. Riles, K. Wette, and M. Lalleman, "Self-gating of O4a h(t) for use in continuous-wave searches," (2024).

[153] F. Acernese *et al.*, Classical and Quantum Gravity **26**, 204002 (2009).

[154] P. B. Covas *et al.* (LSC Instrument Authors), Phys. Rev. D **97**, 082002 (2018).

[155] E. Goetz *et al.*, "O4a lines and combs in found in self-gated C00 cleaned data," (2024).

[156] N. L. Johnson, A. W. Kemp, and S. Kotz, *Univariate Discrete Distributions* (John Wiley & Sons, Ltd., 2005).

[157] C. Palomba, "On the sensitivity of peakmap-based methods for the search of continuous gravitational wave signals," (2025).

[158] M. Di Cesare, *All-sky gravitational wave searches for isolated neutron stars: methods and applications to LIGO-Virgo data*, Master thesis, Sapienza Università di Roma (2021).

[159] B. Behnke, M. A. Papa, and R. Prix, Phys. Rev. D **91**, 064007 (2015).

[160] R. Abbott *et al.*, Physical Review D **103** (2021), 10.1103/physrevd.103.064017.

[161] R. Abbott *et al.*, The Astrophysical Journal **922**, 71 (2021).

[162] R. Abbott *et al.*, Physical Review D **105** (2022), 10.1103/physrevd.105.082005.